OPTIMIZATION OF ASYMMETRIC HOLLOW FIBER MEMBRANES FOR NATURAL GAS SEPARATION

A Thesis
Presented to
The Academic Faculty

by

Canghai Ma

In Partial Fulfillment
Of the Requirements for the Degree
Master of Science in the
School of Chemical and Biomolecular Engineering

Georgia Institute of Technology
May, 2011

OPTIMIZATION OF ASYMMETRIC HOLLOW FIBER MEMBRANES FOR NATURAL GAS SEPARATION

Approved by:

Dr. Williams J. Koros, Advisor
School of Chemical and Biomolecular Engineering
Georgia Institute of Technology

Dr. Yulin Deng
School of Chemical and Biomolecular Engineering
Georgia Institute of Technology

Dr. Wallace W. Carr
School of Polymer, Textile & Fiber Engineering
Georgia Institute of Technology

Date Approved: April, 2011

ACKNOWLEDGEMENTS

This work cannot be accomplished without the help of numerous people. First of all, I would like to thank my advisor, Dr. Koros. He taught me not only how to become a real researcher but also how to overcome obstacles in my life. His guidance, friendship, enthusiasm, and energy always inspires me. Without his help, I could not cross over the hurdles in the study and research. Moreover, I want to thank all the group members. Dr. Junqiang Liu and Omo Esekhile helped me in the fiber spinning and dense film permeance test. Dr. Ryan P. Lively helped solve the spinneret problems and spinning issues I encountered during spinning. Dr. Wulin Qiu assisted me with the synthesis of polymers. Chien-Chiang Chen always shared his experience of research unselfishly. Dr. N. Bessho greatly resolved my puzzles both in study and research. Dr. JR. Johnson and Dr. Oguz Karvan took care of almost everything in our labs so that I could conduct my experiments smoothly. I want to gratefully acknowledge my thesis committee members, Dr. Yulin Deng and Dr. Wallace W. Carr, for their work and guidance in the thesis. I would also like to thank my collaborators, especially, Dr. Stephen Miller, at Chevron for their generous funding support, as well as their polymer supply and technical feedback. Thanks Dr. Daniel Chin, Dr. Oluwassijibomi Okeowo and Dr. Shabbir Husain. Finally, my great thanks are given to my loving parents, Jinmin Ma and Dahua Xu, my brother, Lin Ma and my wife, Hongjuan Cui. They always encouraged me whatever the problem I had; especially, thanks to Hongjuan, who is standing closest to me. Without their unconditional love and care, I cannot overcome all the setbacks in my life.

TABLE OF CONTENTS

LIST OF TABLES

Page

LIST OF FIGURES

Page

LIST OF SYMBOLS AND ABBREVIATIONS

P	Permeability /Barrer
D	Diffusion coefficient/ [m^2/s]
S	Sorption coefficients/ [cc (STP)/ (cc polymer·psi)]
f	Average jumping frequency/Hz
λ	Average jumps length (m) or response factor
k_{Di}	Henry's law constant/[cc(STP)/cc polymer·psi]
C'_{Hi}	Langmuir capacity constant/ [cc(STP)/cc polymer]
b_i	Langmuir affinity constant/ [1/psi]
p_i	Partial pressure of component *i*/psi
n_i	Flux of penetrant *i*
l	Membrane thickness/μ
Δp_i	Partial pressure difference/psi
α_{ij}	Selectivity of component *i* and *j*
$S.F.$	Separation factor
x	Mole fraction of the penetrants in the upstream
y	Mole fraction of the penetrants in the downstream
ρ	Unswollen polymer density/[g/cc]
ω_A	Mass fraction of permeant A
dp/dt	Slope of the downstream pressure vs. time/[torr/s]
V_R	Downstream reservoir volume/cc
A	Membrane area/cm^2
T	Operation temperature/K
Vp	Permeation volumetric flow rate/[cc/s]

Δf	Fugacity difference/psi
ϕ	Fugacity coefficients

SUMMARY

Energy issues have been driving researchers throughout the world studying extensively on natural gas separation. As a common contaminant of natural gas, carbon dioxide (CO_2) must be removed from raw natural gas to meet the composition specification in the pipeline.

Compared to the conventional amine adsorption process to separate CO_2 from natural gas, the membrane separation technology has exhibited advantages in easy operation and lower capital cost. However, the high CO_2 partial pressure in natural gas can plasticize the membranes, which can lead to the loss of methane (CH_4) and low CO_2/CH_4 separation efficiency.

Crosslinking of polymer membranes, either in the form of dense films or asymmetric hollow fibers, have been proven effective to increase the CO_2 induced plasticization resistance by controlling the degree of swelling and segmental chain mobility in the polymer. This research focuses on extending the success of crosslinking to more productive asymmetric hollow fibers.

In this study, the productivity of asymmetric hollow fibers was optimized by reducing the effective selective skin layer thickness. Thermal crosslinking and catalyst assisted crosslinking were performed on the defect-free thin skin hollow fibers to stabilize the fibers against plasticization. The crosslinked fibers were first probed by pure

gas permeation to study the ideal gas transport properties. The natural gas separation performance of hollow fibers was evaluated by feeding CO_2/CH_4 gas mixture with high CO_2 content and partial pressure. The stability of crosslinked fibers over time was also studied by an exposure for a set period of time in a high CO_2 content at the maximum test pressure.

CHAPTER 1

INTRODUCTION

1.1 Natural gas overview

Energy issues have been always an important research topic throughout the world. Natural gas provided about 25% of energy used in the U.S. in 2009. In last decade, the U.S. consumed around 22~23 trillion SCF/yr of natural gas while only produced 19~21 trillion SCF/yr. (In this thesis, "SCF" is used to represent standard cubic feet.)[1]. Raw natural gas varies significantly in the composition from source to source. The main component in natural gas is methane (CH_4), which comprises 75~90 mol% of total. Carbon dioxide (CO_2) is a common contaminant of natural gas and must be removed to a level of <2% to minimize the pipeline corrosion. There are also some other impurities like hydrogen sulfide (H_2S), water, C_3+ hydrocarbon that also must be removed to meet the pipeline specification, as shown in Table 1.1.

Table 1.1: Natural gas composition specifications for delivery in the U.S. pipeline [2].

Component	Specification
CO_2	<2%
H_2S	<4ppm
H_2O	<120ppm
C_3+ hydrocarbon	950~1050 BTU/SCF; T_{dew}<-20^oC
Inert gases (total)	<4%

To meet pipeline specification shown in Table 1.1, ~20% of natural gas requires extensive treatment. Excessive impurities in the natural gas feed must be removed before delivery to the pipeline [2].

1.2 Natural gas separation technology

The main technologies that exist currently to separate CO_2 from natural gas include cryogenic distillation, amine absorption, and membranes [2-4]. Cryogenic distillation is a highly energy intensive technology as gases must be cooled down to form boiling liquid mixture to realize the separation [5]. Amine absorption technology has been widely accepted and used as the stand of natural gas separation. This technology removes CO_2 almost completely but high capital cost, complex operation, corrosion and expensive maintenance makes this approach problematic [4]. Large amounts of absorbent fluid are used in the towers and the heating and cooling of the recirculation fluids requires additional cost and careful operation procedures. The high-maintenance and complex operation further hinders application of amine absorption in remote locations. Membrane separation technology has been developed and attracted researchers' interests throughout the world and can significantly overcome the operational problems that associated with the amine absorption process [2-7]. The membrane approach will be the focus of this study.

1.3 Membrane separation technology

In 1980, Permea launched the high flux asymmetric hollow fiber hydrogen-separating Prism membrane, which was the first large industrial application of membranes technology for hydrogen separation [3]. Since then, membrane technology has become a competitive separation technology and has grown into a $150 million/yr business. The membrane technology does not require a phase change; therefore, the energy cost is significantly reduced. Furthermore, the membrane system is particularly

suitable for use in remote locations where reliability is critical [4]. If membranes achieve a CO_2/CH_4 selectivity of 40 commercially, the membrane technology will replace most amine plants [3].

Many materials can be used to form membranes, including polymers, carbon molecular sieves, zeolites and ceramic [4, 8]; however, for natural gas purification, the polymeric membranes are the dominant materials used. Current polymer membranes are produced as asymmetric hollow fibers modules or spiral-wound modules. Asymmetric hollow fiber modules provide relatively higher surface area to volume ratio and packing density due to their cylindrical morphologies. The small dimension of hollow fibers provides the membrane the capability of withstanding high feeding pressures [2]. They can reduce the effective separating layer to a thin integral "skin" on the outer layer of the fibers [9-10]. The thickness of this skin layer is critical in natural gas separation as a thinner skin offers a higher separation productivity. This optimization of the skin layer is specifically addressed in this thesis. Another issue involving membrane technology is the plasticization of membranes due to the aggressive feed streams with high CO_2 contents. The CO_2 induced plasticization can cause swelling of membranes and the loss of separation efficiency. The thesis will focus on the strategies to suppress the plasticization of membrane in realistic feed streams with high CO_2 concentration. The following are the main objectives of research for this thesis.

1.4 Research objectives

1.4.1 Skin layer optimization of hollow fibers

In this work, a novel polymer called propanediol monoesterified crosslinkable polyimide (PDMC) is used to produce asymmetric hollow fibers [11-12]. PDMC polymer has been proven effective for CO_2 removal of aggressive natural gas streams in the form of dense film [13-14]. Moreover, asymmetric hollow fibers have been spun successfully to achieve high CO_2/CH_4 selectivity and suppress CO_2 induced plasticization under rigid mixed gas feeding. However, the skin layer thickness of the hollow fibers is on the order of 0.2~0.4μ and it would be desirable to reduce this thickness to increase productivity [11-12]. Therefore, in this section, the skin layer of hollow fibers was optimized to achieve a defect-free skin layer thickness on the order of 0.1μ without loss of separation efficiency.

1.4.2 Crosslinking of asymmetric hollow fibers

Covalent crosslinking of hollow fibers has been proven as an effective method to improve the CO_2 induced plasticization resistance and maintain high selectivity [11-14]. However, conventional crosslinking by annealing the hollow fibers in vacuum for a set period of time causes a significant loss of permeance, making the hollow fibers inadequate for industrial applications. Therefore, the work will study the optimization of crosslinking conditions, including the crosslinking temperature and crosslinking time. The less aggressive process conditions must be applied on the hollow fibers to reduce the loss of permeance, which necessities the usage of catalyst in the crosslinking reaction. The addition of catalyst during crosslinking can lower the crosslinking temperature by reducing activation energy of crosslinking reaction. The separation performance of catalyst crosslinked fibers was probed by using ideal gas permeation.

1.4.3 Natural gas separation with hollow fibers

As discussed in Section 1.3, membrane separation technology has exhibited advantages for natural gas purification over the traditional amine absorption process. In this work, natural gas separation performance of hollow fibers was evaluated by using the model feed mixed gas. Different compositions of CO_2/CH_4 were fed to the hollow fibers. High CO_2 concentration and pressure feed streams were also used to study the stability of hollow fibers against aggressive conditions. The mixed gas permeation of both uncrosslinked and crosslinked fibers were conducted to identify the effect of crosslinking on natural gas separation properties.

1.5 Thesis overview

Chapter 1 contains introductory materials, including background on natural gas and membrane separation technology. Research objectives and thesis organization are also described.

Chapter 2 relates the technical background for the work. This includes gas transport fundamentals, hollow fiber spinning techniques, effect of feed composition and pressure on CO_2/CH_4 separation properties, and stabilization strategies against CO_2 plasticization.

Chapter 3 presents the materials and experimental methods. Dense film and hollow fibers are introduced, followed by the characterization of hollow fibers and crosslinking.

Chapter 4 describes the work and results on the skin layer optimization of hollow fibers, which includes the three main aspects: spinning conditions optimization, dope reformulation and molecular weight effect.

Chapter 5 discusses the crosslinking of asymmetric hollow fibers. Ideal gas permeation behavior of thermal crosslinked and catalyst assisted crosslinked hollow fibers are reported to study the gas transport properties of those crosslinked fibers.

Chapter 6 focuses on the natural gas purification with hollow fibers. The mixed gas permeation of both uncrosslinked and crosslinked hollow fibers are investigated to probe the natural gas separation performance.

Chapter 7 provides a summary of the conclusions of this work and recommends paths for future study and investigation.

The appendices contain additional useful information, including a description of making hollow fiber modules, methods for permeation test, and monoesterification reaction procedures.

CHAPTER 2

BACKGROUND AND LITERATURE REVIEW

This chapter provides additional background details in order to understand gas transport in polymer membranes, the formation and characterization of hollow fiber membrane and strategies for stabilizing hollow fibers against plasticization.

2.1 Molecular transport in polymer membranes

2.1.1 Gas transport mechanism in membranes

Several mechanisms exist for gas molecule transport in polymer membranes, depending on the existence and size of membrane pores and the mean free path of penetrants [6, 7, 10, 15-18]. In this work, the two most common gas transport mechanisms for practical membranes are considered: Knudsen diffusion and solution-diffusion process. Knudsen diffusion occurs in membrane pores where the pore size is smaller than the gas molecular mean free path in the bulk. The molecules frequently collide with the pore wall and are hindered in moving across the membrane by these collisions. Some diffusion selectivity occurs based on the difference in the molecular weight of the molecules; however, the low selectivity in Knudsen diffusion is inadequate to meet most practical gas separation requirements. The solution-diffusion model was first qualitatively described by Graham in 1831 as the most widely accepted description of gas transport in polymer membranes without continuous pores [6, 18]. In this model, the permeants dissolve in the membrane materials and then diffuse through the membrane down a concentration gradient. The differences in the amount of gas dissolved in the membrane and the rate of permeants diffusion through the membrane causes the different gases to be separated as they permeate across the membrane. In this case, the

permeability coefficient, P, of a polymer membrane can be represented as the product of the diffusion coefficient, D, and sorption coefficients, S, as shown in Equation 2.1[6].

$$P=D\cdot S \tag{2.1}$$

If the membrane is essentially isotropic and the penetrants can move equally in any of the six coordinate directions, the diffusion coefficient can be written as shown in Equation 2.2 in terms of the average jump length, λ, and average jumping frequency, f. [6, 19]

$$D=f\cdot \lambda^2/6 \tag{2.2}$$

The sorption coefficient S in glassy polymer membranes is most commonly described by the dual mode model, shown in Equation 2.3 [20-21].

$$\frac{C_A}{P_A} = S_A = k_{Di} + \frac{C'_{Hi} b_i}{1 + b_A p_A + b_B p_B} \tag{2.3}$$

In Equation 2.3, k_{Di} is the Henry's law constant, C'_{Hi} is the Langmuir capacity constant, b_i is the Langmuir affinity constant, and p_i is the local effective partial pressure of component i, which is a measure of the local chemical potential for component i. In a typical glassy polymer membrane, there exist segmental packing defects, generally referred to as microvoids or "holes". These packing defects represent "unrelaxed volume" in the nonequilibrium glassy matrix of the selective layer.

The sorption of penetrants in the intersegmental packing defects, called "microvoids", is expressed as Langmuir sorption in dual sorption model, while the sorption of penetrants in more or less well packed environments in the glassy matrix is described by the Henry's Law sorption, shown in Equation 2.3. At lower pressure, the Langmuir sorption dominates the gas in the membrane, as the microvoid offers low energy sorption sites in the glassy matrix. When increasing the pressure, the Langmuir

sites become saturated by penetrants and Henry's Law becomes the dominant mechanism of gas molecular transport in membranes. At higher sorption levels, swelling of the matrix can occur with increases in the apparent value of k_{Di} that lead to large increases in S_A in Equation 2.3 as p_A increases [11].

2.1.2 Characterization of membrane performance

To evaluate the performance of a polymer membrane, two key factors are commonly investigated: permeability and selectivity [6]. The permeability reveals the intrinsic productivity of a membrane material and is defined in terms of the flux of penetrant *i*, normalized by the membrane thickness and the partial pressure difference between the feed and permeate side, as shown in Equation 2.4.

$$P_i = \frac{n_i \cdot l}{\Delta p_i} \tag{2.4}$$

In Equation 2.4, n_i refers to the flux of penetrant *i* through the membrane; l represents the membrane thickness, and Δp_i describes the partial pressure difference across the membrane between its upstream and downstream faces. The common unit of membrane permeability is the Barrer, defined as Equation 2.5.

$$1\ \text{Barrer} = 10^{-10}\left(\frac{\text{cc(STP)}}{\text{cm}^2 \cdot \text{s}}\right) \cdot \frac{\text{cm}}{\text{cmHg}} \tag{2.5}$$

In asymmetric hollow fiber membranes, the actual thickness of membranes is hard to determine unambiguously; therefore, the productivity of this hollow fiber membrane is usually described by the permeance, which is ratio of normalized flux and partial pressure difference, as shown in Equation 2.6.

$$\frac{P_i}{l} = \frac{n_i}{\Delta p_i} \tag{2.6}$$

The unit of permeance is the GPU, which is defined as Equation 2.7.

$$\mathrm{GPU} = 10^{-6}\left(\frac{\mathrm{cc(STP)}}{\mathrm{cm}^2 \cdot \mathrm{s} \cdot cmHg}\right) \tag{2.7}$$

The selectivity measures the intrinsic membrane material separation efficiency. For a given pair of pure gases, if the total downstream pressure is much less than the total upstream pressure, the ideal selectivity, α_{ij} is defined the ratio of the fast gas (i) to the slow gas (j) permeability or permeance, as shown in Equation 2.8.

$$\alpha_{ij} = \frac{P_i}{P_j} = \frac{P_i / l}{P_j / l} \tag{2.8}$$

Equation 2.8 is used to describe the ideal gas separation performance of membranes when it is tested with pure gases. Practically, for mixed gas streams, complications including plasticization and competition among gas molecules may occur (discussed in 2.5). The separation factor, $(S.F.)_{ij}$, is the practical measure commonly used to examine the separation performance, shown in Equation 2.9 [6].

$$(S.F.)_{ij} = \frac{y_i / y_j}{x_i / x_j} \tag{2.9}$$

In Equation 2.9, x and y means the mole fraction of the penetrants in the upstream and downstream of the membrane, respectively; and i and j represent the different penetrants in the mixed gases. The two factors, α_{ij} and $(S.F.)_{ij}$, are equal when the ratio of upstream pressure to downstream pressure is very high (ideally infinite). The relative permeability or permeance ratio is the preferred measure of a membrane's intrinsic separation performance, since the $(S.F.)_{ij}$ includes the effects of feed to permeate pressure ratio, which complicate material performance properties.

To characterize the membrane performance, the permeability and permselectivity must be balanced for commercial application of membranes, since there exists a tradeoff between the permeability and permselectivity. Robeson studied this tradeoff by summarizing separation factor and permeability for different polymer membranes [22].

2.2 Asymmetric hollow fibers

2.2.1 Asymmetric hollow fiber introduction

In the past decade, many new polymer materials have been reported to form membranes and have high permeabilities and selectivities. The two key parameters, permeabilities and selectivities, affect the relative performance of such materials; however, the ability to integrate stable, thin, low-cost membranes into high-surface-area modules must be also considered.

Asymmetric hollow fiber membranes are industrially preferred to improve the productivity and reduce the cost of membranes in gas separation technology. Hollow fiber membranes have surface area to volume ratios over 30 to 50 times than spiral-wound membranes, that is, up to 10,000 m^2/m^3 [23]. The cylindrical structure of the hollow fibers can withstand high transmembrane pressure difference up to 1000 psi [10]. The porous structure of hollow fibers underneath the outer skin layer has ideally negligible transport resistance and increases mechanical stability of membranes against high pressure feeds. The dense skin layer has a thickness as low as 100 nm and performs the separation with high productivity. The morphology of a typical asymmetric hollow fiber membrane is shown in Figure 2.2.

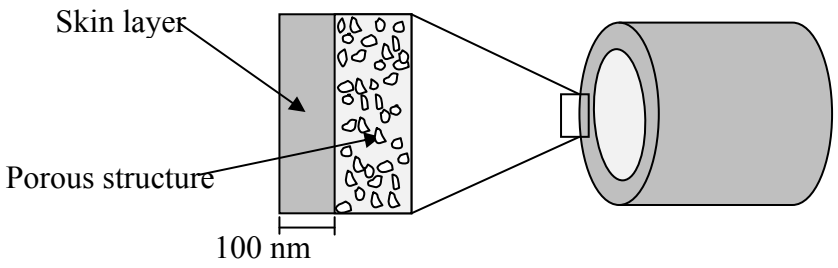

Figure 2.1: A typical asymmetric hollow fiber and schematic of the skin layer (~100 nm thick).

2.2.2 Mechanism of hollow fiber formation

The process to produce asymmetric hollow fiber membranes is called hollow fiber spinning. The formation of hollow fibers is based on the phase separation behavior of polymer solutions. Non-solvent is commonly introduced in the spinning solution to promote rapid phase separation in the spinning. To better understand the spinning mechanism, the ternary phase diagram is useful [10], as shown in Figure 2.2.

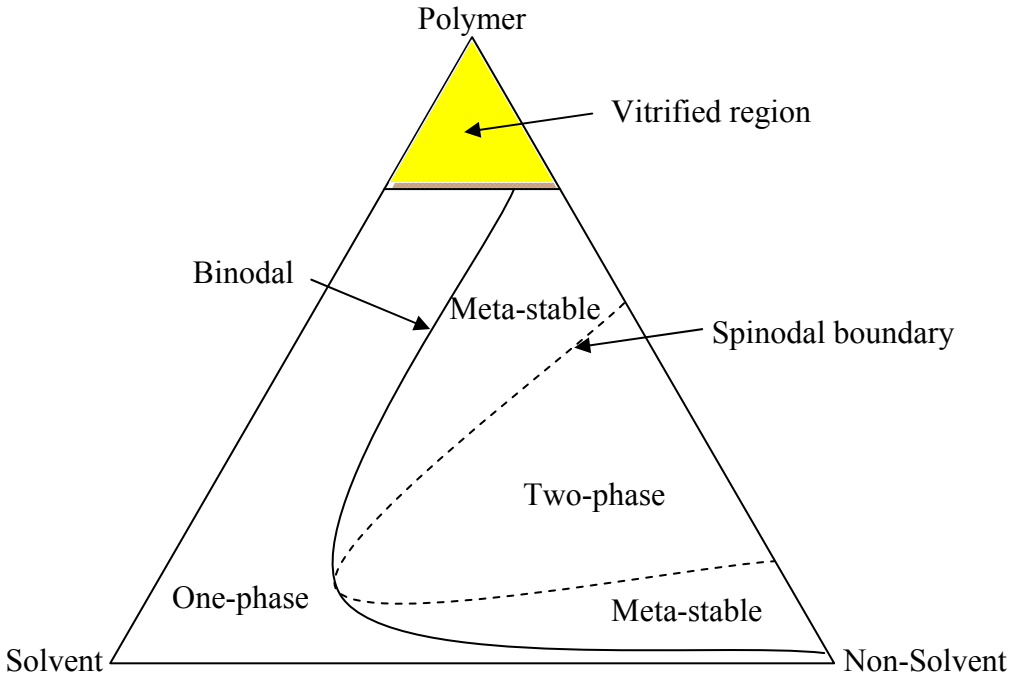

Figure 2.2: Ternary phase diagram showing important boundary lines and phase regions [10].

There are three main regions in the ternary phase diagram as shown in Figure 2.2: stable one-phase, meta-stable phase and two-phase. The binodal (solid line) and spinodal (dashed line) lie within the two phase regions. The polymer solution can move to the two-phase region from the one-phase region either by addition of non-solvent or the removal of solvent, which are two mechanisms of phase separation for polymer solutions. Defect-free hollow fibers with integral dense skin layer can be formed when the polymer concentration is above a certain value prior to phase separation (discussed in 2.3.6) [24-27].

2.3 The dry-jet/wet-quench bath spinning

2.3.1 Overview

The homogeneous polymer solution (called dope) is first extruded with bore fluid through an annular die, called a spinneret, into aqueous quench bath. The invasion of water in the bath causes the dope phase separated into a polymer rich phase and a polymer lean phase. The polymer rich phase forms the solid structure of hollow fibers while the polymer lean phase forms the porous support structure. The phase separation occurs either through the solvent evaporation over non-solvent from the dope or immersion in aqueous quench bath. The spinning technique used in this work is called dry-jet and wet-quench spinning. In this process, the dope initially passes through an "air gap" (wet-jet) and forms the nascent fibers during phase separation in the aqueous quench bath (wet-quench). Figure 2.3 depicts the procedures of dry-jet/wet-quench bath spinning.

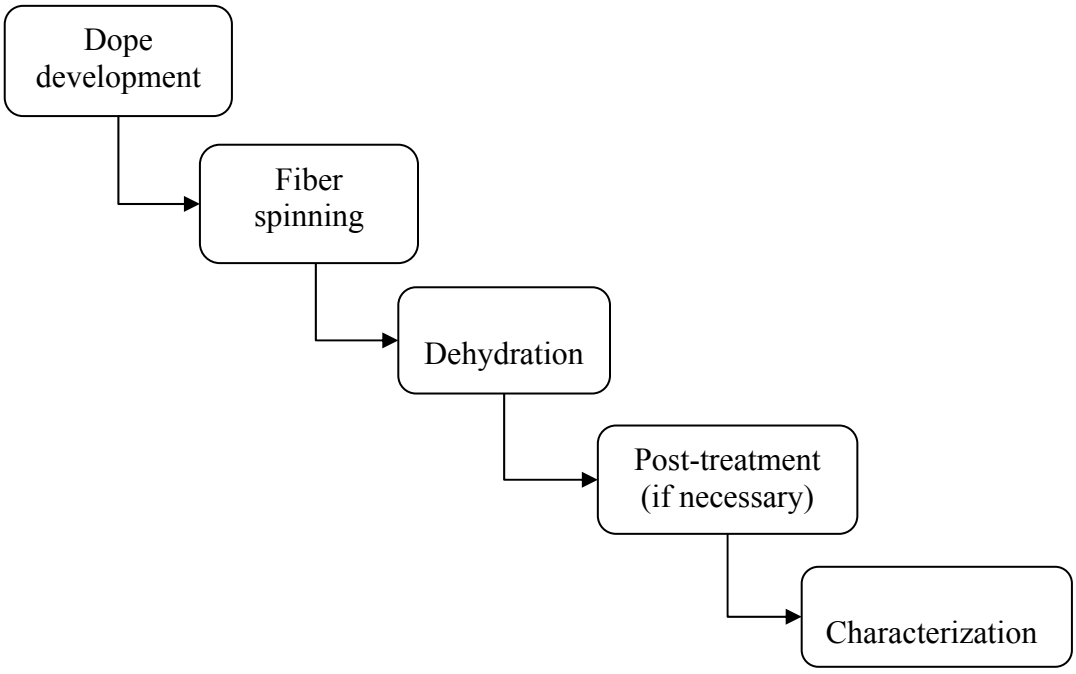

Figure 2.3: Flow diagram showing a typical hollow fiber spinning process [11].

2.3.2 Dope development

The dope for hollow fiber spinning usually consists of polymer, solvent, and non-solvent. The polymer acts as the membrane solid phase and determines the morphology and performance of hollow fibers. The solvent keeps the solution homogeneously in a single phase. The non-solvent in the dope can accelerate phase separation. Inorganic composites, such lithium nitrate, can also serve as non-solvent to tune the dope viscosity and thus improve spinnability. The details of formulating a spinnable dope will be discussed in Chapter 3.

2.3.3 Hollow fiber spinning

Asymmetric hollow fibers are spun through the hollow fiber spinning system, as shown in Figure 2.4.

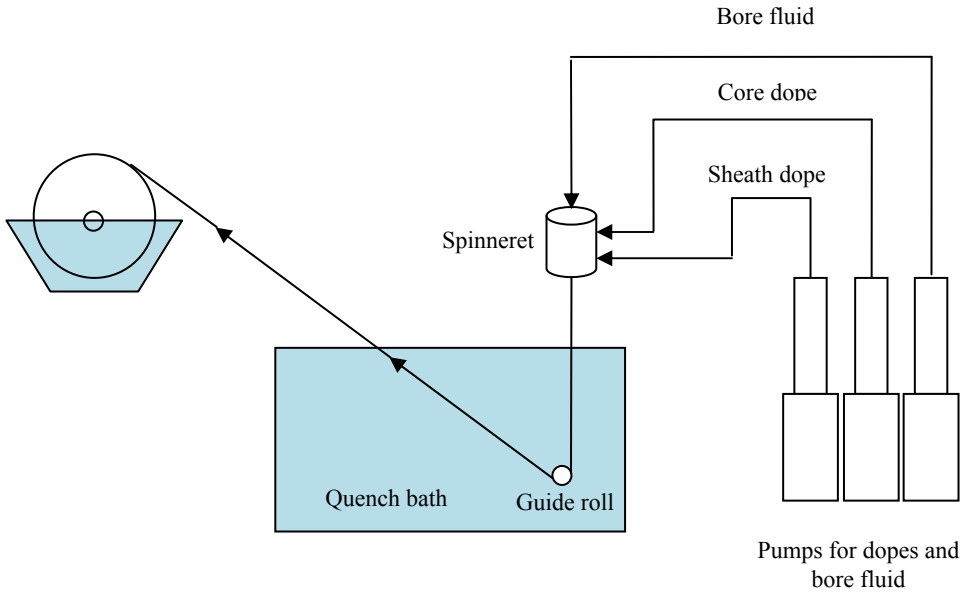

Figure 2.4: Flow diagram showing dry-jet and wet-quench spinning of asymmetric hollow fibers.

The bore fluid serves to prevent the collapse of nascent fibers. Another dope (sheath dope) can be used to form dual-layer hollow fibers. This advanced composite spinning technique is well discussed and studied in literatures [28-31] but it is not the topic of this thesis.

In any case, for the monolithic spinning with only one dope fluid, the dope is co-extruded with bore fluid through the spinneret. Before reaching the quench bath, the extruded nascent fibers are exposed in the air with controlled humidity, temperature and air gap. During this dry-jet period, the volatile component will evaporate from the dope and increase the polymer concentration in the outer layer of fibers. In addition, sufficient removal of volatile component can cause phase separation and influence the morphology of fibers, especially the skin layer thickness (discussed in Section 2.3.6). When the nascent fiber enters the aqueous quench bath, phase separation occurs rapidly, as the dope demixes into polymer rich and polymer lean phase. The solvent diffuses from fibers into quench bath while the non-solvent diffuses into the fiber. The fibers with solid and porous structure are formed during this phase separation. If the nascent skin composition reaches the vitrified region prior to immersion, it will not phase separate and a defect free skin layer is formed. After the dry-jet and wet-quench process, the hollow fibers are wound in a rotating drum. The take-up rate and the extrusion rate determine the draw ratio (ratio of take-up rate and extrusion rate), which can control the diameter of fibers and effluence the separation performance of fibers significantly.

2.3.4 Fiber dehydration

Solvent and non-solvent must be removed from hollow fibers without collapsing the fiber structure. The fibers from the quench bath contain water and must be dehydrated before being potted into modules. However, the wet fibers must not be dried directly because the capillary force in the fiber induced in dehydration will collapse the pores and

destroy the fibers. Therefore, solvent exchange must be done as the final spinning step. Generally, the first step uses alcohol (e.g. ethanol or methanol) to replace water in the fibers. Then the alcohol is washed out by a volatile non-solvent (e.g. hexane or heptane). This non-solvent can easily evaporate in the air. With this two-step solvent exchange, the fiber surface tension can be greatly reduced and therefore, the fibers can be dried under vacuum and heating without collapsing the fiber pores.

2.3.5 Post spinning treatment

After solvent exchange, the hollow fibers are ready to be potted into modules. However, post treatment or annealing the hollow fibers can significantly improve the gas separation performance [11, 32]. The objective of post treatment is to caulk the fiber outer surface with a highly permeable polymer layer, thereby repair the pinholes defects in the fibers. Two post treatment methods are often used for hollow fibers. The first one uses the high molecular weight polydimethylsiloxane (PDMS) solution in heptanes. The solution is heated so that the crosslinking of PDMS chains can caulk the defects in the fibers. The other post treatment method is called reactive post treatment. Two solutions are applied on the defective fibers: diethyltoluenediamine in iso-octane and trimesoyl chloride/PDMS mixture in iso-octane.

Annealing is commonly used in both dense films and hollow fibers. Annealing can effectively stabilize the hollow fibers against plasticization (discussed in 2.5.1) so that high separation performance is achieved in the presence of plasticizers, such CO_2 or H_2S. Annealing at a moderate temperature can initiate the crosslinking reaction of crosslinkable polymer and stabilize the fibers against aggressive feed (discussed in Section 2.6). Annealing at a high temperature is used to pyrolyze the polymer and obtain robust structure with stable separation performance. Post spinning treatment has an important role in performance optimization.

2.3.6 Skin layer formation

Clausi and Carruthers studied the skin layer formation in spinning as noted earlier and proposed that the vitrification of the skin layer occurs prior to phase separation, caused by the evaporation of solvent and non-solvent. Figure 2.5 shows the ternary phase diagram depicting the skin layer formation [25, 27].

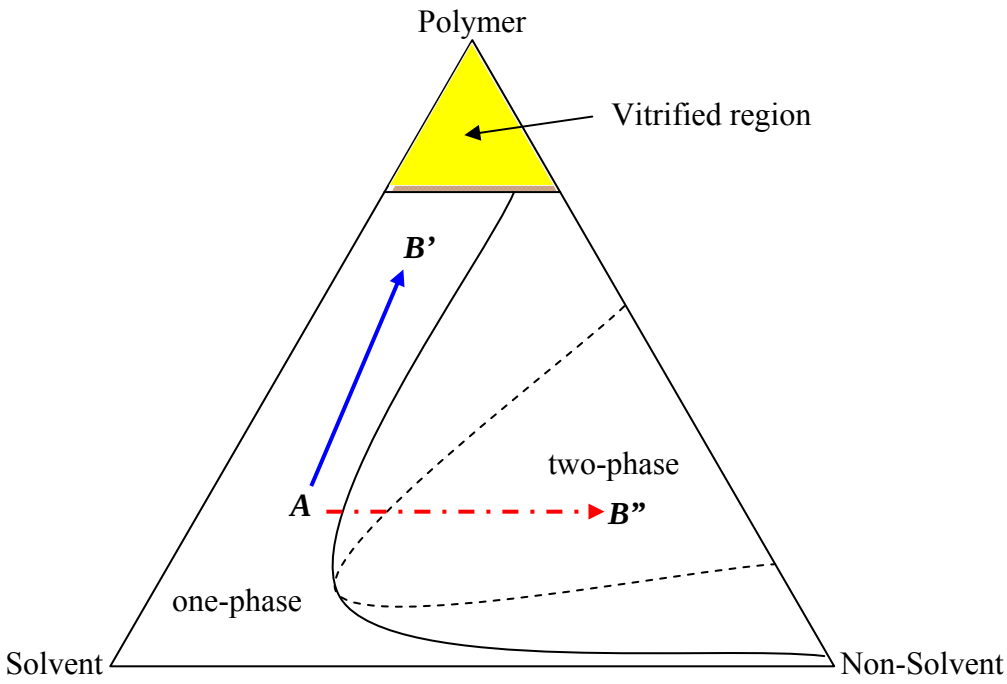

Figure 2.5: Ternary phase diagram showing the skin formation. The solid line represents the trajectory of the skin layer formation during the dry-jet step and the dashed line describes the trajectory of the substructure formation.

In Figure 2.4, point *A* represents the initial polymer concentration of the dope solution. The increase in polymer concentration on the outer surface of the fiber is represented by point *B'*, which can be caused by the evaporation of solvent and/or non-solvent, and moisture adsorption in the air gap. *B''* represents the lower local polymer concentration on the inside wall of the bore, resulting from the influx of solvent in the

bore fluid. The solid line describes the skin path leading to the formation of the outer layer of fibers, while the dashed line represents the path leading to formation of the open, porous substructure. A possible phase separation mechanism regarding the formation of defect-free skin layer is called nucleation and growth. In this case, the vitrification of nascent skin occurs while polymer lean domains are nucleated and grow in the substrate region to intersect and create a low substrate resistance unless the intersection and rupture of the polymer lean domains fails to occur, thereby causing close cell supports with high transport resistance. The formation of support structure is also thought sometimes to involve so-called, "spinodal decomposition", and this leads to desirable naturally bicontinuous polymer lean and polymer rich phases with low substrate resistance. The loss of solvent and non-solvent occurs in the region underneath the vitrified skin to create an interconnected open support with a minimum of substrate resistance [6].

2.4 Hollow fiber characterization

2.4.1 Scanning Electronic Microscopy(SEM)

To examine the ovality and concentricity of the fibers, microscopy with a magnificatioin of 10x or 20x is commonly used. However, to better observe the substructure of fibers, SEM is needed to provide higher magnification up to 40,000x. To prepare the sample for SEM test, the fibers are first soaked in hexane and then cryogenically fractured in liquid nitrogen to perserve their inner substructure. Since the fibers are non-conductive, the cross-section of fiber must be coated with a thin layer of gold in order to be revealed in the microscopy. Besides the ovality and concentricity mentioned above, SEM images can show the macrovoid, porous structure and even the thin skin layer of fibers. The exact skin layer thickness is often determined by gas permeation test (discussed in 2.4.2).

2.4.2 Gas Permeation

Gas permeation is used to study gas separation performance of hollow fibers. The fabrication process of a double-ended laboratory scale module is described in Appendix A. Once the fibers are potted into modules, there are mainly two different approaches to conduct the gas permeation. The most common one is feeding the gas through bores. Generally, pure gas permeation prefers bore-fed system. Under higher feed pressure, the feed is often introduced into the shell side. Shell-fed modules can overcome the concentration polarization in the feed when mixed gas feeding is used at a low stage cut. The stage cut equals the ratio of the permeate rate to feed flow rate, shown in Equation 2.10. Shell-fed system is generally preferred for mixed gas permeation when elevated feed pressure is required.

$$\text{stage cut} = \frac{\text{permeate molar flow rate}}{\text{feed molar flow rate}} \tag{2.10}$$

For pure gas permeation, the module is fed through the bores and there is no retentate flow. Noncondensable gases, like O_2, N_2, He, are often used to find the ideal selectivity of fibers. The substructure resistance must be taken into account in gas permeation and asymmetric hollow fibers must have substructure resistances less than one tenth of the skin resistance for the most permeable gas in order to avoid up to 10% loss of selectivity [33]. The N_2/He selectivity usually reveals potential substructure resistance information because the higher permeation rate of He is more easily inhibited by small substructure resistance as opposed to the case for less permeable gas such as N_2 and O_2. If the fibers have almost intrinsic O_2/N_2 selectivity but the N_2/He selectivity is below the intrinsic value, there is likely a certain amount of substructure resistance.

Even though the fiber shows intrinsic selectivity for both O_2/N_2 and N_2/He in pure gas permeation, mixed gas permeation with CO_2/CH_4 is still necessary to study the gas

separation performance under practical feed conditions for natural gas in order to study plasticization and competition effects. In mixed gas permeation, as discussed above, the feed is in the shell side and the retentate flow must be controlled to avoid concentration polarization in the feed. The retentate flow must meet a stage cut of less than 1%. As noted earlier, the stage is defined as Equation 2.10. The detailed mixed gas permeation is described in Appendix B.

2.5. Effect of feed composition and pressure on CO_2/CH_4 separation

2.5.1 CO_2 plasticization in hollow fibers

The penetrants can interact with glassy polymers when the feed is aggressive. The plasticization effect is often observed when a large partial pressure of CO_2 is fed at high pressure. Plasticization is apparent when the permeability is increased in the presence of aggressive gases. In this process, the penetrant-polymer interaction increases the segmental mobility of polymer chains and causes increased diffusion coefficients of penetrants, thereby increasing the permeability. In a microscopic respect, the plasticization occurs when a decrease of the glass transition temperature and a softening of the materials are observed. The effects of plasticization are illustrated in Figure 2.6 [34].

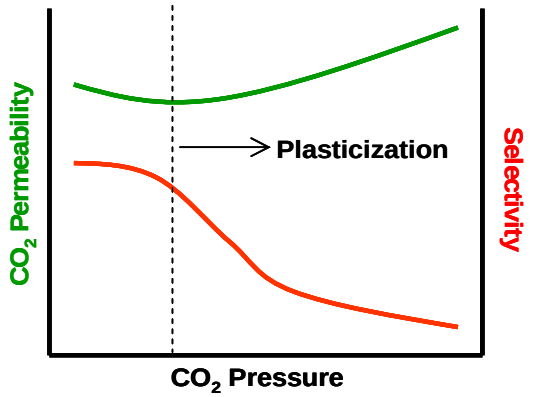

Figure 2.6: CO_2 permeability isotherm and selectivity at different CO_2 pressure, the dashed line represents the CO_2 plasticization pressure [12].

The plasticization pressure is defined as the pressure when the permeability starts to increase with the increasing penetrant pressure, as shown in dashed line in Figure 2.6. After the plasticization pressure is reached, the permselectivity decreases with pressure. The loss of permselectivity is due to the relatively greater increase of permeability for slow gas molecules (e.g. CH_4) than CO_2. To develop a commercial membrane with sufficient separation performance, the plasticization must be controlled and limited to a level at which a high permeability and selectivity can be both maintained.

2.5.2 Competition effects in gas mixtures

Besides the CO_2 induced plasticization effect on glassy polymer membranes, the competitive effects of penetrants must also be taken into account to study the mixed gas separation properties. According to the dual mode sorption model, the permeabilities of penetrants are decreased due to the competition effects between penetrants on Langmuir sorption sites [21].

$$\frac{C_A}{P_A} = S_A = k_{Di} + \frac{C'_{Hi} b_i}{1 + b_A p_A + b_B p_B} \tag{2.11}$$

For instance, in CO_2/CH_4 gas mixtures, as CO_2 is the more condensable penetrant, CO_2 can exclude CH_4 and dominate the sorption process. As a result, CO_2 molecules "slow down" the permeation of CH_4 as it permeates through the membrane. Since the competition effect does not happen in pure gas measurements, the CO_2/CH_4 selectivity in mixed gases is relatively higher than pure gas measurements in the absence of plasticization [14]. Hillock showed that the CO_2/CH_4 selectivity in gas mixtures is higher than the pure gas selectivity while the CO_2 permeability is equal in the two cases in the dense film study [13]. However, there exists subtle balance between competition sorption and plasticization. Visser studied the competition sorption and plasticization effects in hollow fibers and pointed out that plasticization effects could be completely counterbalanced by competitive sorption once the inert gas composition reached a certain level [35].

2.5.3 Bulk flow effect

According to Fick's first law, the total permeation flux of a penetrant through a glassy polymer membrane with respect to a fixed frame of reference is equal to the sum of the bulk flux and diffusive flux, shown in Equation 2.12~2.14 [14, 36-37].

$$n_A = n_A^{bulk} + n_A^{diffusion} \tag{2.12}$$

$$n_A^{bulk} = (n_A + n_B + n_P)\omega_A \tag{2.13}$$

$$n_A^{diffusion} = -\rho D_{Am} \frac{d\omega_A}{dx} \tag{2.14}$$

The polymer flux, n_p is equal to zero since the membrane is stationary, ρ is the unswollen polymer density, and ω_A is the mass fraction of permeant A in the membrane. The membrane permeability can be derived using Equation 2.12~14.

When studying the transport of permeants through polymer membranes, the bulk flux contribution is usually assumed to be negligible when the sorption levels of the permeants are low (ω_i<0.05). However, if the permeation flux of one permeant is much higher than the others in a gas mixture, the bulk flux cannot be neglected. Ebra-Lima and Paul researched the effect of bulk flux on the permeant transport properties in a highly swollen membrane [36]. In mixed gas permeation, the bulk flux of the slower permeating component (e.g. CH_4) is a function of the sorption level of the permeant and the flux of the faster gas (e.g. CO_2). Kamaruddin and Koros modeled the diffusion-based permeability of each permeant in a binary mixture by considering the bulk flow contribution to the transport [37]. They studied the CO_2/CH_4 mixture using 6FDA-TADPO polypyrrolones membranes and showed that if the bulk flow contribution to the flux of each component is neglected, the CO_2/CH_4 selectivity can be overestimated over the experimental observed membrane selectivity [38].

2.5.4 Non-ideal gas phase thermodynamics

As discussed in 2.1.2, the partial pressure difference through the membrane is usually used as the driving force to calculate the permeance of each permeant, shown in Equation (2.4). However, the true driving force is the penetrant fugacity difference, which is approximately equal to partial pressure difference only at low feed pressure. At high feed pressure, the permeant permeance can be overestimated by using the partial pressure difference instead of penetrant fugacity difference because the permeants are not ideal any more. The non-ideal behavior of gas feed can significantly affect the separation performance and must be taken into account to analyze the permeance and permselecitivty.

The fugacity coefficients for a multicomponent mixture can be estimated by the commercial process simulator Aspen. Commonly used equations to calculate the fugacity

coefficients include Peng-Robinson, Virial Equation of State, Soave-Redlich-Kong Equation [39-40].

2.6 Strategy for stabilizing hollow fibers

2.6.1 Covalent crosslinking

Covalent crosslinking has been investigated by former researchers [11-14, 41-54] and shown to stabilize polymer membranes against CO_2 induced plasticization by suppressing the degree of swelling and segmental chain mobility in the polymer. Wind studied the effect of copolymer composition, crosslinking agent and thermal treatment on crosslinking and found that the covalent crosslinking could suppress the CO_2 plasticization in dense film. Hillock applied zeolites in the propane diol monoesterified crosslinkable (PDMC) polymer and showed that the mixed matrix membrane had the potential to separate CO_2 from CH_4 more effectively than the traditional pure polymer membrane, while also providing stability of membranes against the CO_2 plasticization. Wallace focused on the development of asymmetric hollow fibers from PDMC material and found crosslinking at moderate temperature stabilized the membrane against both liquid solvent exposure and high CO_2 feed pressure. Omole developed high molecular weight PDMC polymer and investigated the PDMC fibers at aggressive feeding. The PDMC fibers exhibited good CO_2 induced plasticization resistance and decent selectivity at high CO_2 partial pressure or toluene contaminant feed [54].

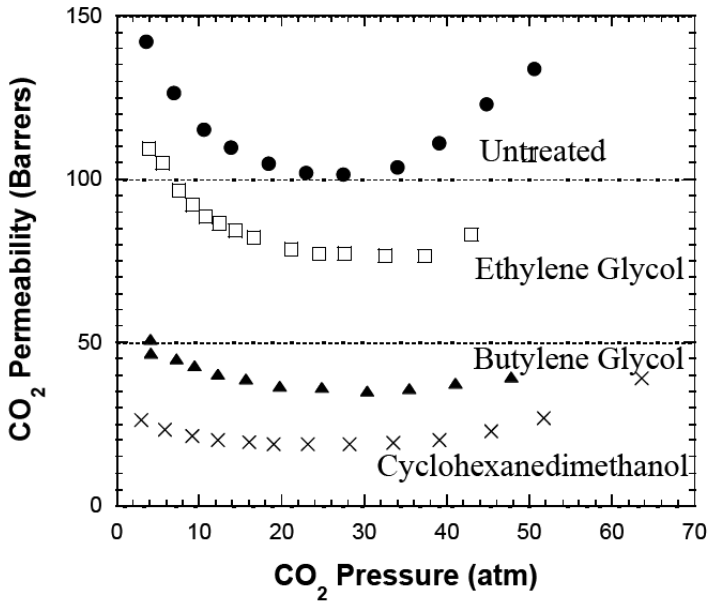

Figure 2.7: CO_2 permeation isotherms for 6FDA-DAM: DABA (2:1) membranes crosslinked with ethylene glycol, butylene glycol, and 1, 4-cyclohexanedimethanol [14, 47].

2.6.2 Antiplasticization

Antiplasticization refers to the phenomenon by which some low molecular weight additives retard the segmental motions of polymer chains, leading to increase in modulus and strength, losses in elongation at break and impact resistance. The lower molecular weight additives are called plasticizers when present above a critical level; however, below this level, they acts as antiplasticatizers. Antiplasticization response is often accompanied with a decrease in permeability of permeants and may also lead to an increase or a decrease in the permselectivity for a multicomponent mixture. Nevertheless, adding plasticizers in the polymer have potential when an increase permselectivity is required at the expense of productivity. Extensive studies have shown that most low molecular weight compounds miscible with polymer will produce antiplasticiztion to some degree at low concentrations. Maeda and Paul studied the antiplasticization phenomenon with low molecular weight aromatic compounds at low concentrations and

found the permselectivity of CO2/CH4 behaves quite differently depending on the concentration of additives, as shown in Figure 2.8.

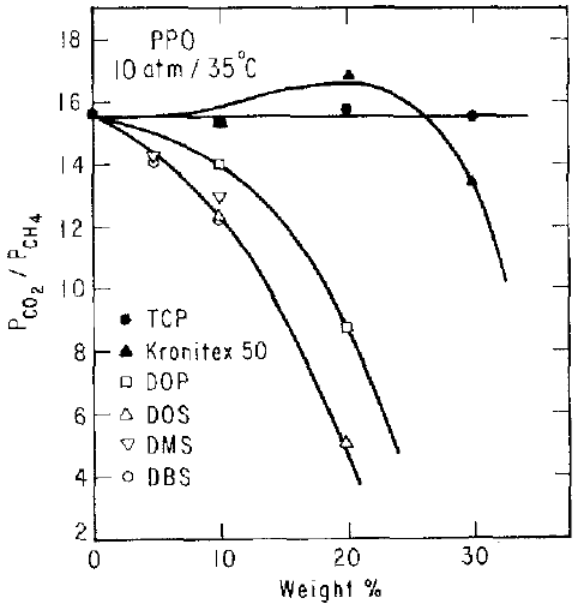

Figure 2.8: Permselectivty for CO_2/CH_4 using different additives and concentration in poly (phenylene oxide) [55-57].

CHAPTER 3

MATERIALS AND EXPERIMENTAL METHODS

3.1 Materials

3.1.1 Polymer synthesis

The material used in this study is mainly provided by Chevron Energy Technology Company, which is a polyimide copolymer. Besides the supply from Chevron, the mononesterification of 6FDA-DAM: DABA to form the desired polymer was done in the laboratory by the author on the non-esterified samples not provided by Chevron. This copolymer is chosen based on its excellent CO_2/CH_4 separation performance and decent CO_2 induced plasticization resistance, which has been well investigated by former researchers [11-13, 48-54]. The polymer is synthesized from 4, 4'-(hexafluoroisopropylidene) diphthalic anhydride (6FDA), 2, 4, 6-trimethyl-1, 3-diaminobenzene (DAM) and 3, 5-diaminobenzoic acid (DABA) and called 6FDA-DAM: DABA. The DAM: DABA diamine ratio is 3: 2 in this work. The details of synthesis can be found in reference [11-12]. The acid pendant group of DABA units in backbone of the copolymer is additionally monoesterified with 1, 3-propanediol and produce ester bonds, which have the potential to form crosslinked structure and stabilize the polymer against plasticization. This monoesterification reaction will be discussed in 3.1.2. The structures of monomers and 6FDA-DAM: DABA are shown in Figure 3.1.

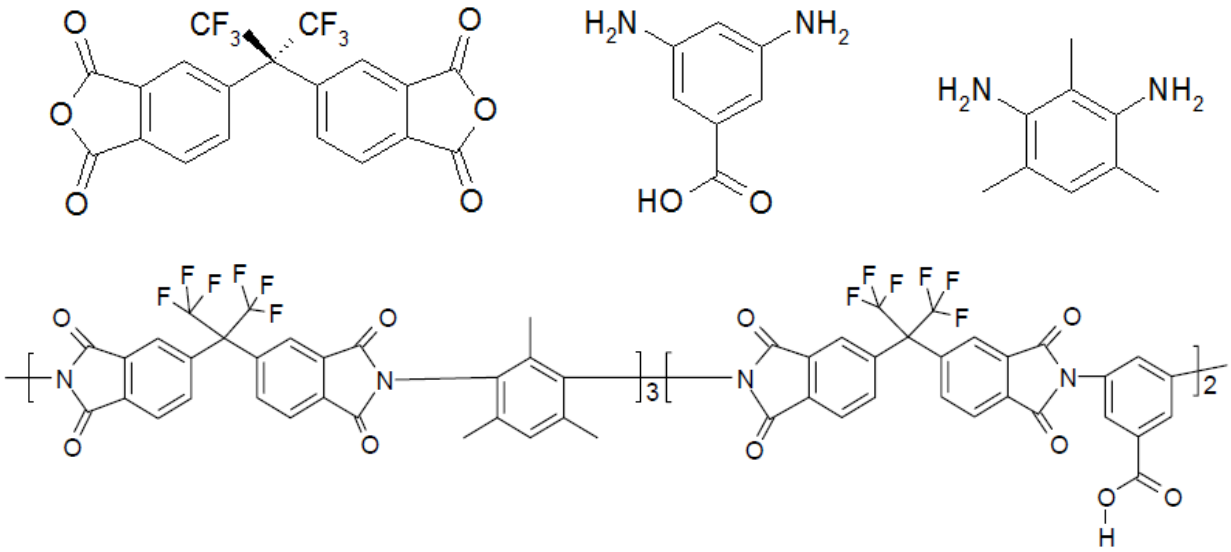

Figure 3.1: Chemical structures of monomers (top) and 6FDA-DAM: DABA (bottom) polymer used in this work.

3.1.2 Monoesterification

Different polyalcohols (e.g. ethylene glycol, butylenes glycol) have been studied to react with the acid group (-COOH) in DABA units of 6FDA-DAM: DABA polymer to form covalent bonds [14]. Among those polyalcohols, 1, 3-propane diol is advantageous in terms of permeability and CO_2 plasticization resistance. The reaction mechanism of acid groups in DABA units with diols, such as 1, 3-propanediol, called monoesterification, is demonstrated in Figure 3.2.

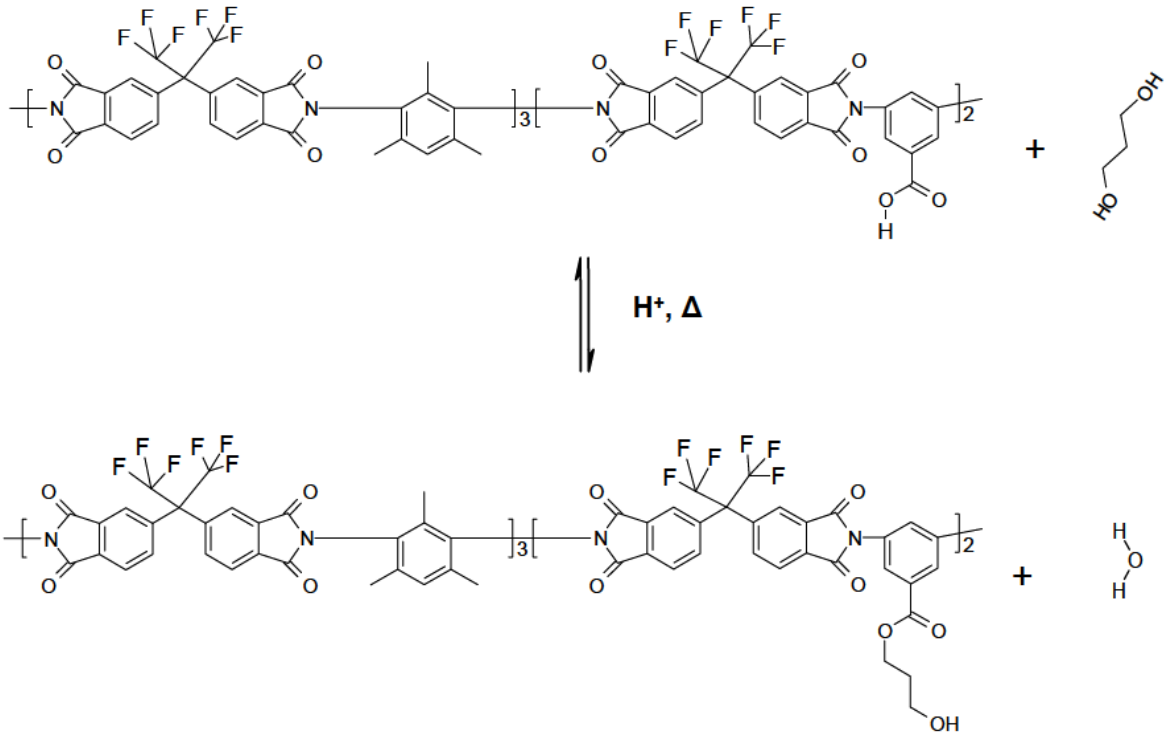

Figure 3.2: Monoesterification reaction for synthesizing 1, 3-propanediol monoesterified crosslinkable (PDMC) polyimide (3:2).

The polymer produced after monoesterification is called PDMC, which stands for propane-diol monoesterified crosslinkable polymer. PDMC polymer has –OH groups in the DABA units and can be dissolved in solvents, like NMP or THF. This monoesterification process is described in more details in appendix C.

3.1.3 Polymer characterization

3.1.3.1 Gel permeation chromatography

Gel permeation chromatography (GPC) is the most widely used technique for polymer analysis in order to determine their molecular weights and polydispersity index (PDI). This technique uses monodisperse polymer standards (e.g. solutions of monodispersed polystyrene in THF) to plot the logarithm of the molecular weight versus the retention volumes (or times). With this calibration curve, the gel permeation chromatogram of unknown polymer samples in the same solvent can be obtained and the molecular weights and the PDI can be calculated.

3.1.3.2 Nuclear magnetic resonance spectroscopy (NMR)

Solution ^{1}H NMR experiment can quantify the reaction conversion of monoesterification. The methylene proton closest to the ester bond shows a peak at 4.2ppm in the spectra, shown in Figure 3.3, and the peak does not overlap with any others either from the polymer or solvent (dimethyl sulfoxide, DMSO). The conversion of monoesterification is determined by the ratio of methlyene proton peak area to the aromatic protons in the DAM monomer, compared to the theoretical ratios at complete conversion from the copolymer composition. More details on this technique can be found in reference [14].

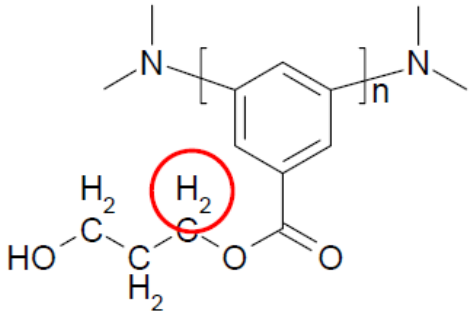

Figure 3.3: Monoesterified DABA moiety showing the proton used for the solution ^{1}H NMR determination of degree of monoesterification.

3.2 Dense film study

3.2.1 Dense film membrane preparation

Solution casting is used to prepare dense film membrane sample in this work. The polymer is first dissolved in solvent with a polymer concentration at 5~20%. Preferred solvents are moderate volatile, such as THF. Strong solvents, like NMP, are not usually suitable due to their low volatility. A uniform dense film is spread across a flat plate (e.g. glass plate) by using a casting knife as shown in Figure 3.4. The cast knife controls the gap between the blade and the substrate, thereby determining the thickness of dense films. After casting, the solution is placed in the environment of solvent and the evaporation of solvent in the polymer solution leaves a thin and uniform dense film. The dense film is dried in vacuum with heating to remove solvent residence in the film prior to the gas permeation (will be discussed in 3.2.2).

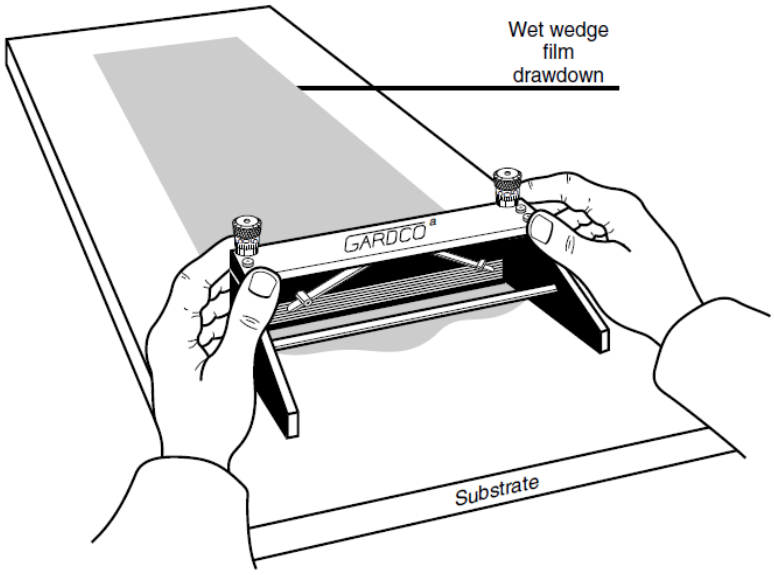

Figure 3.4: A schematic showing the dense film solution cast with a casting knife [10].

3.2.2 Dense film permeation

The dense film gas permeation is carried out in a gas permeation system within a dense film cell. The details to mask the dense film into permeation cells are described in reference [58]. A schematic depicting the dense film permeation system is shown in Figure 3.5.

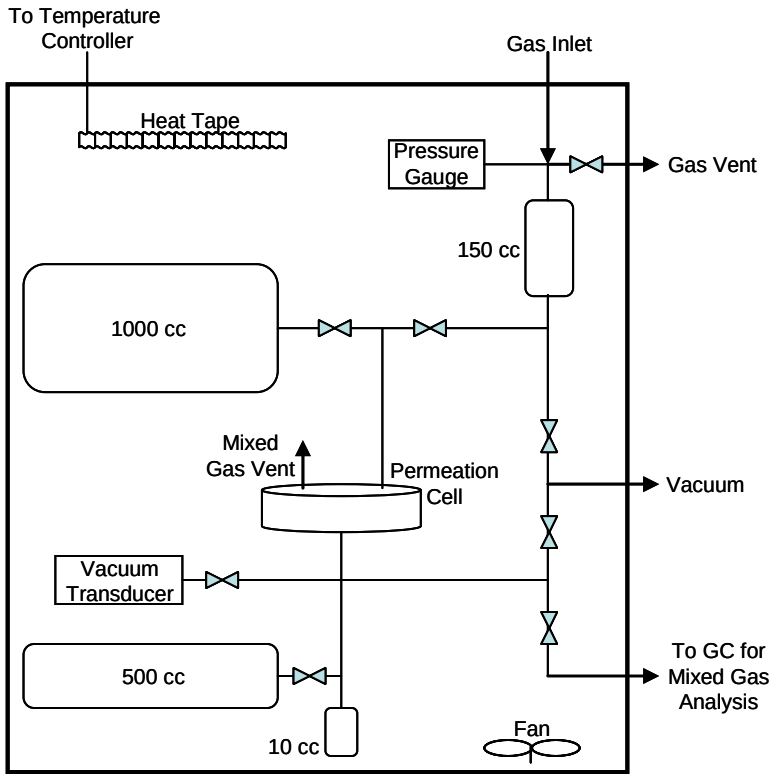

Figure 3.5: Constant-volume, variable-pressure gas permeation system for dense film permeation [59].

The permeability of a dense film membrane is calculated by monitoring the change of downstream pressure with time, as shown in Equation 3.1 [12].

$$P = \frac{1.1583\times10^{3}\cdot(\frac{dp}{dt})\cdot l\cdot V_R}{A\cdot T\cdot\Delta p} \tag{3.1}$$

In Equation 3.1, *dp/dt* is the slope of the downstream pressure vs. time in torr/min; l is the membrane thickness in microns; V_R is the downstream reservoir volume in cm^3; A is the dense film area in cm^2; T is the operation temperature in Kelvin; the driving force is the fugacity difference across the membrane, which is approximately equal to partial pressure difference Δp at low feed pressure. The unit of permeability is Barrer, as discussed in 2.1.2.

3.3 Hollow fiber preparation

3.3.1 Dope formulation

The first step for hollow fiber spinning is to form a spinnable dope. The dope formulation is critical for hollow fiber morphology and separation performance because the thermodynamics interaction of dope (or nascent fiber) with air or quench medium significantly affects the formation of skin layer and porous structure.

The spinning dope consists of polymer, solvent and non-solvent [60-61]. Polymer is the framework of the hollow fibers and therefore, the polymer concentration in the dope must allow fibers sufficient mechanical strength and decent separation performance. Increasing the polymer concentration will cause an increase of viscosity and thereby reduce the spinnability. A good choice for the polymer concentration is often in the range between 25~35%.

The solvent dissolves the polymer to form a homogeneous single phase polymer solution. Depending on the properties of polymer and experimental conditions, higher boiling point solvents, such as NMP (N-methyl-2-pyrrolidone), dimethylformamide (DMF), dimethyl sulfoxide (DMSO), are often used due to their polymer solubility and miscibility with water or ethanol. NMP is preferred in this work as it has low volatility, low toxicity and high boiling point (~204°C). On the other hand, THF is also added in the dope to promote the skin layer formation during phase separation. The volatility of THF can produce a polymer rich phase in the outer layer of nascent fibers in the air gap and therefore, accelerate the formation of skin layer in hollow fibers [25, 27].

Solvent and non-solvent mixtures are used to keep the dope in a single stable phase so that the dope composition is near enough to the binodal and phase separation occurs rapidly. Health and safety issues must be taken into account. Apparently, water is

a good choice of the non-solvent as most polymers are hydrophobic. However, only a small amount of water needed in the dope for phase separation, which causes a rather narrow window of stable ternary phase solution [11]. On the other hand, alcohols provide more flexibility for the dope composition than water. The volatility of alcohols also affects the skin layer formation [27]. Ethanol is often preferred as the non-solvent due to the good volatility and low toxicity. Besides ethanol, lithium nitrate can be added as the non-solvent since it can modify the dope viscosity and accelerate phase separation due to its ability to form a complex with solvents discussed above.

With the chosen polymer, solvent and non-solvent, a ternary phase diagram must be constructed to make a spinnable dope. The ternary phase diagram shows both the single phase, two-phase region and the binodal curve, as discussed in 2.2.2. Due to the complex solution properties, the most common and effective method to determine the binodal is through experiments, called the cloud point technique [11-12]. In this technique, the concentration of components in the dope is varied and the solution is visually determined if it is one-phase or two-phase. The binodal is located between the one-phase and two-phase regions.

Once the ternary phase diagram is accomplished, the dope composition is chosen near the binodal. The binodal also indicates the composition of bore fluid. In a polymer/solvent/water system, this composition is usually determined by extrapolating towards the solvent/water axis a line tangent to the binodal at the polymer concentration of the dope, shown in Figure 3.6.

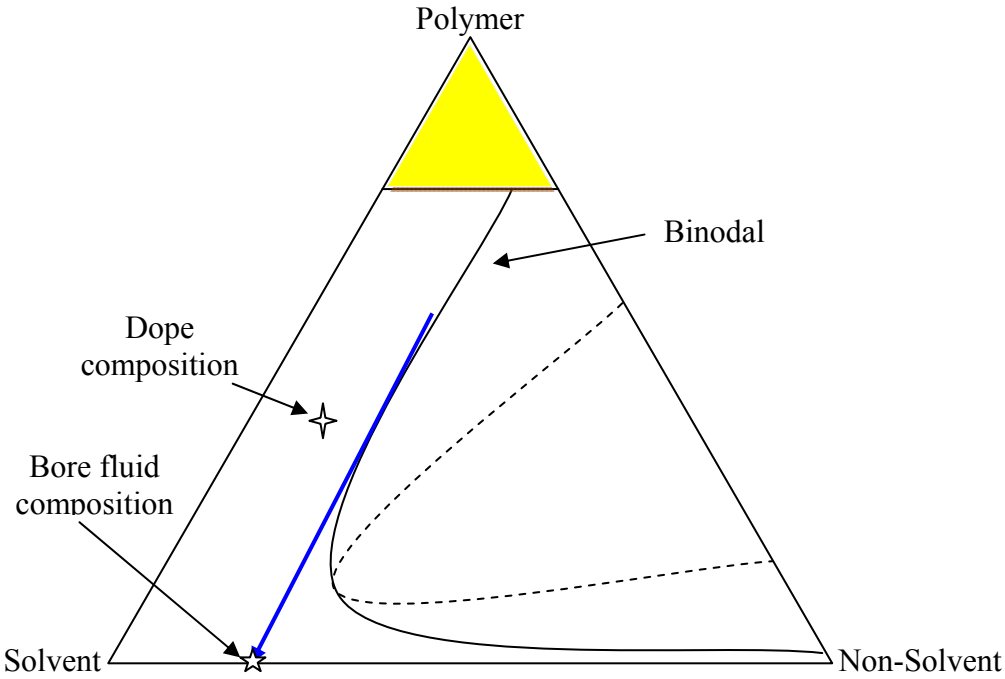

Figure 3.6: Ternary phase diagram showing the determination of the bore fluid composition [11-12].

The initial dope composition is often determined by intuition and prior experience and somehow depends upon the properties of solvent and non-solvent. Macroscopically, the dope must be a single phase and have a viscosity similar to thick honey (about 10,000 cP) [11]. It also must have sufficient volatile solvent/non-solvent for skin layer formation. To modify the dope composition, a common approach is by tuning the ratios of components in the dope, for instance, keeping the ratio of polymer to solvent same and reducing the composition of polymer. Another method is adding inorganic salt in the dope, such as lithium nitrate, which can control the viscosity and reduce the phase separation time. The complex nature and multiple requirements that must be met require that the spinning includes a great deal of trial and error in dope formulation.

3.3.2 Hollow fiber spinning

Once the dope formulation and characterization (e.g. viscosity test) are accomplished, the hollow fiber spinning process is ready to be done. To spin hollow fibers with desired separation performance successfully, the following parameters must be considered: spinneret type, extrusion rate, draw ratio, air gap and quench bath.

3.3.2.1 Spinneret

Spinnerets have different dimensions depending upon the requirement of the specific fiber formation goals. Generally, a spinneret with a smaller dimension produces smaller fibers, which can withstand high feed pressure. For instance, 200 μm outer diameter fibers can withstand high pressure up to 1000 psia in the gas permeation in some cases [10]. The spinneret dimension also significantly affects the CO_2/CH_4 separation performance [12]. The other important factor regarding the spinneret is the temperature, which is crucial for hollow fiber formation as it affects kinetics and evaporation in the air gap to form the nascent skin. For example, the "pulsing" problem of fibers can be resolved by lowering the spinneret temperature because the viscosity of dope is increased at lower temperature and this often damps such instabilities. On the other hand, a high spinneret temperature can reduce the viscosity of dope and improve the spinnability of viscous dope. Nevertheless, the spinneret temperature must be below the crosslinking temperature of PDMC polymer. Usually, an appropriate spinneret temperature is between room temperature and 80^{o}C.

3.3.2.2 Extrusion rate and draw ratio

The ratio of take-up rate to extrusion rate defines the practical draw ratio. Both the extrusion and take-up rate can affect the fiber diameter. A faster extrusion rate tends to produce larger outer diameter fibers. At the same extrusion rate, the draw ratio is increased with the take-up rate and eventually the radial dimension of fibers is reduced. It

has to be noted that a high draw ratio may introduce elongational forces at the outer layer of nascent fibers. This stress may orientate the segmental chains in polymer and cause a higher permselectivity; however, if excessive, defects and even fiber breaks can occur [12, 62-63].

3.3.2.3 Air gap

The air gap primarily determines the time that the nascent fibers exposed in the air during spinning [25]. A higher air gap means a longer residence time of nascent fibers in the air and may promote the formation of a thick skin layer; however, the air gap height is limited by many factors, such as the elasticity of dope and draw ratio. The spinning line can be broken easily at a high air gap as the gravity and elongational stress overcome the strength of the nascent fibers. At the same air gap, a higher draw ratio produces a stronger tension stress in the fiber, which tends to break the fibers. Therefore, the air gap must be controlled carefully so that a stable and smooth spinning line can be established.

3.3.2.4 Quench bath

Three common parameters are considered in the quench bath: the quench medium, the depth and the temperature. The quench medium affects the phase inversion to form the skin layer. As an environmental friendly medium, water is commonly used as the quench batch medium since most polymers are hydrophobic. Nevertheless, other solvents can be added to the water depending on the requirement of membrane formation. The quench bath depth is also critical in the formation of hollow fibers, as it determines the residence time of fibers in the quench medium. A deeper quench bath may help the formation of skin layer and porous structure of hollow fibers as the nascent fibers have a longer residence time in the quench bath. The quench temperature affects significantly the diffusion of solvent and non-solvent during fiber coagulation process. An elevated temperature can promote the transport of components in the nascent fibers and is

preferred in this work, since the crosslinkable polymer is more hydrophilic than other polymers and requires a longer phase separation time. The quench bath medium, the height and the temperature must be controlled carefully to allow complete phase separation so that the nascent fibers are not squeezed by the guide roll to form oval structures.

3.4 Hollow fiber characterization

3.4.1 Microscopy

As discussed in Chapter 2, the microscopy or SEM images can provide details of the cross-section of hollow fibers, including the ovality, concentricity, substructure of fibers and so on. For instance, due to the slow phase separation, the nascent fibers are not completely solidified before reaching the guide roll and can partially collapse; therefore oval fibers are formed, shown in Figure 3.7.

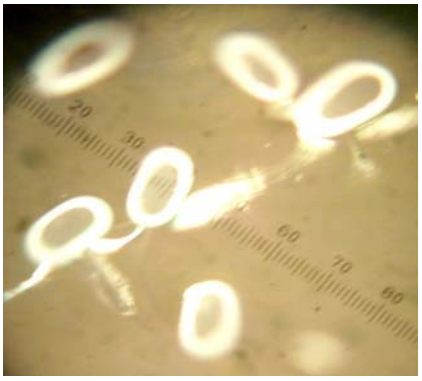

Figure 3.7: Microscopy depicting the oval hollow fibers [11].

Nonconcentric fibers may also be produced in spinning, as shown in Figure 3.8. For such fibers, the wall thickness is not uniform, and at some point, the wall is quite thin and vulnerable, making the fibers unable to withstand high feed pressure. The non-concentricity of fibers is primarily caused by the non-concentric spinneret needle,

therefore the needle in the spinneret must be carefully adjusted to the center of the spinneret to form uniform fiber structure.

Figure 3.8: SEM image showing the non-concentric hollow fibers.

3.4.2 Pure gas permeation

Pure gas permeation is conducted in a dead end, counter-current flow module with the feed in the bore side of the hollow fibers. The feed gas permeates across the hollow fibers and the permeate flow rate is tested by a bubble meter or digital flow meter in the shell side. Multiple modules can be connected by using the bore feed to allow a higher experimental efficiency if the same test conditions are used, as shown in Figure 3.9.

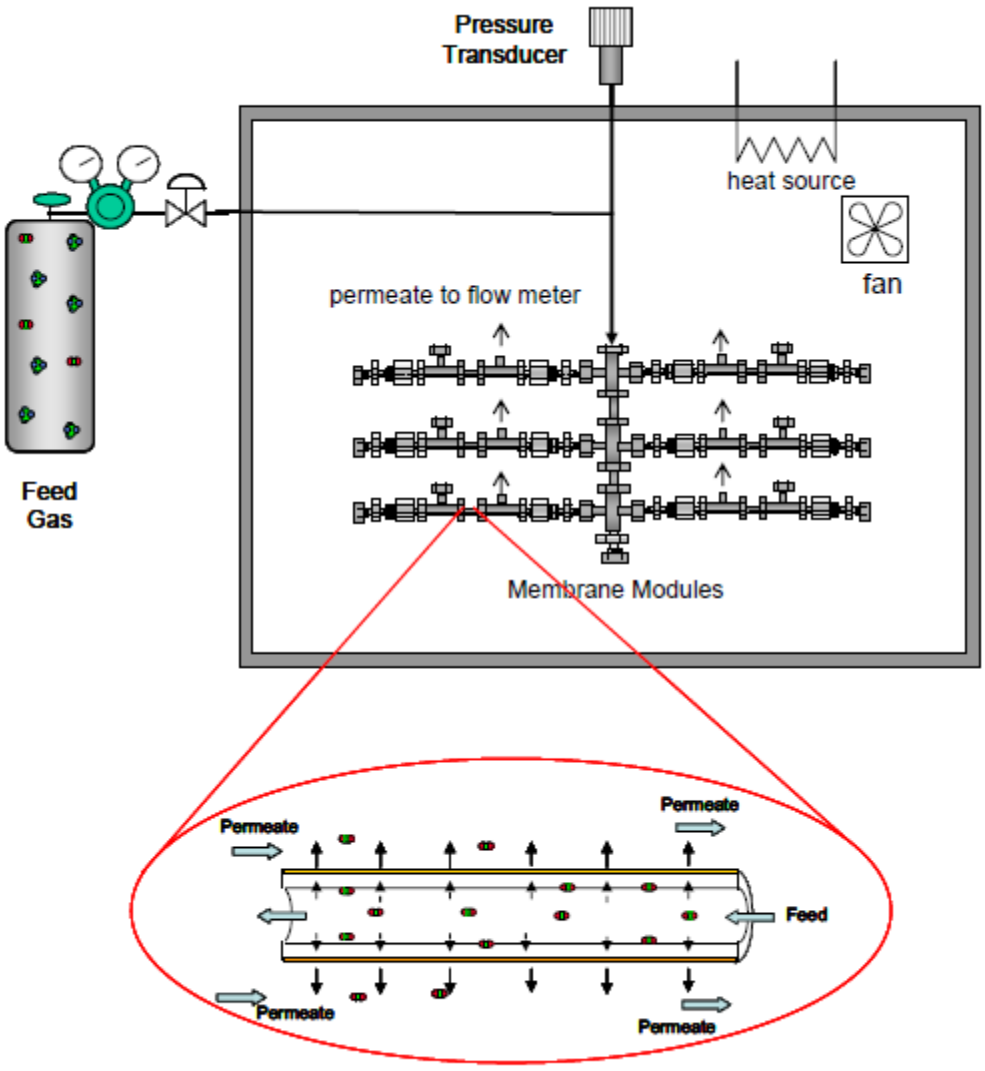

Figure 3.9: Schematic depicting the pure gas permeation system with bore feed and permeate stream at atmosphere [12].

The permeance *P/l* in GPU for each module is calculated by its individual permeation volumetric flow rate *Vp* in ml/s; the test temperature *T* in *Kelvin*; membrane area *A* in cm^2; the transmembrane pressure or fugacity difference (Δp or Δf) in psia, as shown in Equation 3.2 [11-12].

$$\frac{P}{l} = 10^{-6} \cdot \frac{Vp \cdot 273.15}{5.17 \cdot A \cdot T \cdot \Delta p} \tag{3.2}$$

3.4.3 Mixed gas permeation

Unlike pure gas permeation, the mixed gas permeation experiment is carried out with feed in the shell side to allow a higher feed pressure [11-12, 32]. The permeate flow rate is often measured by a bubble flow meter. In this experiment, the retentate flow rate is controlled by a valve so that the ratio of permeate to retentate flow rate (called stage cut) is below 1%. This low stage cut can eliminate concentration polarization in the feed. The gas composition of permeate and retentate flow is analyzed by the gas chromatography (GC). The permeance in GPU of each component in the gas mixture through the hollow fibers is calculated by the following parameters: volumetric flow rate of permeate (*Vp*) in ml/s; mole fraction of component *i* in permeate (y_i); mole fraction of component *i* in the upstream (x_i); the operating temperature *T* in Kelvin; membrane area (*A*) in cm_2; feed pressure (p_x) in psia; and permeate pressures (p_y) in psia; fugacity coefficients of component *i* in the upstream and permeate streams, (ϕ_{xi}) and (ϕ_{yi}) respectively, as shown in Equation 3.3.

$$\frac{P}{l} = 10^{-6} \cdot \frac{Vp \cdot y_i \cdot 273.15}{5.17 \cdot A \cdot T \cdot (p_x \cdot \phi_{xi} \cdot x_i - p_y \cdot \phi_{yi} \cdot y_i)} \tag{3.3}$$

3.4. 4 Post-treatment

In practical spinning, some hollow fibers may exhibit selectivities much lower than intrinsic values due to small pinholes, leading to Knudsen transport; therefore such fibers are defective. The defects may be cured by a post treatment. There are mainly two approaches for the post-treat: PDMS and reactive post-treatment. The details of post-treatment can be found in reference [11, 32]. Some fibers can be completely cured with an intrinsic selectivity, indicating that the fibers are not badly defective before post-treatment. In other cases, the selectivity cannot be improved after post-treatment, which means that the defects in fibers are too large to be caulked. On the other hand, although post treatment is undesirable in the practical application due to potential failure in swelling feed, it can reveal some insights regarding intrinsic transport properties in preliminary studies. For instance, the pure gas permeation after post treatment may help to determine the transport resistance either from the skin layer or porous substructure.

3.5 Hollow fiber crosslinking

3.5.1 Thermal crosslinking

There are different approaches to stabilize the hollow fiber membrane, mainly including polymer blending and annealing [64-67]. Recent work demonstrates that crosslinking the polyimide membrane can increase the pressure that plasticization occurs, thereby stabilizing the membrane under aggressive CO_2 feed [11-14]. The most common studied crosslinking strategy is annealing the hollow fibers under vacuum for a set period of time, called thermal crosslinking. The process is straightforward; the fibers are directly placed in a preheated vacuum oven and sit for several hours. The key parameters for thermal crosslinking include the crosslinking temperature and crosslinking time. The reaction mechanism of covalent crosslinking is shown in Figure 3.10.

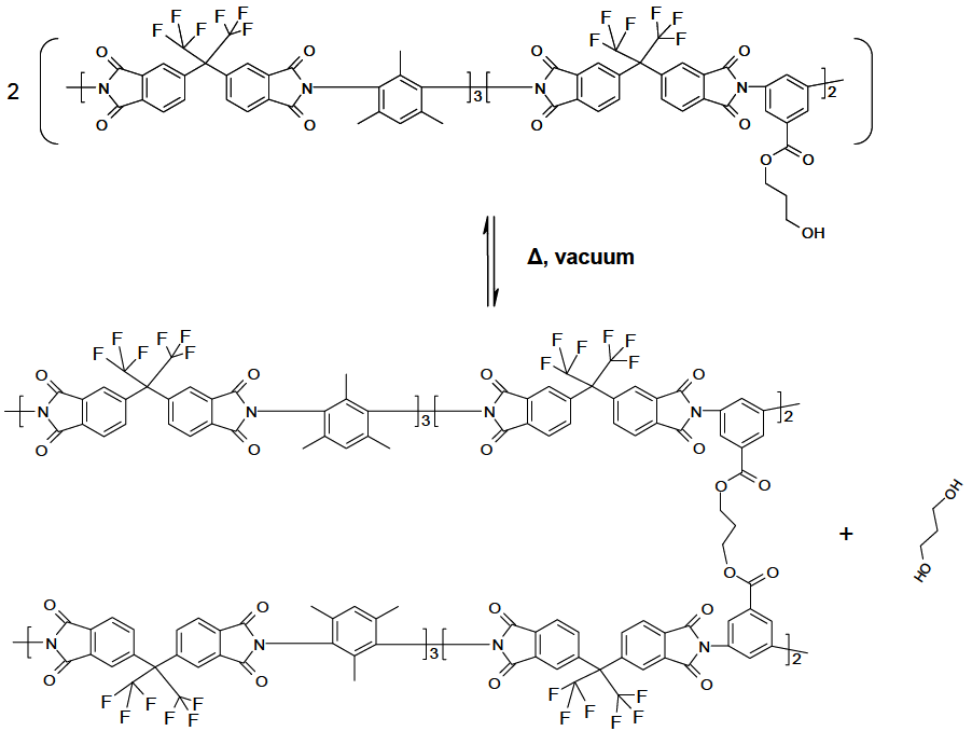

Figure 3.10: Schematic showing the thermal crosslinking of PDMC (3:2).

Dynamic vacuum creates a driving force for the crosslinking reaction as the by-product, 1, 3-propane diol, is removed in this process. Although the thermal crosslinking can suppress the CO_2 induced plasticization to some degree and achieve high CO_2/CH_4 selectivity under rigid feed streams, the CO_2 permeance must not be compromised. A high crosslinking temperature tends to cause a significant drop of permeance while a low temperature may be insufficient to crosslink the fibers. Therefore, the crosslinking conditions must be examined carefully to obtain both enough plasticization resistance and high CO_2 permeance.

3.5.2 Catalyst assisted crosslinking

Thermal crosslinking is often conducted at high temperature, which tends to form a rather thick skin layer and reduce the CO_2 permeance. Some attempts have been made to increase the permeance by crosslinking fibers at a lower temperature with catalyst. The

crosslinking reaction can be accelerated by an acid as the catalyst since it can reduce the activation energy of the reaction. P-toluenesulfonic acid (PTSA) are commonly used in catalyzing polyesterification reactions, including the monoesterification and transesterification [11, 68].

To prepare a catalyst assisted crosslinked dense film, the catalyst is first dissolved in the solution and then the solution is cast into a dense film using the technique discussed in 3.2.1. The dense film with catalyst can be crosslinked under vacuum at a lower temperature. On the other hand, the way to add catalyst in hollow fibers is different. Catalyst can be added to the dope but it is likely to be washed out during the wet-quench, water bath and/or solvent exchange steps. Therefore, an alternative to add the catalyst is dispersing catalysts into fibers in the solvent exchange step. The catalyst, like PSTA, is miscible with ethanol but immiscible with hexane. Thus, the catalyst can be dissolved in the ethanol and fibers are soaked in this catalyst-ethanol mixture instead of pure ethanol in solvent exchange. The swelling of fibers in ethanol helps fibers adsorb more catalyst. When this catalyst-ethanol is replaced by hexane, the catalyst is unlikely to be washed away because of immiscibility of catalyst in hexane. Then the fibers can be annealed under vacuum and the crosslinking reaction with catalyst occurs simultaneously [11].

3.6 Crosslinking characterization

3.6.1 Dissolution experiment

A dissolution experiment is commonly performed to qualitatively determine the degree of crosslinking of fibers [11, 48]. The uncrosslinked fibers are easily dissolved in solvents, like THF, but the crosslinked polymer has “infinite” high molecular weight, making it insoluble in THF or even NMP. In the experiment, fibers crosslinked with different approaches are placed in vials with THF for a period of time and the degree of

crosslinking can be judged visually. Completely crosslinked fibers will be not dissolved in the THF. Some crosslinked fibers may be highly swollen but not completely soluble in THF, which means a certain degree of crosslinking has still occurred.

3.6.2 TGA-IR Analysis

TGA-IR (thermo gravimetric analysis-infra-red) is commonly used to analyze the effect of temperature on polymer samples. The crosslinking process can also be studied by the TGA-IR experiment. In this work, Netzsch STA 409 TGA instrument and Bruker Tensor 27 FTIR spectrometer with a flow-through gas cell and a LN-MCT external detector were used, shown in Figure 3.11.

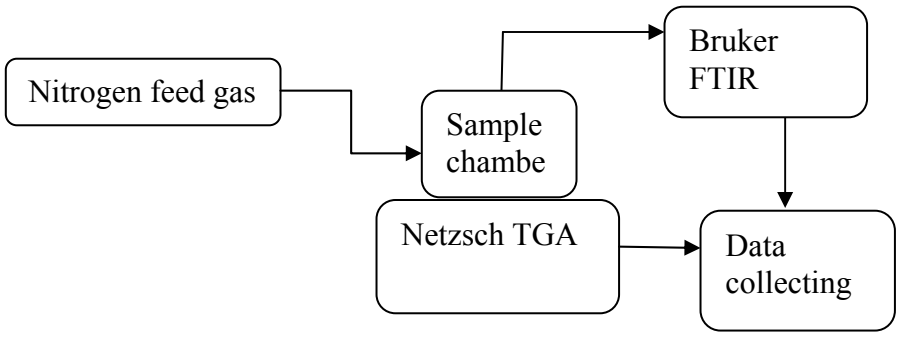

Figure 3.11: Schematic showing the TGA-IR systems.

TGA quantifies the produced components by weight loss during heating treatment while IR qualitatively identifies those components. Ideally, the ratio of actual weight loss of 1, 3-propane diol to theoretical weight loss from stoichiometry can determine the degree of crosslinking. However, polymer samples often contain NMP, making the TGA difficult to separate 1, 3-propane diol and NMP. In this case, an IR spectrum is necessary to quantify the degree of crosslinking. There are specific and stand-alone peaks in both 1, 3-propane diol and NMP. The wavelength at 3670, 2900, 1740 cm-1 represent the OH, CH, C=O stretches. The ratio of the peak integrals helps quantitatively determine the crosslinking degree, though there exists relatively large uncertainty [11, 14].

3.6.3 Nuclear magnetic resonance spectroscopy (NMR)

^{13}C NMR can quantitatively determine the degree of crosslinking [11-12]. The peak area in NMR spectra for both uncrosslinked and crosslinked samples are the most of interest. Specifically, the aliphatic carbon from 1, 3-propane diol in crosslinked sample shows the percentage of diol involved in crosslinking reaction. The peak area of this aliphatic carbon can be used to calculate the degree of crosslinking by comparing the spectra of uncrosslinked and crosslinked samples. However, NMR analysis must be conducted carefully as the peaks on solid state spectra are usually broad.

CHAPTER 4

SKIN LAYER OPTIMIZATION OF HOLLOW FIBERS

4.1 Introduction

In Chapter 2, the dry-jet/wet quench bath spinning was presented to produce effective asymmetric hollow fibers. Details of dope formulation, spinning and characterization were described in Chapter 3. This chapter will apply the spinning technique on the propanediol monoester crosslinkable (PDMC) polymer by following the flow diagram shown in Figure 4.1.

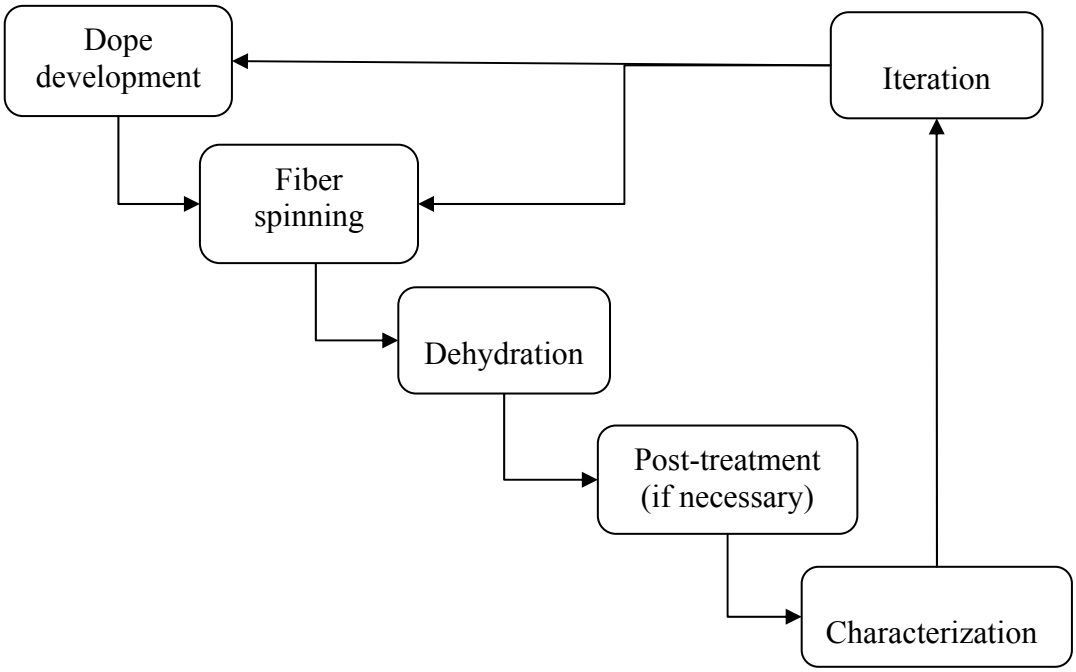

Figure 4.1: Flow diagram showing the hollow fiber spinning process [11].

In this chapter, three main approaches were first considered to improve the productivity of natural gas separation by reducing the effective skin layer thickness

without introducing defects: spinning conditions optimization, dope reformulation and polymer molecular weight effect.

4.2 Hollow fiber spinning optimization

Researchers have developed the dry-jet/wet quench spinning process to fabricate defect-free hollow fibers from PDMC polymer with a skin layer thickness on the order of 0.2~ 0.4 μ [11-12]. One apparent technique to continuously reduce the skin layer thickness without introducing defects is optimizing the spinning conditions, as the spinning parameters significantly affect the phase separation of the hollow fiber skin layer. Clausi [25] studied the formation of defect-free polyimide hollow fibers by varying spinning conditions and showed that a lower air gap formed a thinner skin layer when the dope composition and other spinning parameters remained the same. In this chapter, the optimization of spinning conditions was performed on PDMC hollow fiber to study the feasibility of reducing the defect-free skin layer thickness on the order of 0.1 μ, which is commercially preferable in terms of separation productivity.

4.2.1 Hollow fiber spinning

In the spinning optimization work, the monoesterified PDMC polymer (3:2) was provided by Chevron Energy Technology Company. The molecular weight is 74,800 (Mw) with polydispersity index of 1.8. This polymer sample is termed "PDMC-74.8k/1.8". The dope formula of xlp2 spinning is shown in Table 4.1. The method to make the dope was described in reference [11-12].

Table 4.1: Hollow fiber spinning dope composition of xlp2.

Component	Wt%
PDMC-74.8k/1.8	35.0
NMP	35.0
Ethanol	8.5
THF	15.0
$LiNO_3$	6.5

In the dope as shown in Table 4.1, NMP and THF are used as the solvents. The volatility of THF promotes the skin formation of hollow fibers in the dry-jet step. Instead of using water, ethanol is chosen as the non-solvent since it allows more flexibility of dope make-up [11]. Moreover, ethanol can also avoid phase separation of the skin in the air gap when THF evaporates. To be more specific, ethanol can also evaporate and offset the solvent loss, so the skin is not likely to phase separate in the air gap, thereby promoting the formation of a defect-free skin layer. Lithium nitrate ($LiNO_3$) is added as non-solvent as both the promoter of phase separation in the quench bath and modifier of dope viscosity.

The hollow fibers were fabricated through the dry-jet/wet quench spinning process. The main spinning parameters used in the spinning included the air gap, draw ratio and spinneret temperature. The quench bath temperature was heated to 55^{o}C and quench batch height was 102 cm. The hollow fiber spinning conditions are summarized in Table 4.2. These conditions were used on the basis of experience gained from prior researchers and also personal experience with the “PDMC-74.8k/1.8” sample to obtain spinnable fibers.

Table 4.2: Hollow fibers spinning conditions for xlp2.

Spinning State	Spinneret temp (°C)	Air gap (cm)	Take-up rate (m/min)	Nominal draw ratio
2	50	30	50	4.2
3	50	10	50	4.2
4	50	20	25	2.1
5	50	10	25	2.1
6	75	30	50	4.2
7	75	1	50	4.2

Dope extrusion rate: 180ml/hr; bore fluid flow rate: 60ml/hr; bore fluid composition: 80/20w.t% NMP/H_2O; aqueous quench bath temperature: 55 ^oC.

During this spinning, three parameters that significantly affect the hollow fibers spinning were studied: the spinneret temperature, air gap, and take-up rate. The spinneret temperature was between 50°C and 75°C. An elevated spinneret temperature reduces the dope viscosity and increase the evaporation of volatile components in the dope, thereby affecting the skin layer formation. The air gap was varied from 1 to 30cm since it fixes the nascent fiber residence time in the air gap and may affect the degree of phase separation. The take-up rate was also studied as a high take-up rate can produce fibers with smaller dimensions, preferred by industrial application in terms of productivity. Moreover, a smaller fiber diameter can help fibers withstand high feed pressure [10].

After spinning, the hollow fibers were soaked in a water bath for three days to remove residual solvents. The water was changed twice a day. After water bath, the solvent exchange was conducted with ethanol and hexane. Each solvent exchange was divided into three washes, which were three 20 min baths with ethanol and three 20min

baths with hexane. After solvent exchange, the fibers were dried in the hood for 1 hr. Then the fibers were kept in vacuum for 2 hrs at 70°C to allow enough drying without crosslinking of fibers [69].

4.2.2 Hollow fiber characterization

Scanning Electron Microscope (SEM) test is commonly used to study the cross sectional structure of hollow fibers. Besides the ovality and concentricity, high magnification of SEM can reveal the skin layer and porous substructure of fibers. A typical SEM image is shown in Figure 4.2.

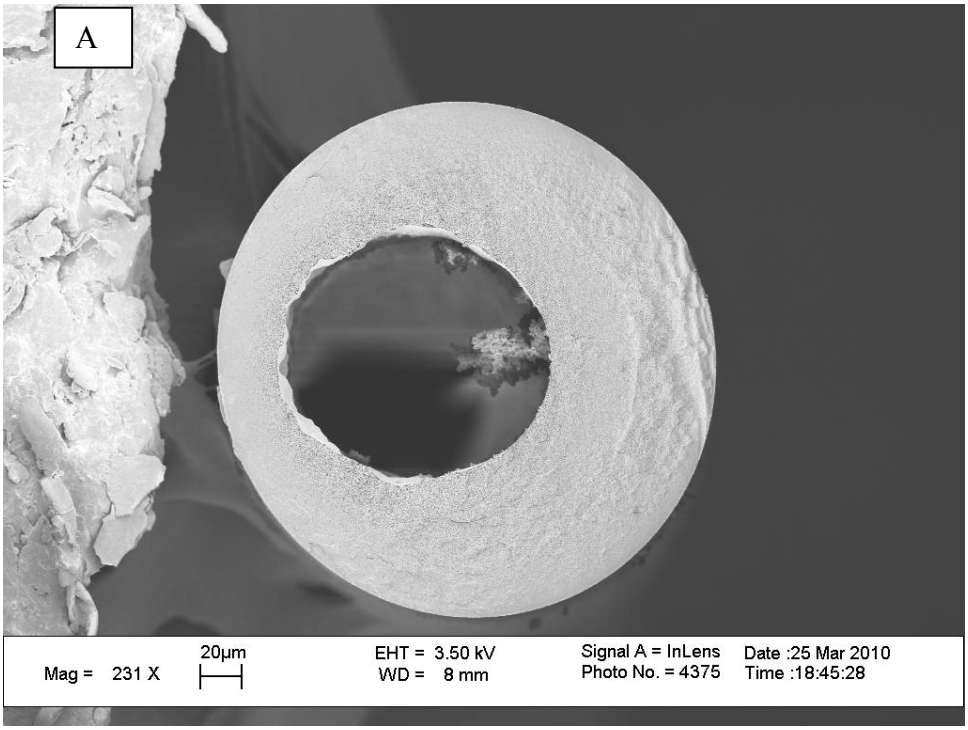

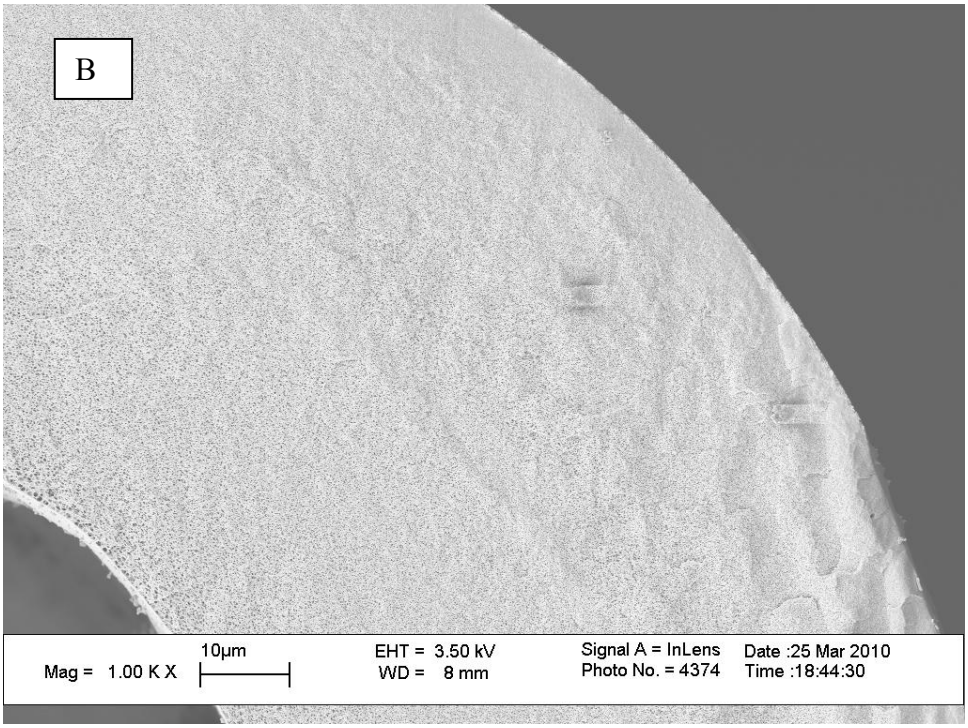

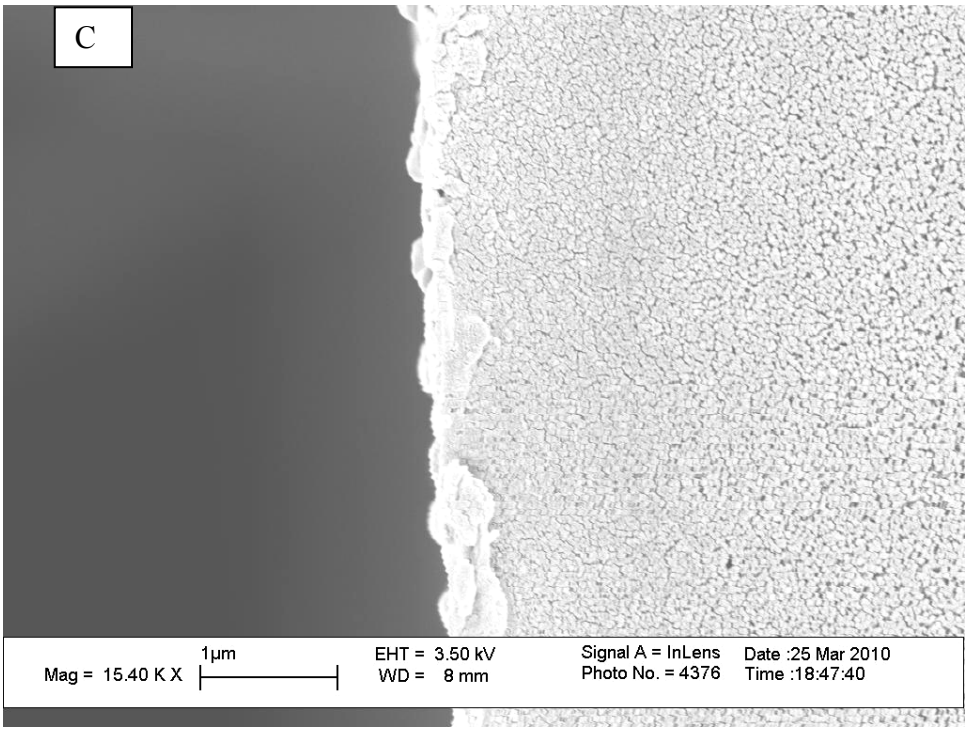

Figure 4.2: SEM images showing cross sectional structure of xlp2 State 3 uncrosslinked hollow fibers. Figure (A) shows the cross-section of the fiber; Figure (B) and (C) show the apparent skin layer structure with porous transition layer.

Figure 4.2 showed that the hollow fibers are not as concentric as expected. This is due to the difficulty in keeping the needle in the spinneret perfectly straight when spinning the high viscous dope at high pressure. The non-concentricity of the hollow fibers seems not be a serious problem as long as the separation performance of hollow fibers is not undermined by this morphology. Nevertheless, concentric hollow fibers must be always pursued both in the laboratory study and industrial application to provide high pressure feed capability. The skin layer and porous substructure are apparent in the hollow fibers, suggesting the phase separation occurred completely.

As discussed in Chapter 2, the separation performance and productivity of hollow fibers are characterized by the gas permeation. The uncrosslinked hollow fibers from xlp2 spinning were tested with pure gas and the permeation results are summarized in Table 4.3.

Table 4.3: Pure gas separation properties of uncrosslinked xlp2 fibers.

Spinning State	O_2 Perm. (GPU)	$\alpha_{O2/N2}$	$\alpha_{He/N2}$	Skin layer thickness/μ
2	15.8±1.2	4.7±0.4	31.7±4.0	0.45±0.04
3	20.4±0.9	5.9±0.6	-	0.35±0.02
4	13.9±0.2	5.4±0.3	-	0.51±0.01
5	16.3±1.3	4.9±0.5	-	0.44±0.04
6	16.6±0.9	4.5±0.3	30.3±1.4	0.43±0.02
7	36.4±2.5	3.3±0.2	-	0.20

Test conditions: feed pressure: ~100 psia, temperature: 35^{o}C.

In Table 4.3, the hollow fibers skin layer thickness (l) is estimated by the ratio of O_2 permeability and O_2 permeance at the same test conditions, shown in Equation 4.1 [27].

$$l = \frac{Permeability}{Permeance} = \frac{P}{P/l} \tag{4.1}$$

The O_2 permeability of uncrosslinked PDMC dense film at 100 pisa, 35°C is 7.1 Barrer [12]. Based on the O_2 permeance from Table 4.2, the skin layer thickness (l) in μ is determined.

State 2 fibers are nearly defect-free as the O_2/N_2 selectivity is almost intrinsic (the dense film value $\alpha_{O2/N2}$=4.8); minor defects may exist in State 2 fibers as the He/N_2 selectivity is below the intrinsic (the dense film value $\alpha_{He/N2}$=40); State 3 fibers are defect-free since both the O_2/N_2 and He/N_2 selectivity are above the intrinsic values. The values slightly above intrinsic dense film presumably reflect orientation induced during fiber extrusion, which can increase size and shape selectivity. The skin layer thickness from these two states is ~0.4 μ. Nevertheless, State 3 fibers have a thinner skin than State 2 due to the lower air gap in State 3.

State 4 and 5 fibers are defect-free. As shown in Table 4.2, State 3 and 5 fibers have the same spinning conditions, except that State 3 have a higher take-up rate. It seems a higher take-up rate tends to produce a thinner skin layer, as State 3 fibers have a skin layer (0.35 μ) thinner than State 5 (0.44 μ). It is also found that a lower air gap produce a thinner skin layer since State 5 has an air gap lower than State 4.

State 6 fibers are defect-free. The fibers spun at higher spinneret temperature (State 6) have a relatively thinner skin than those at lower spinneret temperature (State 2). It seems that the spinneret temperature does not significantly affect the skin formation perfection for this spinning dope; however, an excessively high spinneret temperature can cause a decrease of dope viscosity and nascent fiber instabilities.

State 7 fibers have the thinnest skin layer thickness low to 0.18 μ. However, the O_2/N_2 selectivity is lower than intrinsic value, suggesting that the fibers are somewhat defective; therefore the real skin layer thickness is underestimated. Those defects are probably due to the excessively low air gap, which causes the nascent fibers to form an excessively thin and not completely perfect nascent skin layer.

To sum up the work on spinning conditions optimization, the PDMC hollow fibers exhibit defect-free selective skin layer by using the nominal same dope composition indicated in reference [12, 52]. The fibers have a delicate morphology and uniform structure; however, the skin layer thickness for most spinning states is on the order of 0.4 μ. The skin layer thickness of State 7 fibers is reduced to 0.2 μ but the true selective skin layer is presumably not correctly estimated using Equation (4.1) due to the defective skin. Since the spinning conditions used in the xlp2 spinning do not produce defect-free fibers with the desired thin skin layer (ideally 0.1 μ), the dope composition must be modified, which will be discussed in Section 4.3.

4.3 Dope reformulation for hollow fiber spinning

4.3.1 Phase separation study

As discussed in Section 4.2, various spinning conditions have been studied to form defect-free selective hollow fibers. However, the hollow fibers do not exhibit the desired skin layer thickness (ideally 0.1 μ without defects) as expected. This necessitates the study on dope reformulation so that the defect-free skin layer thickness can be reduced to the desired level.

To start the dope reformulation, the binodal of the dope must be determined to ensure that the reformulated dope composition locates in the single phase region. The commonly used technique to find the binodal is through experimental method, called the cloud point determination [11]. The polymer concentration was between 26% and 32% while the solvent/non-solvent ratio was varied accordingly. The status of each dope sample was observed visually and determined if it was one-phase or two-phase. The results of the cloud point experiments are summarized and plotted in a ternary phase diagram, as shown in Figure 4.3.

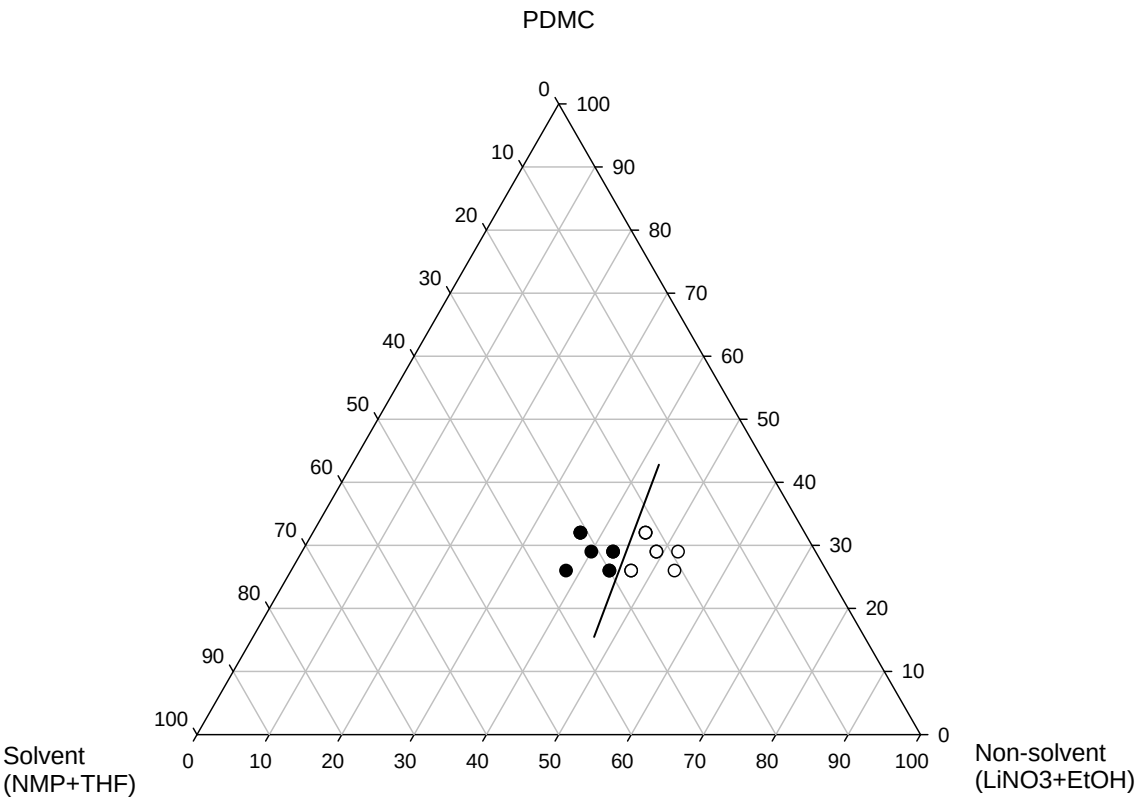

Figure 4.3: Ternary phase diagram depicting the binodal (solid line) of low molecular weight PDMC polymer/solvent/non-solvent system.

In Figure 4.3, the solid points represent the single phase samples and the open circles represent the two-phase samples. The binodal (shown as the solid line) lies between the single phase region and two-phase region. With the binodal information, the dope composition used in Section 4.2 is verified as being safely in the 1-phase region. The xlp2 dope composition used in Section 4.2.1 for hollow fibers spinning was: 35% PDMC polymer, 35% NMP, 15% THF, 8.5% EtOH and 6.5% $LiNO_3$. The relative location of this dope composition (indicated as open star) is shown in Figure 4.4.

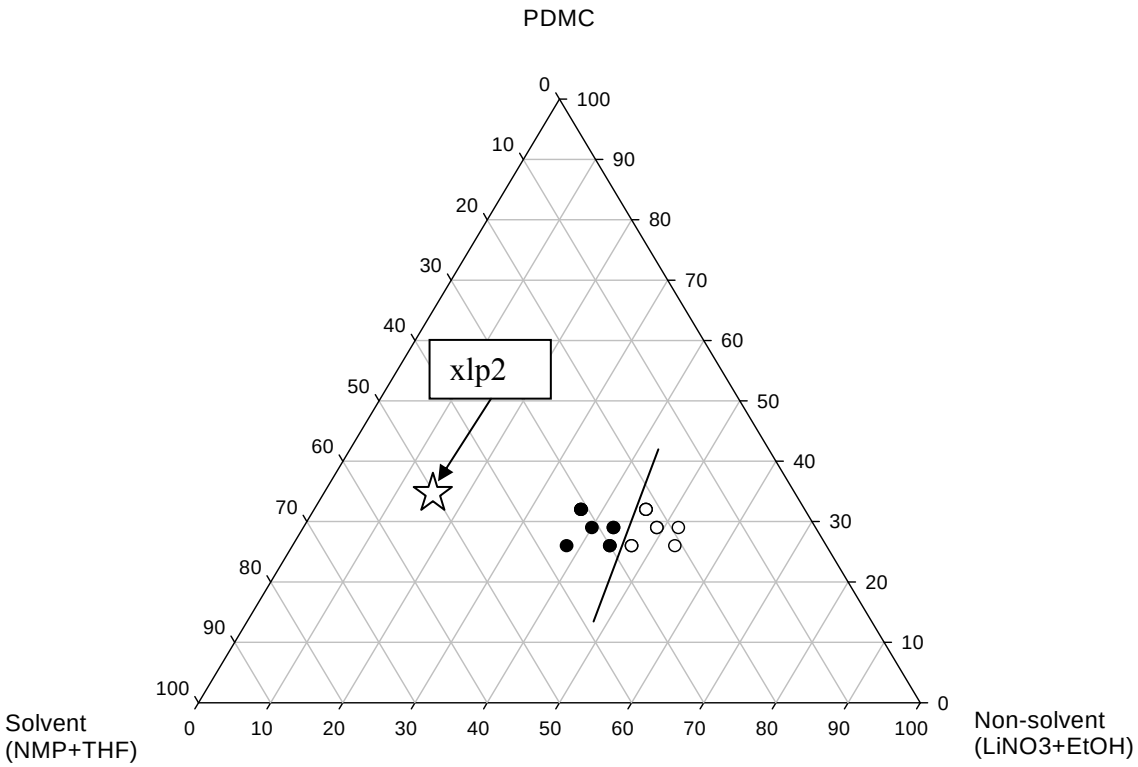

Figure 4.4: Ternary phase diagram depicting the binodal (solid line) of low molecular weight PDMC polymer and xlp2 dope composition (open star).

From Figure 4.4, while the dope composition of xlp2 spinning is safely in the one phase region, it is essentially too far from the binodal, which is probably the reason of the thick skin layer (~0.4μ). Although reference [12] indicated that the hollow fibers spun at this dope composition (solid point) showed high CO_2/CH_4 selectivity and CO_2 plasticization resistance, the CO_2 permeance of crosslinked fibers were not as high as expected, making them inadequate for commercial application. Therefore, the dope composition must be reformulated to meet the industrial requirement in terms of high productivity and intrinsic selectivity.

4.3.2 Hollow fiber spinning

Attempts have been made to reduce the skin layer thickness through dope reformulation. Starting from the middle range between the xlp2 spinning and the binodal, the dope was reformulated as CM5 and the CM5 dope composition is shown as the open triangle in Figure 4.5.

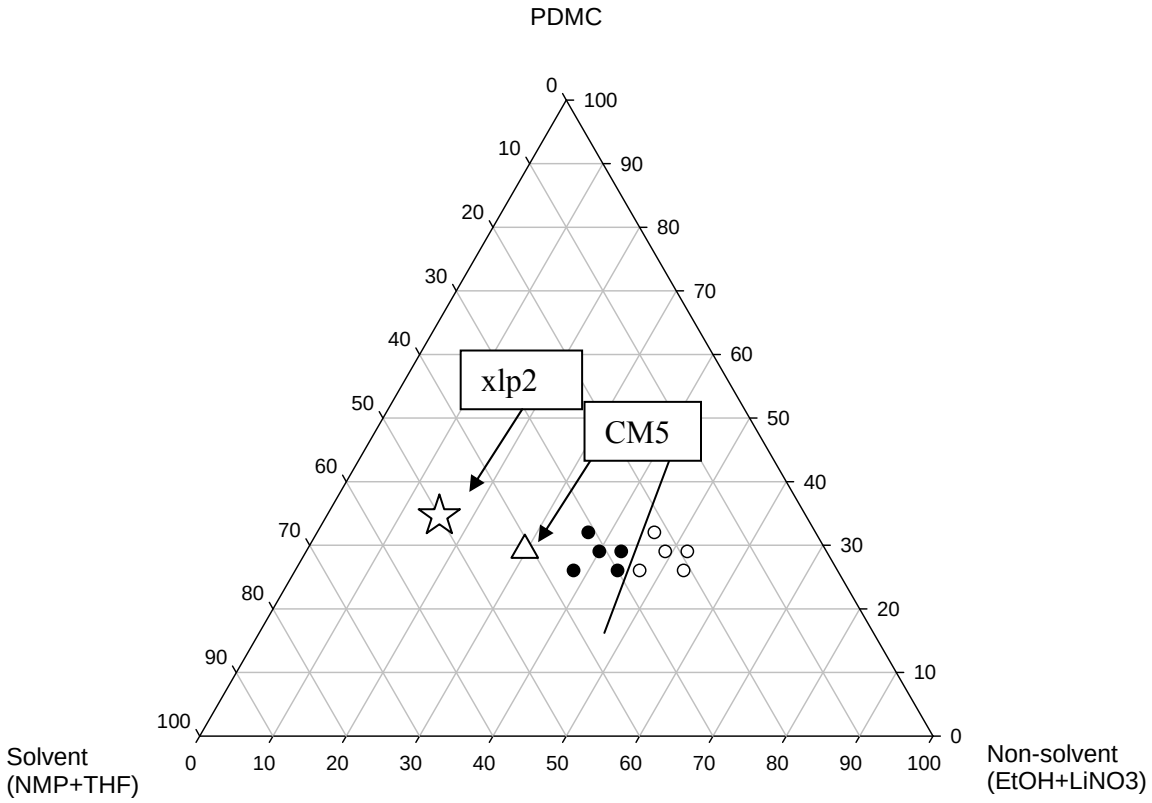

Figure 4.5: Ternary phase diagram depicting the binodal (solid line) of low molecular weight PDMC polymer, xlp2 dope composition (open star) and CM5 dope composition (open triangle).

In the CM5 dope, the ratio of PDMC to solvent was kept the same as xlp2 (=35: 50) to allow enough solvent in the dope. The polymer concentration was reduced from 35% to 29% due to difficulties of syringe test on the high viscous dope with 35% polymer concentration. The composition of CM5 dope is listed in Table 4.4. This moves the dope composition in the direction of the binodal line, while giving "room" to manipulate spinning variables in the air gap without danger of crossing the binodal line and creating a highly defective skin.

Table 4.4: Hollow fibers spinning dope composition of CM5.

Component	Wt%
PDMC-74.8k/1.8	29.0
NMP	29.0
Ethanol	23.1
THF	12.4
$LiNO_3$	6.5

In CM5 spinning, two main spinning parameters, dope flow rate and air gap, were studied to reduce the skin layer thickness. The dope flow rate was between 120 and 180 ml/hr, which was essentially the same as the reference [12]. The air gap varied from 2 to 33 cm to optimize skin layer thickness without defects. 33 cm air gap has been studied in reference [12] and shown decent natural gas separation performance. It also indicated a good spinnability. In this work, an air gap lower to 2 cm was studied to reduce the skin layer thickness. The spinning conditions of CM5 fibers are summarized in Table 4.5.

Table 4.5: Hollow fibers spinning conditions for CM5.

State ID	Dope extrusion rate (ml/hr)	Air gap (cm)	Nominal draw ratio
1	180	2	4.2
2	180	33	4.2
3	120	33	6.3
4	120	2	6.3
5	120	5	6.3
6	180	5	4.2

The quench bath temperature: ~50°C; bore fluid composition: 80/20 wt% NMP/H_2O; bore fluid flow rate: 1/3 of dope flow rate; take-up rate: 50m/min; the spinneret temperature: 70°C.

4.3.3 Hollow fiber characterization

The SEM images were taken for uncrosslinked CM5 State 2 fibers to observe the cross sectional structure, shown in Figure 4.6.

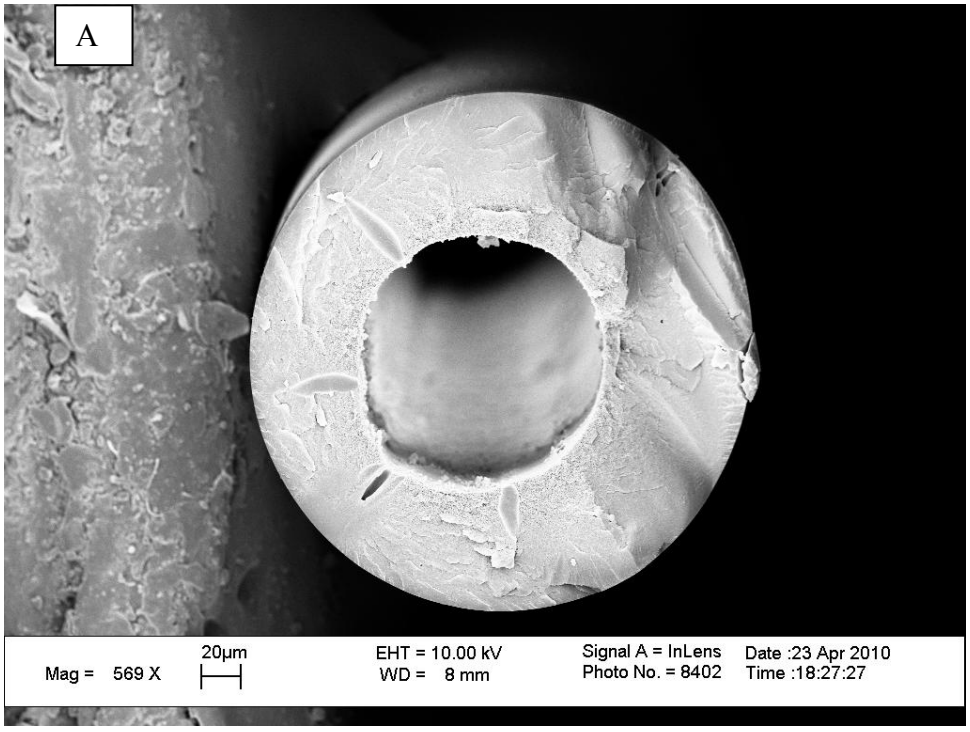
A
Mag = 569 X
20µm
EHT = 10.00 kV
WD = 8 mm
Signal A = InLens
Photo No. = 8402
Date :23 Apr 2010
Time :18:27:27

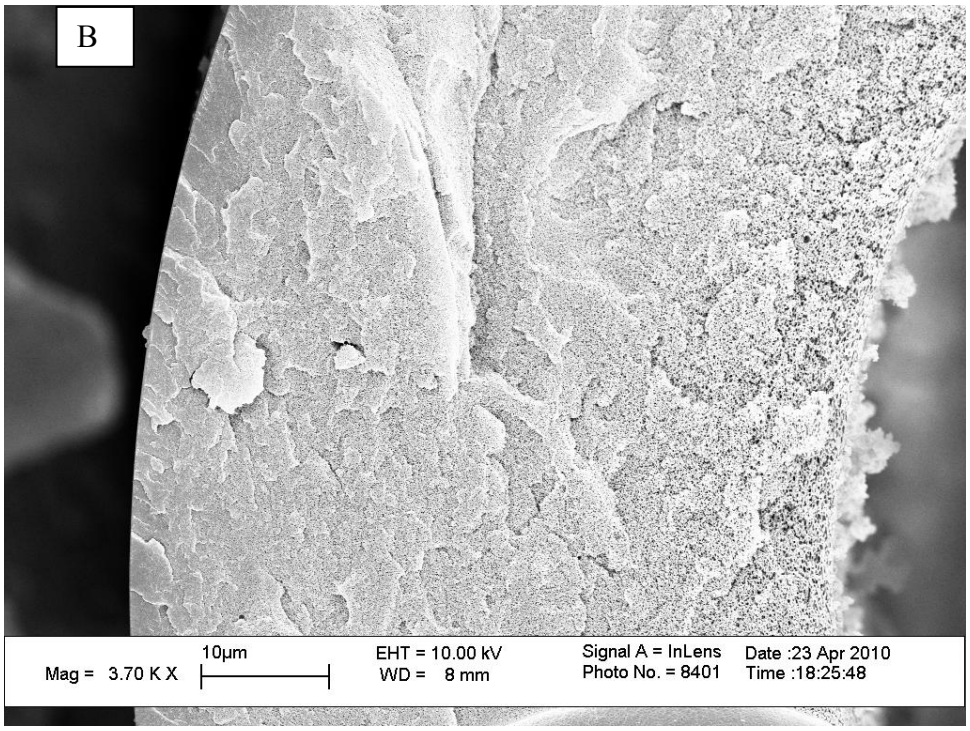
B
Mag = 3.70 K X
10µm
EHT = 10.00 kV
WD = 8 mm
Signal A = InLens
Photo No. = 8401
Date :23 Apr 2010
Time :18:25:48

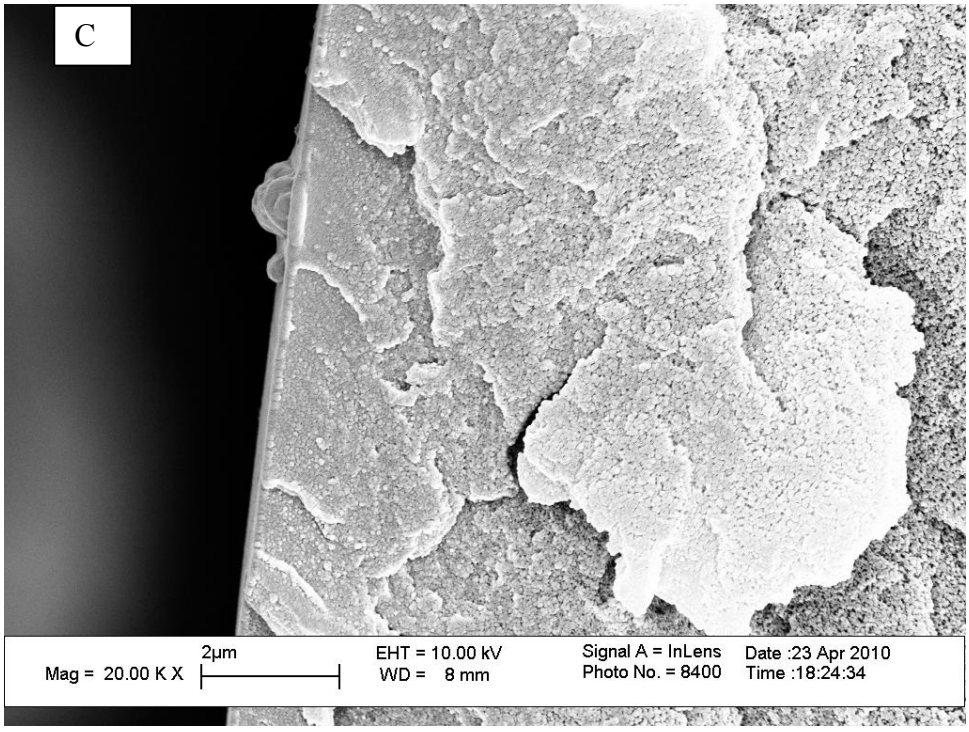

Figure 4.6: SEM images showing the cross-sectional structure of uncrosslinked CM5 Statue 2 fibers. Figure (A) shows the cross-section of the fiber; Figure (B) and (C) show the apparent skin layer structure with porous transition layer.

From above SEM images in Figure 4.6, the CM5 State 2 fibers show highly concentric structure, even better than xlp2 fibers, showing the learning achieved vs. the original spinning experiments. The concentricity indicates that the alignment of spinneret needle was quite accurate and the needle in the spinneret withstood the dope flow during spinning. The skin layer and porous substructure are apparent for the uncrosslinked fibers. Minor macrovoids are present in the hollow fibers.

The CM5 fibers were then tested with pure gas to study the ideal gas separation properties and the gas permeance data are shown in Table 4.6.

Table 4.6: Pure gas separation properties of uncrosslinked CM5 fibers.

Spinning state	O_2 Perm. (GPU)	$\alpha_{O2/N2}$	$\alpha_{He/N2}$	Skin layer thickness/μ
1	33.7	4.9	42	0.21
2	16.3	4.9	32	0.44
4	23.2	4.9	33	0.31
5	21.6	4.2	29	0.33
6	22.8	6.2	41	0.31

Test conditions: feed pressure: ~100 psia, temperature: 35°C.

From Table 4.6, defect-free fibers are obtained in CM5 spinning. All spinning states (except State 5) exceed the intrinsic O_2/N_2 selectivity (dense film $\alpha_{O2/N2}$=4.8). This represents a significant advancement. Possible minor sub-structure resistance may exist in State 2, 4 and 5 since the He/N_2 selectivity is below the dense film value (dense film $\alpha_{He/N2}$=40). Nevertheless, the skin layer thickness is lower than 0.21 μ for CM5 State 1 fiber based on O_2 permeance. This skin layer thickness is reduced ~50% vs. xlp2 fibers, suggesting that the reformulated CM5 dope composition can effectively reduce the skin layer thickness without introducing defects. However, the defect-free skin layer thickness of CM5 State 1 fibers is on the same order of the reference [12], which means further optimization of spinning conditions must be done to reduce the skin layer thickness to the desired level.

Since the CM5 spinning with a reformulated dope composition do not reduce the thin skin layer thickness to the extent expected, attempts have been made to move the dope composition closer to the binodal to form a thinner skin layer of hollow fibers. The CM8 spinning were performed with the dope composition still closer to binodal than CM5, as shown in Figure 4.7.

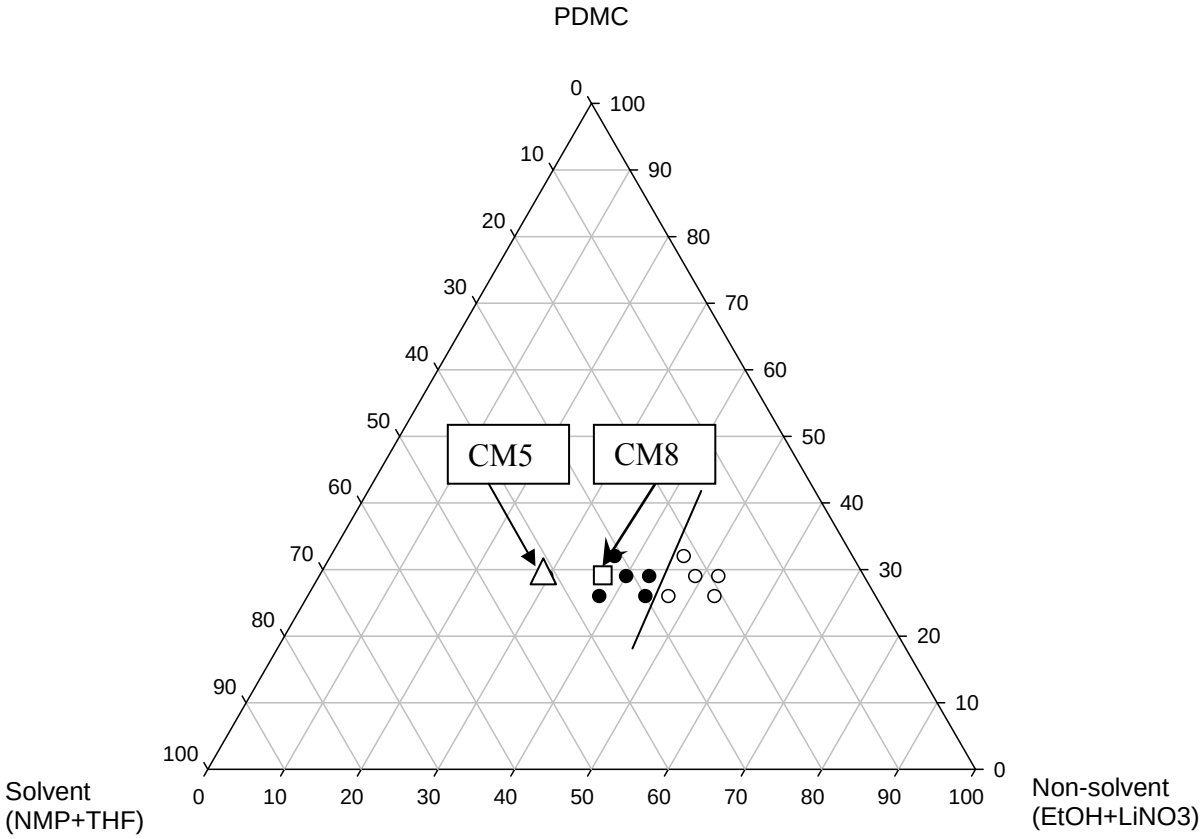

Figure 4.7: Ternary phase diagram depicting the CM8 dope composition (open rectangle point), CM5 dope composition (open triangle point) and binodal (solid line) of PDMC polymer.

The CM8 dope composition was shown in Table 4.7.

Table 4.7: Hollow fiber spinning dope composition of CM8.

Component	Wt%
PDMC-74.8k/1.8	29.0
NMP	23.8
Ethanol	30.5
THF	10.2
$LiNO_3$	6.5

The air gap was studied in the CM8 spinning. The spinning conditions used for CM8 fibers are summarized in Table 4.8.

Table 4.8: Hollow fibers spinning conditions for CM8.

Spinning state	Air gap/cm
1	5
2	2
3	1

The quench bath temperature: ~50°C; dope extrusion rate: 180ml/hr; bore fluid flow rate: 60ml/hr; bore fluid composition: 80/20 wt% NMP/H_2O; take-up rate: 50m/min; spinneret temperature: 70°C.

The CM8 fibers were tested with pure gas and the permeance data are shown in Table 4.9.

Table 4.9: Pure gas separation properties of uncrosslinked CM8 fibers.

Spinning state	O_2 Perm. (GPU)	$\alpha_{O2/N2}$	$\alpha_{He/N2}$	Skin layer thickness/μ
1	45.8	2.0	14	0.15
2	49.6	2.7	26	0.14
3	80.3	2.3	17	0.09

Test conditions: feed pressure: ~100 psia, temperature: 35^{o}C.

From Table 4.9, the CM8 fibers are somewhat defective. Again, the real skin layer thickness for each state is underestimated due to the defective nature of the skins. The defects are possibly due to that the reformulated dope composition is too close to the binodal. The THF concentration in CM8 is 22% lower than that in CM5 dope. Since the volatile THF plays as a key role in promoting the formation of skin layer, the lower concentration can cause the skin layer to be inadequately vitrified, which can lead to defective fibers as the skin undergoes phase separation. The lower THF content is clearly detrimental to the formation of skin layer and cause the defects of the hollow fibers.

To additionally reduce the skin layer thickness, the dope composition was back to the one used in previous successful CM5 spinning. The CM9 spinning was conducted by using the nominal same dope composition as CM5 spinning (as shown in Figure 4.2). The air gap was varied from 0.5 to 2cm in the CM9 spinning to thin the skin layer down while seeking to maintain a defect-free selective skin. Other spinning parameters were kept the

same as CM5 spinning since the air gap primarily affects the skin layer thickness. The spinning conditions used for CM9 fibers are summarized in Table 4.10.

Table 4.10: Hollow fiber spinning conditions for CM9.

Spinning state	Air gap/cm
1	2
2	1
3	0.5

The quench bath temperature: ~50°C; dope extrusion rate: 180ml/hr; bore fluid flow rate: 60ml/hr; bore fluid composition: 80/20 wt% NMP/H_2O; take-up rate: 50m/min; spinneret temperature: 70°C.

The CM9 fibers were tested with pure gas, and the permeance data are shown in Table 4.11. At least two modules were prepared to check for the experimental reproducibility for each state.

Table 4.11: Pure gas separation properties of uncrosslinked CM9 fibers.

Spinning state	O_2 Perm. (GPU)	$\alpha_{O2/N2}$	$\alpha_{He/N2}$	Skin layer thickness/μ
1	84.2±25	2.0±0.5	14±6.5	0.09
2	37.2±5.3	4.8±0.1	45±4.5	0.19±0.02
3	31.5±2.6	4.9±0.2	56±7	0.23±0.02

Test conditions: feed pressure: ~100psia, temperature: 35^{o}C.

From Table 4.11, CM9 State 1 fibers are somehow defective due to initial unstable spinning line. Again, the real skin layer thickness of CM9-1 fibers was under-

estimated by Equation 4.1 due to the defective nature of the skins; CM9 State 2 fibers have defect-free skin layer thickness lower to 0.19 μ, which is relatively lower than the CM5 State 1 fibers (0.21 μ); CM9 State 3 fibers are defect-free, with a skin layer thickness close to CM9 State 2.

To sum up Section 4.3, the dope composition was reformulated to obtain thinner skin hollow fibers. It shows that the location of dope composition in the ternary phase diagram significantly affects the transport properties, including the selectivity and permeance. A moderate composition (CM5 and CM9 spinning) is needed to produce defect-free fibers with skin layer thickness lower to 0.19 μ. If the dope composition is too close to the binodal, as suggested by CM8, defects are likely formed in the fibers due to the lower THF and higher ethanol concentration.

In Section 4.2 and 4.3, the spinning optimization and dope reformulation were studied to reduce the skin layer thickness without introducing defects. However, the skin layer thickness of hollow fibers is still above the desired level (ideally 0.1 μ without defects). These factors, which called into question the quality of the basic "PDMC-74.8k/1.8" polymer batch and suggested the need to study another polymer batch with different molecular weight. This will be discussed in Section 4.4.

4.4 Polymer molecular weight effect on hollow fiber separation

4.3.1 Materials

In this section, a new batch of higher molecular weight 6FDA-DAM: DABA (3:2) polymer was used and monoesterified by the author. This 6FDA-based polyimide have a molecular weight about 360,000 (Mw) and polydispersity of ~2. Prior to spinning, the 6FDA polymer needs to be monoesterified with 1, 3-propane diol to form the PDMC polymer. This monoesterification reaction was done in the laboratory. The details of monoesterification experiment are described in Appendix C.

The first attempt to spin the new polymer batch used the nominal same dope composition as CM5, shown in Figure 4.5.

4.3.2 Hollow fiber spinning

For CM 10 spinning, the main studied spinning parameter was the air gap. The air gap up to 33 cm represented a good spinnability and 1 cm air gap was used to minimize the skin layer thickness. Other spinning conditions remained the same as CM9 spinning. Table 4.12 shows the CM10 spinning conditions.

Table 4.12: Hollow fiber spinning conditions for CM10.

Spinning state	Air gap/cm
1	33
2	2
3	1

The quench bath temperature: ~50°C; bore fluid composition: 80/20 wt% NMP/H_2O; the dope flow rate: 180 ml/hr; bore fluid flow rate: 60 ml/hr; take-up rate: 50 m/min; the spinneret temperature: 70°C.

4.3.3 Hollow fiber characterization

The pure gas permeation was first performed on CM10 State 3 fibers, the permeation results are shown in Table 4.13. At least two modules were prepared to check the experimental reproducibility for each state.

Table 4.13: Pure gas separation properties of uncrosslinked CM10 State 3 fibers.

Spinning state	O_2 Perm. (GPU)	$\alpha_{O2/N2}$	$\alpha_{He/N2}$	Skin layer thickness/μ
3	63±7	4.6±0.1	39±1	0.11±0.01

Test conditions: feed pressure: ~100psia, temperature: 35°C.

From Table 4.13, the uncrosslinked CM10 State 3 fibers have defect-free skin layer roughly at 0.1 μ and there is no substrate resistance since the $\alpha_{He/N2}$ is intrinsic (dense film $\alpha_{He/N2}$=40). The desired skin layer thickness (0.1 μ) without defects is achieved in the CM10 spinning with higher molecular weight PDMC polymer. This result is highly significant and strongly suggests that the higher molecular weight PDMC sample is critical for achieving both thin skins and defect-free skins.

The cross sectional structure of the CM10 State 3 fibers is evaluated by SEM images, shown in Figure 4.8.

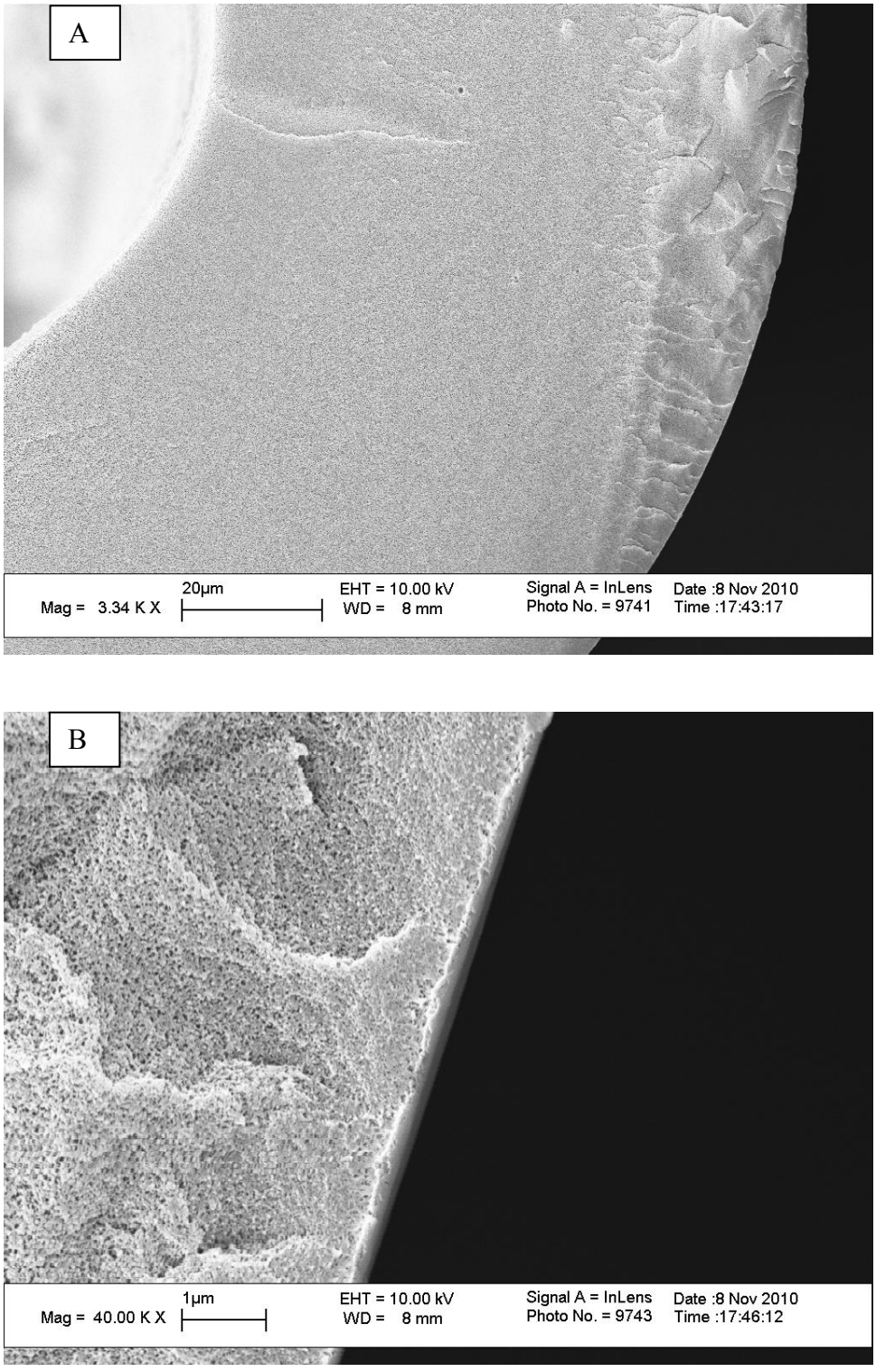

Figure 4.8: SEM images showing cross sectional structure of uncrosslinked CM10 State 3 fibers. Figure (A) shows the cross-section of the fiber; Figure (B) shows the apparent skin layer structure with porous transition layer.

From Figure 4.8, the CM10 State 3 fibers show the apparent thin skin layer and porous sub-structure. No macrovoid presented in the cross section indicates good phase separation.

To summarize the study of the polymer molecular weight effects on hollow fibers, it seems that a higher molecular weight polymer tends to produce the defect-free hollow fibers with desired skin layer thickness. Defect-free CM10 fibers with a skin layer thickness roughly at 0.1 μ were successfully spun. No substructure resistance was found in those fibers. To further probe the separation performance of defect-free hollow fibers with practical feed streams, the fibers must be crosslinked to stabilize their separation properties. Chapter 5 will discuss the approaches of crosslinking and the ideal gas separation performance of crosslinked hollow fibers. The natural gas separation of both uncrosslinked and crosslinked will be described in Chapter 6.

CHAPTER 5

CROSSLINKING OF ASYMMETRIC HOLLOW FIBERS

5.1 Introduction

In Chapter 2, covalent crosslinking have been described as an important membrane stabilization strategy. Crosslinking combines high efficiency, ease of execution and commercially viable application with desired separation performance and plasticization resistance [11-14]. This chapter will focus on the application of crosslinking to hollow fibers. The crosslinking method involves varying temperature and exposure times to optimize the plasticization resistance and productivity. Attempts have been made to use catalysts to assist crosslinking by lowering the crosslinking temperature. The bulk of this chapter will discuss the ideal gas separation properties (O_2/N_2 selectivity) of crosslinked fibers.

5.2 Materials and methods

Hollow fibers were spun from 6FDA-DAM: DABA (3: 2) polymer. Prior to spinning, the 6FDA-based polyimide was monoesterified with 1, 3-propane diol to form PDMC polymer [11-13]. The monoesterification was done either in Chevron or in our laboratory, as discussed in previous sections. Two polymer batches with different molecular weight were studied, as studied in Chapter 3. The chemical structure of PDMC polymer is shown in Figure 5.1.

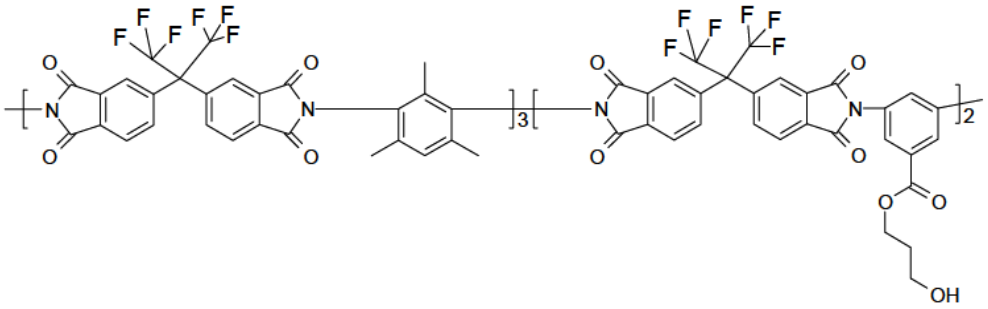

Figure 5.1: Chemical structure of PDMC polymer for hollow fiber spinning.

5.3 Thermal crosslinking

Hollow fiber spin runs were done on the dry-jet/wet-quench spinning system [70]. Crosslinking was conducted on defect-free uncrosslinked hollow fibers. Table 5.1 shows the ideal gas separation performance of uncrosslinked hollow fibers from xlp2 spinning.

Table 5.1: Pure gas separation properties of uncrosslinked xlp2 fibers.

Spinning State	O_2 Perm. (GPU)	$\alpha_{O2/N2}$	$\alpha_{He/N2}$	Skin layer thickness/μ
2	15.8±1.2	4.7±0.4	31.7±4.0	0.45±0.04
3	20.4±0.9	5.9±0.6	-	0.35±0.02
4	13.9±0.2	5.4±0.3	-	0.51±0.01
5	16.3±1.3	4.9±0.5	-	0.44±0.04
6	16.6±0.9	4.5±0.3	30.3±1.4	0.43±0.02
7	36.4±2.5	3.3±0.2	-	0.20

Test conditions: feed pressure: ~100psia, temperature: 35°C.

As discussed in Section 4.2, the skin layer thickness of xlp2 State 7 fibers is underestimated by Equation 4.1 due the defective nature of the skin. The crosslinking reaction, as discussed in Chapter 2 and 3, was carried out by heating fibers in a preheated

vacuum for a set period of time at a constant temperature. Fibers were stored in aluminum foil and sit in the vacuum oven to allow crosslinking reaction occur. Dynamic vacuum creates a driving force to promote the completion of reaction by removing the byproduct-1, 3-propane diol. In the work, crosslinking temperature was between 150^{o}C to 200^{o}C while the crosslinking time was from 1 to 2 hrs.

After crosslinking, the hollow fibers were potted into modules and tested with pure gas. Only one module was prepared for each state since this crosslinking was early in the author's work. The gas permeation data on crosslinked fibers are shown in Table 5.2.

Table 5.2: Pure gas separation properties of crosslinked xlp2 fibers (200^{o}C, 2hrs).

State ID	O_2 Perm. (GPU)	$\alpha_{O2/N2}$
2	15.3	5.3
3	15.4	5.0
4	8.9	5.8
5	9.7	6.0
6	7.4	5.3
7	20.2	3.6

Test conditions: feed pressure: ~100 psia, temperature: 35^{o}C.

All of the crosslinked fibers show slightly improved O_2/N_2 selectivity vs. uncrosslinked fibers. The increase in O_2/N_2 selectivity is between 2% and 15% over uncrosslinked fibers. This increase does not necessarily suggest a significant change of material properties in terms of selectivity. On the other hand, the O_2 permeance dropped between 36% and 56% after crosslinking. The permeance decrease is consistent with the

skin densification. The densified transient layer causes an increase of the effective skin layer thickness and thereby reduces the permeance. To overcome the loss of permeance, less aggressive crosslinking conditions must be utilized, such as lowering the crosslinking temperature or reducing the crosslinking time. This involves the usage of catalyst during crosslinking, which will be discussed in Section 5.4.

5.4 Catalyst assisted crosslinking

To achieve both high CO_2 permeance and CO_2/CH_4 selectivity for industrial application, the crosslinking conditions must be further optimized. The key factor that affects crosslinking degree is the crosslinking temperature. It had been suggested that the catalyst can lower the activation energy of esterification [11, 68] and thereby reduce the crosslinking temperature. In this work, p-toluenesulfonic acid (PTSA), DuPont™ Tyzor® tetra-isopropyl titanate (TPT) and methanesulfonic acid (MSA) were studied to assist the crosslinking reaction [11-12]. The concentration of catalyst was 2g catalyst in 1L ethanol, unless specified otherwise. The details of crosslinking are described in Chapter 3.

The xlp2 State 3 fibers were first crosslinked with PTSA. The pure gas permeation data are shown in Table 5.3.

Table 5.3: Pure gas separation properties of PTSA crosslinked xlp2 State 3 fibers.

Membrane form	O_2 Perm. (GPU)	$\alpha_{O2/N2}$	$\alpha_{He/N2}$
uncrosslinked	20.4±0.9	5.9±0.6	41.8
Crosslinked @PTSA, 150^{o}C 2 hrs	3.7	6.4	48.8

Test conditions: feed pressure: ~100 psia, temperature: 35^{o}C.

From Table 5.3, the PTSA assisted crosslinked hollow fibers show $\alpha_{O2/N2}$ over intrinsic value (dense film $\alpha_{O2/N2}$=4.8), suggesting defect-free crosslinked fibers achieved. No substructure resistance is found in crosslinked fibers since the $\alpha_{He/N2}$ is above the intrinsic selectivity ($\alpha_{He/N2}$=40). However, the O_2 permeance dropped about 82% after catalyst crosslinking. The drop of permeance is likely due to the swelling of fibers in the ethanol/catalyst system. A lower catalyst concentration may be useful to reduce the loss of permeance.

For the thinner skin layer CM5 State 1 hollow fibers, three main crosslinking approaches were studied, as shown in Table 5.4. The thermal crosslinking was done either at 200^{o}C for 2 hrs or at 190^{o}C for 1hr. PTSA was used as the catalyst, but the catalyst concentration was only 1g catalyst in 1L ethanol. The catalyst concentration was significantly reduced compared to the reference [11], which used 103g catalyst in 1L ethanol for the catalyst crosslinking. The pure gas permeation results on those crosslinked fibers are shown in Table 5.4.

Table 5.4: Pure gas separation properties of crosslinked CM5 State 1 fibers.

Fibers form	O_2 Perm. (GPU)	$\alpha_{O2/N2}$
Uncrosslinked	33.7	5.2
Crosslinked@200^{o}C, 2hrs	7.6	5.1
Crosslinked@190^{o}C, 1hr	9.7	5.7
Crosslinked@PTSA, 150^{o}C,1.5hrs	1.6	4.3

Test conditions: feed pressure: ~100psia, temperature: 35^{o}C.

From Table 5.4, the thermal crosslinked CM5 State 1 fibers are defect-free with a moderate O_2 permeance. The 190^{o}C crosslinked fibers have a higher permeance than

200°C crosslinked ones. The PTSA crosslinked fibers have nearly intrinsic O_2/N_2 selectivity (dense film $\alpha_{O2/N2}$=4.8). However, the application of catalyst in the crosslinking process causes a significant drop of the O_2 permeance, that is, ~95% decrease vs. uncrosslinked fibers. The lower catalyst concentration used in CM5 crosslinking do not preserve the permeance as expected. This may suggest that the process of catalyst crosslinking must be modified to embed the catalyst into the fibers appropriately. One possible way to embed the catalyst is dissolving the catalyst in ethanol during the solvent exchange. The fibers are likely to adsorb the catalyst effectively. The hexane is unlikely washing away the catalyst since PTSA does not dissolve in the hexane. This method may significantly reduce the effect of swelling on the permeance of fibers as it avoids the second time of contact of fibers and ethanol.

The PTSA crosslinked hollow fibers were tested with SEM to examine the morphology after catalyst crosslinking. The SEM images are shown in Figure 5.2.

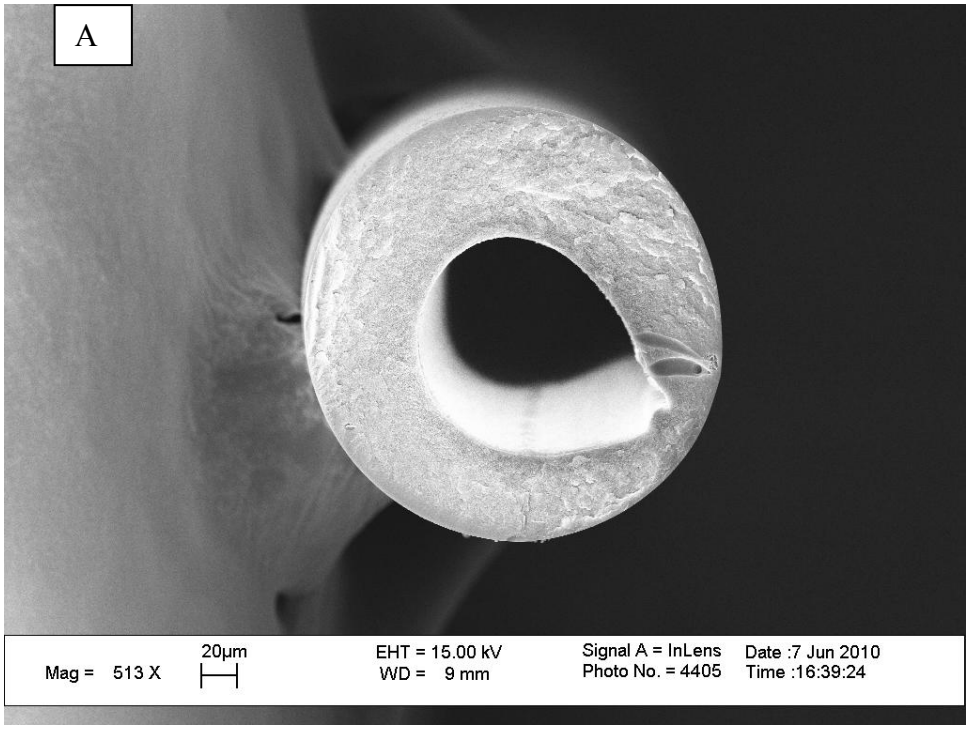

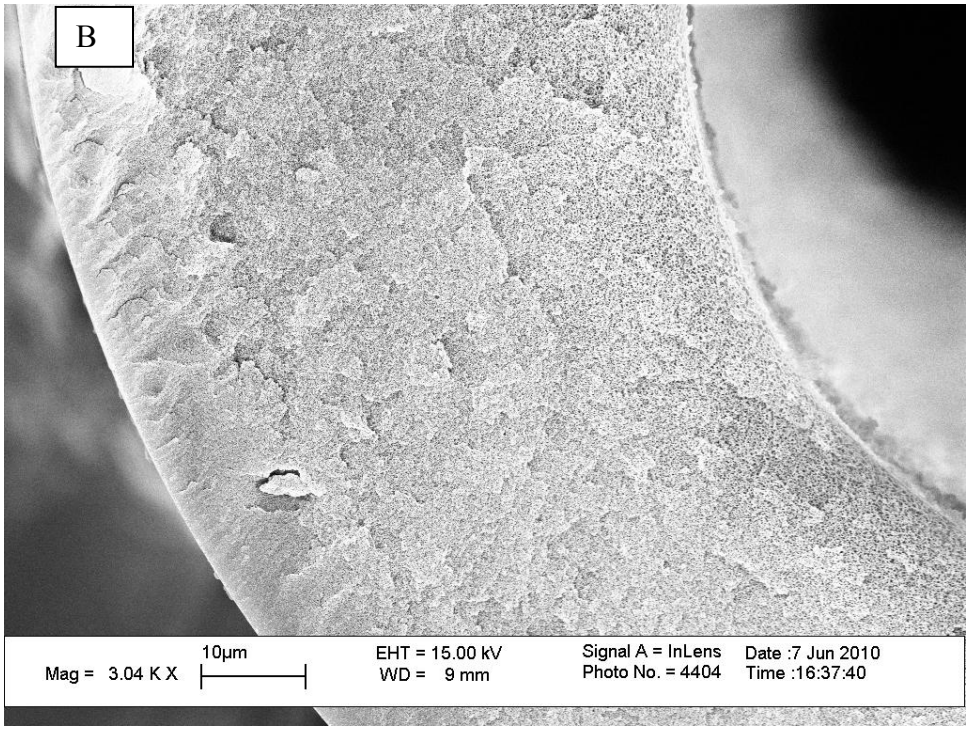
B
10µm
Mag = 3.04 K X
EHT = 15.00 kV
WD = 9 mm
Signal A = InLens
Photo No. = 4404
Date :7 Jun 2010
Time :16:37:40

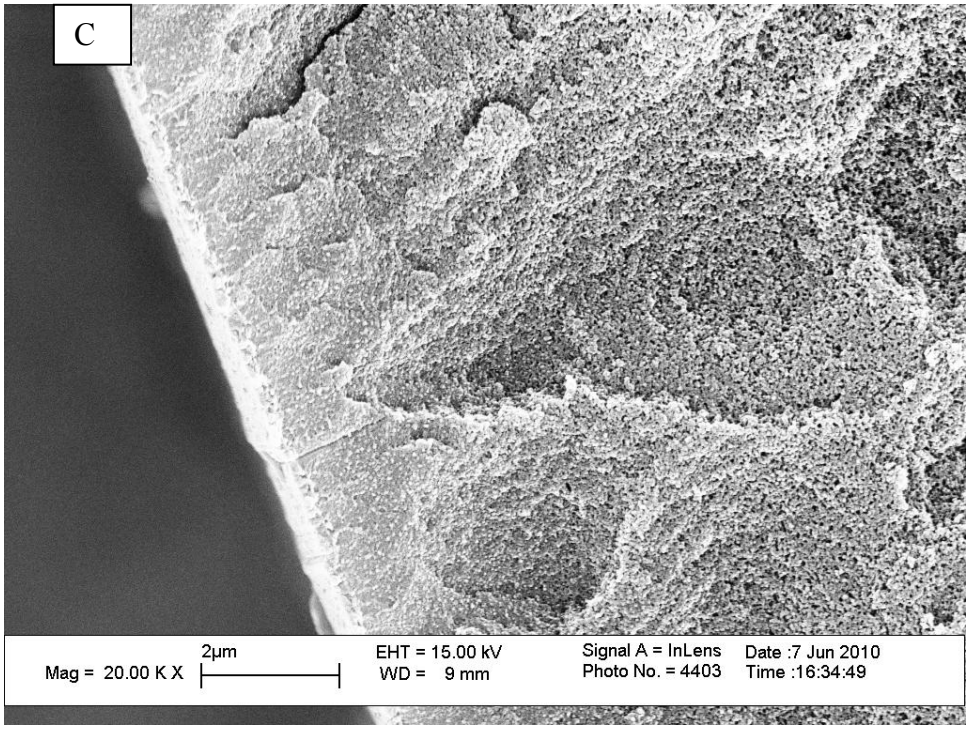
C
2µm
Mag = 20.00 K X
EHT = 15.00 kV
WD = 9 mm
Signal A = InLens
Photo No. = 4403
Date :7 Jun 2010
Time :16:34:49

Figure 5.2: SEM images showing cross sectional structure of PTSA crosslinked CM5 State 1 fibers. Figure (A) shows the cross-section of the fiber; Figure (B) shows the apparent skin layer structure with porous transition layer.

Figure 5.2 showed that the crosslinked fibers show delicate morphology after crosslinking. The crosslinked fibers are nearly concentric and quite circular. The crosslinked fibers have robust skin layer and supporting sub-structure. The fibers were not collapsed during the aggressive crosslinking conditions.

CHAPTER 6

NATURAL GAS SEPARATION WITH HOLLOW FIBERS

6.1 Introduction

Membrane separation technology has advantages for natural gas purification over the traditional amine separation process, as discussed in Chapter 1. In the past sections, defect-free hollow fibers with a skin layer thickness roughly at 0.1μ were successfully fabricated. The hollow fibers were crosslinked either by thermal crosslinking or catalyst assisted crosslinking. Both uncrosslinked and crosslinked fibers were characterized by SEM measurement and ideal gas permeation. This chapter will focus on the separation of CO_2/CH_4 mixtures using these fibers.

The fibers used in this section are identical to those studied in previous sections. The dope composition and spinning conditions were described in Section 4.2. All permeation tests in this chapter were done with mixed gas. 20/80 and 50/50 CO_2/CH_4 model gas mixtures were used to simulate the industrial natural gas well. 50/50 CO_2/CH_4 mixtures were also applied to allow high pressure feed gas permeation. All gas permeation tests were done at 35^{o}C and 200 psia total pressure, unless stated otherwise.

This section contains the natural gas separation properties of both uncrosslinked and crosslinked fibers. The CO_2/CH_4 selectivity and CO_2 permeance of hollow fibers were studied with different feed compositions and high feed pressure. The stability over time of CO_2/CH_4 separation performance of crosslinked fibers was finally evaluated by feeding the fibers with 50/50 CO_2/CH_4 at the maximum test pressure of 650 psia, which corresponds to a CO_2 partial pressure of 325 psia.

6.2 Natural gas separation with uncrosslinked hollow fibers

The mixed permeation was first performed on uncrosslinked hollow fibers from xlp2 spinning with 20/80 CO_2/CH_4 mixed gas. Xlp2 spinning used the "PDMC-74.8k/1.8" polymer and the details of dope composition and spinning parameters of xlp2 spinning can be found in Table 4.1~4.2. The details of mixed gas permeation, including the permeance and selectivity calculation, are described in Appendix B. The permeation results are summarized in Table 6.1.

Table 6.1: Mixed gas separation properties of uncrosslinked xlp2 spinning fibers.

State ID	CO_2 Perm. (GPU)	$\alpha_{CO2/CH4}$
3	98	22.8
4	57	32.0
5	65	22.5
6	64	28.8

Test conditions: 20/80 CO_2/CH_4, pressure: ~200 psia, 35^{o}C.

For the gas mixture studied in this chapter, the fugacity difference across the membrane was used as the driving force of permeation instead of pressure difference to eliminate the effect of non-ideality of gas phase at high pressure (discussed in Section 2.5.4).

The uncrosslinked xlp2 fibers exhibit high CO_2/CH_4 selectivity and CO_2 permeance up to 98 GPU. The State 4 fibers have nearly intrinsic selectivity (the dense film $\alpha_{CO2/CH4}$~34) [12-13]. The CO_2/CH_4 selectivity of other states (State 2, 5, and 6) is lower than the dense film, yet still meets the minimum target of separation performance

set by our sponsors--Dr Miller, et al. ($\alpha_{CO2/CH4}$>20). As shown in Section 4.2.2, the State 6 fibers has a He/N_2 selectivity of 30.3 which is lower than the intrinsic value (dense film $\alpha_{He/N2}$=40) [12], indicating that there may exist minor substructure resistance in those fibers. Nevertheless, the lower selectivity for CO_2/CH_4 separation necessitates further spinning optimization of the uncrosslinked fibers.

Another spinning (CM5 spinning) was conducted to optimize the spinning conditions to improve the CO_2/CH_4 selectivity. CM5 spinning used the "PDMC-74.8k/1.8" polymer and the details of dope composition and spinning parameters of xlp2 spinning are described in Table 4.4~4.5. The uncrosslinked CM5 fibers were tested with CO_2/CH_4 mixed gas. The permeation data are shown in Table 6.2.

Table 6.2: Mixed gas separation properties of uncrosslinked CM5 hollow fibers.

State ID	CO_2 Perm. (GPU)	$\alpha_{CO2/CH4}$
1	99	33.9
2	56	29.5
6	62	26.2

Test conditions: 10/90 CO_2/CH_4, pressure: ~200 psia, temperature: 35^{o}C.

Table 6.2 shows that hollow fibers from CM5 state 1 have intrinsic CO_2/CH_4 selectivity (the dense film $\alpha_{CO2/CH4}$=34.0) with a CO_2 permeance up to 99 GPU. This high CO_2 permeance is due to the low air gap used during the spinning. State 1 had an air gap only 2 cm and this produced a thin skin layer thickness lower to 0.21μ (discussed in Section 4.3). State 2 and 6 have relative lower CO_2 permeance due to a higher air gap than State 1. State 1 fibers have the highest CO_2 permeance and intrinsic selectivity,

thereby favored by the industrial application. Although high permeance and adequate selectivity was achieved in CM5 spinning, the CO_2 permeance can be further improved, as will be shown in CM9 and CM10 spinning.

Note that although CM9 and CM10 had the same dope compositions, CM9 was based on the lower molecular weight sample ("PDMC-74.8k/1.8") used for xlp2 and CM5. On the other hand, CM10 was based on a higher molecular weight sample not obtained from Chevron that was monoesterified in our labs. The dope composition of CM9 and CM10 spinning is identical with CM5 spinning and the details of dope composition are shown in Table 4.4. The details of CM9 and CM10 spinning conditions can be found in Table 4.10 and 4.12. The uncrosslinked hollow fibers from the identical dope compositions, but different polymer molecular weight samples, CM9 and CM10, were tested with mixed gas and Table 6.3 shows the permeation results.

Table 6.3: Mixed gas separation properties of uncrosslinked CM9-2 and CM10-3 fibers.

Fiber state	CO2 Perm. (GPU)	$\alpha_{CO2/CH4}$
CM9-2	214±17	25.6±2.8
CM10-3*	237±23	27.7±2.7

Test conditions: 50/50 CO_2/CH_4, 200psia, 35^oC; *20/80 CO2/CH4.

From Table 6.3, the CO_2 permeance of uncrosslinked hollow fibers is significantly improved compared to CM5 in the CM9 and CM10 spinning. The CO_2 permeance of CM9 State 2 fibers is 214 GPU with a CO_2/CH_4 selectivity of 25.6. The lower selectivity of CM9-2 fibers is likely due to the aggressive spinning conditions (air gap=1 cm) for the low molecular weight polymer (Mw~74,800). The high molecular

weight polymer in CM10 spinning produced an even higher CO_2 permeance up to 237 GPU with acceptable intrinsic CO_2/CH_4 selectivity, suggesting the polymer used in CM10 spinning have better overall separation properties than that in CM9 spinning. As discussed in Section 4.3 and 4.4, the He/N_2 selectivity of uncrosslinked CM9-2 and CM10-3 fibers are close or above the intrinsic values (dense film $\alpha_{He/N2}$=40) [12], suggesting that there is no apparent substructure resistance in those fibers.

To summarize, a CO_2 permeance of 237 GPU with acceptable CO_2/CH_4 selectivity are achieved for the uncrosslinked PDMC hollow fibers. However, since the uncrosslinked PDMC hollow fibers are easily plasticized by high CO_2 pressure [11-12], the hollow fibers are subsequently crosslinked in order to suppress the CO_2 plasticization in natural gas purification. Section 6.3 will discuss the natural gas separation with crosslinked fibers.

6.3 Natural gas separation with crosslinked hollow fibers

The crosslinked hollow fibers from xlp2 spinning were tested with mixed gas. Recall that xlp2 refers to the lower molecular weight "PDMC-74.8k/1.8" formulated into a spin dope with composition close the two phase boundary in Figure 4.4. The mixed gas permeation results are shown in Table 6.4.

Table 6.4: Mixed gas separation properties of crosslinked xlp2 hollow fibers.

State ID/ membrane form	CO_2 Perm. (GPU)	$\alpha_{CO2/CH4}$
3	66	27.6
4	38	36.0
5	41	36.7
6	30	31.4
Crosslinked dense film (200°C, 2hrs)	63 Barrer	31

Fiber test conditions: 20/80 CO_2/CH_4, pressure: ~200 psia, 35°C; dense film test conditions: pure gas at ~100 psia, 35 °C; crosslinking conditions: 200°C, 2 hrs.

Table 6.4 shows that CO_2 permeance dropped dramatically from 57~96 GPU (shown in Table 6.1) to 30~66 GPU after crosslinking. The CO_2 permeance of crosslinked fibers decreased (up to 53%) while the CO_2/CH_4 selectivity increased considerably (up to 63% for State 5). State 3 fibers have a CO_2 permeance up to 66 GPU and the selectivity is close to the dense film value. This high permeance is due to the lowest air gap (10 cm) in the spinning. No uncertainty limits can be reported due to only single module testing done with the small spin states done with xlp2. State 4, 5 and 6 fibers have CO_2/CH_4 selectivity above the dense film value, which may be due to polymer chain orientation during spinning [12, 62-63]. State 6 fibers have the lowest permeance due to the highest air gap (30 cm). The densification of hollow fiber transient layer during crosslinking causes a thicker effective skin layer and thereby reduces the CO_2 permeance. On the other hand, minor defects, like local micro-void packing defects, in the uncrosslinked fibers may be cured by the densification effect so that the increase of selectivity is observed.

DuPont™ Tyzor® tetra-isopropyl titanate (TPT) was also used to assist the crosslinking of xlp2 State 3 fibers. The mixed gas permeation of catalyst assisted crosslinking on xlp2 State 3 fibers were shown in Table 6.5.

Table 6.5: Mixed gas separation properties of crosslinked xlp2 State 3 fibers.

Membrane form	CO_2 Perm. (GPU)	$\alpha_{CO2/CH4}$
Uncrosslinked	98	22.8
Crosslinked@200°C, 2 hrs	66	27.6
Crosslinked@TPT, 200°C, 2 hrs	16	32.7
Crosslinked@TPT, 200°C, 2 hrs*	15.7	38.6

Test conditions: 20/80 CO_2/CH_4, pressure: ~200 psia, 35°C; *: 50/50 CO_2/CH_4.

Table 6.5 shows that the catalyst crosslinked fibers have close to intrinsic or even higher CO_2/CH_4 selectivity (thermal crosslinked dense film $\alpha_{CO2/CH4}$=31). Moreover, the CO_2/CH_4 selectivity of thermal crosslinked fibers is increased 21% vs. uncrosslinked fibers while the catalyst crosslinked fibers increase ~43% vs. uncrosslinked ones. On the other hand, the thermal crosslinked fibers exhibit a high CO_2 permeance up to 66 GPU, only ~33% decrease vs. uncrosslinked fibers while the tetra-isopropyl titanate (TPT) crosslinked CO_2 permeance is reduced ~84% vs. uncrosslinked ones. The catalyst crosslinked fibers show a CO_2 permeance of ~16 GPU. While the catalyst crosslinked fibers are advantageous over thermal crosslinking in terms of selectivity, the lower CO_2 permeance makes them less desirable for practical application. Different crosslinking methods were explored in CM5 fibers, as discussed in Section 5.4.

The CM5 State 1 fibers were crosslinked using different approaches, as discussed in Section 5.4. Instead of using previous crosslinking conditions for xlp2 fibers, a lower temperature and a shorter time was used for CM5 State 1 fibers. This was pursued to see if less loss in permeance could be achieved vs. the data in Table 6.5. The results of mixed gas permeation of CM5 State 1 fibers are shown in Table 6.6.

Table 6.6: Mixed gas separation properties of crosslinked CM5 State 1 fibers.

Crosslinking approach	CO_2 Perm. (GPU)	$\alpha_{CO2/CH4}$
Uncrosslinked	97.4±7.7	36.6±0.3
Crosslinked@190°C,1hr	46.1±2.3	42.4±0.5
Crosslinked@PTSA 150°C,1.5hrs	7.1±0.3	40.7±1.9

Test conditions: 50/50 CO_2/CH_4, pressure ~200 psia, 35^{o}C.

Table 6.6 shows that the 190^{o}C thermal crosslinked CM5-1 fibers have a high CO_2/CH_4 selectivity above the intrinsic value (dense film $\alpha_{CO2/CH4}$=31) and CO_2 permeance higher than 46.1 GPU, suggesting defect-free crosslinked fibers were achieved. Moreover, the P-toluenesulfonic acid (PTSA) crosslinked CM5-1 fibers also have a CO_2/CH_4 selectivity above dense film value. However, the CO_2 permeance of PTSA crosslinked CM5-1 fibers is only 7.1 GPU. As discussed in Section 5.4, the lower PTSA catalyst concentration (only 0.006 M vs. 0.6 M in reference [11]) used in CM5 crosslinking does not preserve the permeance as expected. This may suggest future work must be done on the catalyst crosslinking optimization to overcome the loss of permeance.

Mixed gas test were also carried out on the CM9 State 2 fibers. Recall that these samples were prepared with the same low molecular weight “PDMC-74.8k/1.8” sample

used for CM5; and the same dope composition is an attempt to improve the CO_2 permeance. The permeation results are shown in Table 6.7. At least two modules were made to check the experimental reproducibility for this state.

Table 6.7: Mixed gas separation properties of crosslinked CM9 State 2 fibers.

Fiber state	CO_2 Perm. (GPU)	$\alpha_{CO2/CH4}$
Uncrosslinked	214±17	25.6±2.8
Crosslinked@200°C, 2 hrs	102±5	26.2±0.2

Test condition: ~200 psia, 35°C, 50/50 CO_2/CH_4.

From Table 6.7, the uncrosslinked CM9 State 2 fibers have a CO_2 permeance up to 214 GPU with a $\alpha_{CO2/CH4}$ of 25.6. After crosslinking at 200°C for 2 hrs, the crosslinked CM 9 State 2 fibers show CO_2 permeance of 102 GPU. This is a significant improvement of CO_2 permeance for crosslinked fibers, ~77% increase vs. the data reported in reference [12] (CO_2 permeance=57 GPU). On the other hand, the crosslinked CM9 State 2 fibers have a CO_2/CH_4 selectivity of 26.2, which is essentially close to the intrinsic value (dense film $\alpha_{CO2/CH4}$=31). The improvement of CO_2 permeance is likely due to the lower air gap used in CM 9 spinning (air gap =1 cm for State 2), compared to CM 5 spinning (air gap=2 cm for State 1), as shown in Table 4.5 and 4.10. A lower air gap tends to form a thinner skin layer due to less evaporation of THF during spinning and thereby increases the permeance of hollow fibers.

Moreover, mixed gas test were performed on the crosslinked CM10 State 3 fibers. Recall that these samples were prepared with the new higher molecular weight dope, but with the same dope composition as CM5 and CM9. The crosslinking conditions and

permeation results are shown in Table 6.8. At least two modules were made to check the experimental reproducibility of this state.

Table 6.8: Mixed gas separation properties of crosslinked CM10 State 3 fibers.

Fiber state	CO_2 Perm. (GPU)	$\alpha_{CO2/CH4}$
Uncrosslinked*	237±23	27.7±2.7
Crosslinked@200°C, 2 hrs	65±2	32.4±0.5

Test conditions: 50/50 CO_2/CH_4, ~200 psia, 35°C; *: 20/80 CO_2/CH_4, ~200 psia, 35°C.

The mixed gas permeation of uncrosslinked fibers was not done with 50/50 CO_2/CH_4 due to difficulties in keeping a stage cut lower than 1% during the permeation for the high flux membranes. Table 6.8 shows that the crosslinked CM10 State 3 fibers had a CO_2 permeance of 65 GPU. Moreover, the CO_2/CH_4 selectivity of crosslinked fibers is 32.4, which is slightly higher than the dense film value. This is likely due to the chain orientation during the spinning process [12, 62-63].

To sum up the natural gas separation with crosslinked PDMC hollow fibers, the crosslinked fibers achieve a high CO_2 permeance up to 102 GPU (CM9 State 2 fibers) by thermal crosslinking at 200°C for 2 hrs. This high CO_2 permeance is ~77% increase vs. the reference [12]. The CO_2/CH_4 selectivity of crosslinked fibers is close to or above the dense film value, suggesting defect-free crosslinked fibers achieved. To further probe the separation performance and stability of crosslinked fibers under realistic feed conditions, the mixed gas permeation was conducted by using high feeding pressure of 50/50 CO_2/CH_4 and exposing the fibers in the high pressure for a set period of time (such as

5~24 hrs). Section 6.4 and 6.5 will discuss the high pressure mixed gas permeation of crosslinked hollow fibers.

6.4 Effect of feed pressure on hollow fiber performance

The separation properties of crosslinked hollow fibers were further evaluated by using the 50/50 CO_2/CH_4 gas mixture at a feed pressure up to ~700 psia. Figure 6.1~6.2 show the mixed permeation results of crosslinked fibers from CM9 State 2 spinning. The fibers were crosslinked at 200°C for 2hrs.

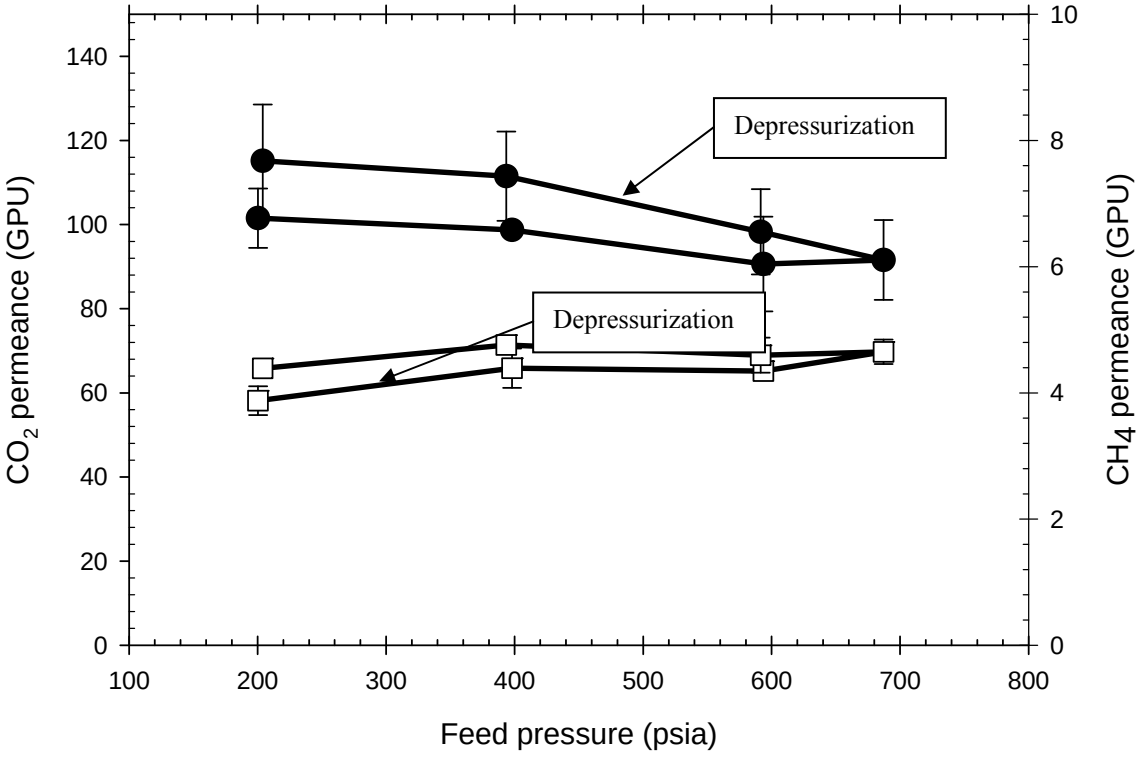

Figure 6.1: CO_2 and CH_4 permeances of crosslinked hollow fibers vs. feed pressure using 50/50 CO_2/CH_4 at 35°C. Two modules were prepared to check the reproducibility for each state.

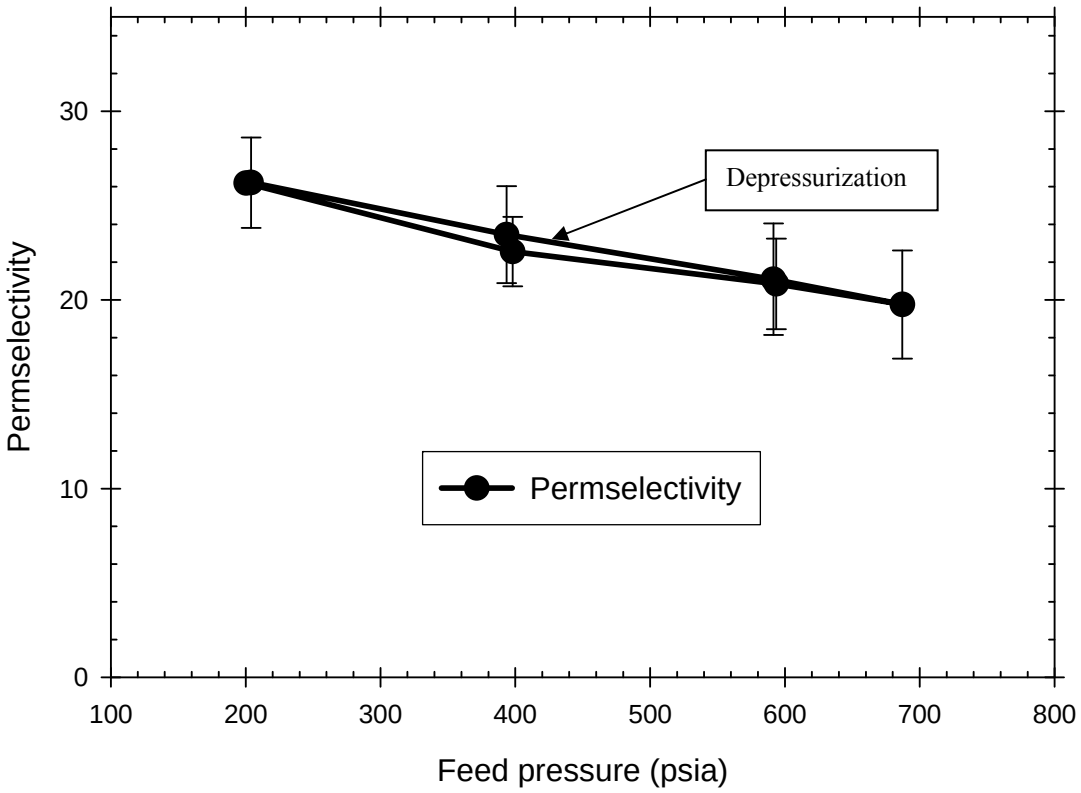

Figure 6.2: Permselectivity of crosslinked hollow fibers vs. feed pressure using 50/50 CO_2/CH_4 at 35°C. Two modules were prepared to check the reproducibility for each state.

From Figure 6.1, the crosslinked hollow fibers do not show any significant upswing in the curve of CO_2 permeance vs. feed pressure, suggesting the crosslinked fibers are stable under the maximum test feeding pressure of 700 psia, which corresponds to a CO_2 partial pressure of 350 psia. Figure 6.2 shows that this high feed pressure did not cause a significant loss of permselectivity of CO_2/CH_4. After depressurization, the crosslinked fibers regained the high permselectivity at the previous feed pressures. The stable permeance and high selectivity under such aggressive feed conditions clearly suggests that the crosslinked fibers can significantly suppress the plasticization induced by the high CO_2 partial pressure.

6.5 Stability of hollow fiber performance over time

Further experiments were performed on the crosslinked hollow fibers to study their resistance to plasticization in the presence of high CO_2 partial pressures over long time periods. The mixed gas permeation of crosslinked CM9 State 2 fibers (200°C, 2 hrs) were done with 50/50 CO_2/CH_4 at the maximum test pressure of 650 psia, which corresponds to a CO_2 partial pressure of 325 psia.

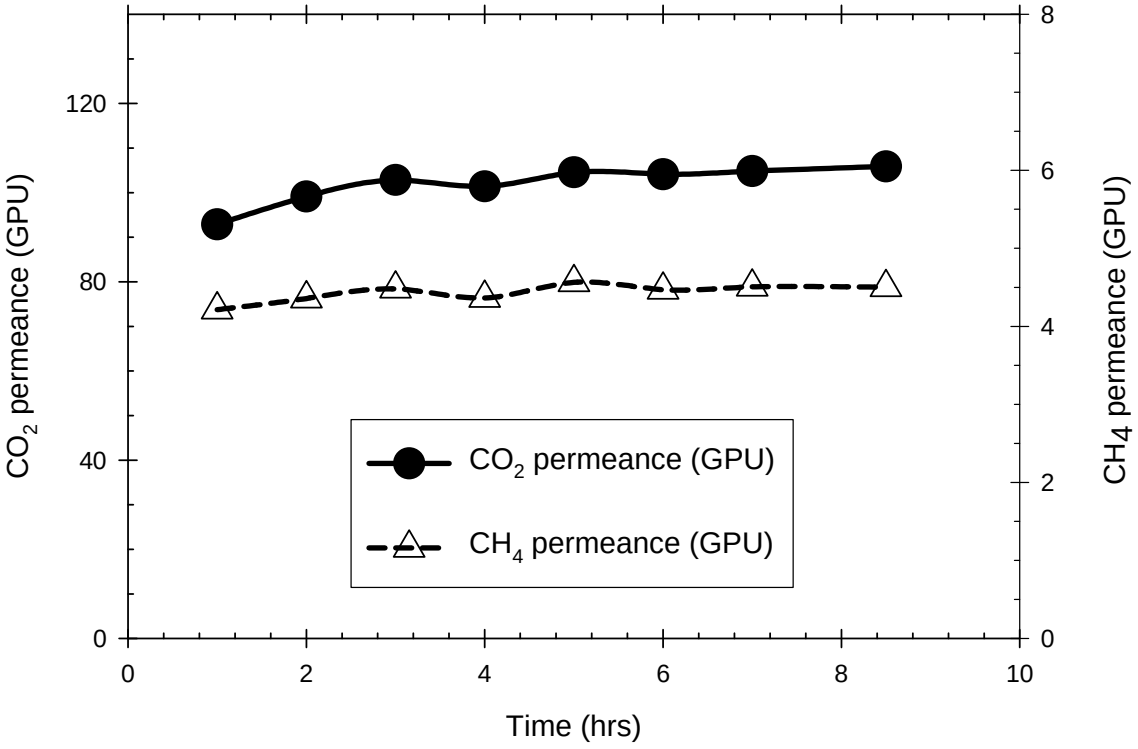

Figure 6.3: Stability over time of CO_2 and CH_4 permeances of crosslinked hollow fibers under high feed 50/50 CO_2/CH_4, test conditions: ~650 psia, 35°C.

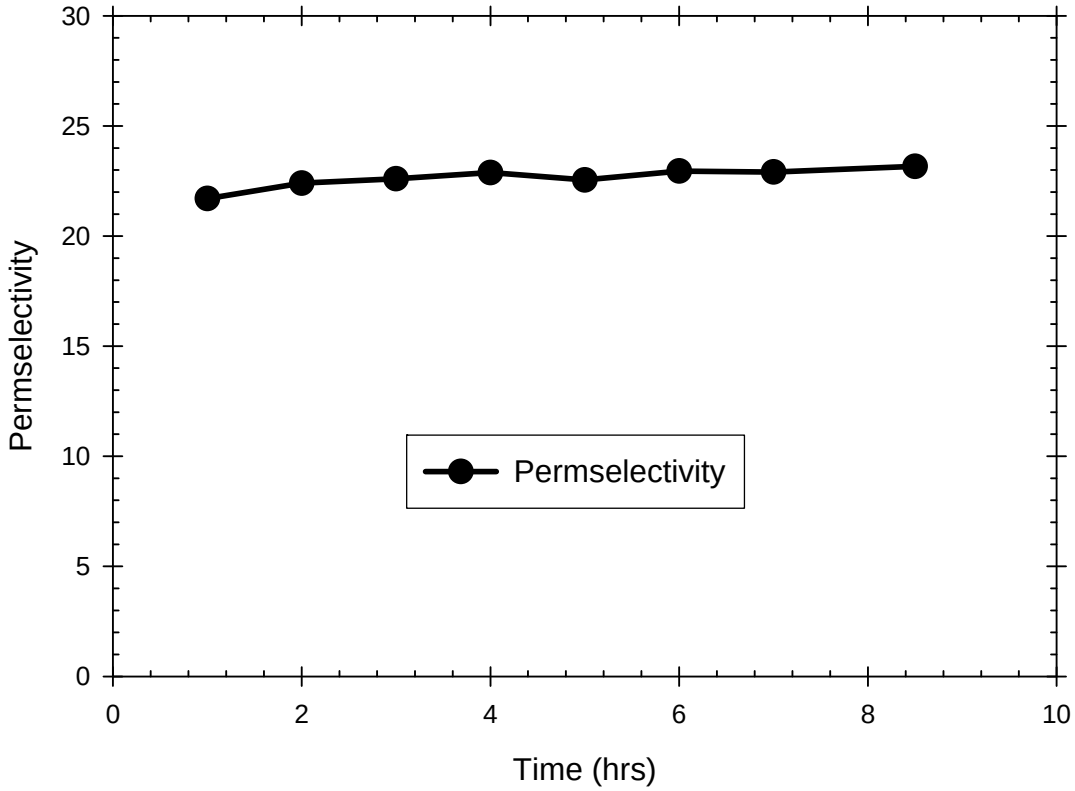

Figure 6.4: Stability over time of permselectivity of crosslinked hollow fibers under high feed 50/50 CO_2/CH_4, test conditions: ~650 psia, 35^oC.

Figure 6.3~6.4 show that the crosslinked fibers perform well and maintain high CO_2 permeance and permselectivity with 325 psia CO_2 in the feed during the ~9 hrs exposure. There is a slight increase of permeance and permselectivity initially (first 3 hrs). Nevertheless, the crosslinked fibers retain the good separation performance after the 9 hrs exposure of high feeding CO_2 content, suggesting that the CO_2 induced plasticization was well controlled by the thermal crosslinking.

CHARPTER 7

CONCLUSIONS AND RECOMMENDATIONS

Membrane separation technology is promising in the field of natural gas separation. This work focuses on the study of 6FDA-DAM: DABA (3: 2) based polymer to develop PDMC asymmetric hollow fibers with commercial viable separation performance. The final chapter summarizes conclusions of this work and provides recommendations for further research.

7.1 Conclusions

7.1.1 Formation of ideally thin defect-free skin layer of hollow fibers

Defect-free selective hollow fibers with ideally thin skin layer were successfully fabricated through the dry-jet/wet quench bath spinning process. The hollow fibers with desired skin thickness were spun from the propanediol monoesterified crosslinkable (PDMC) polymer consisting of 6FDA dianhydride and DAM: DABA (3: 2) monomers. The defect-free hollow fibers exhibit ideally circular and concentric morphology. The skin layer thickness of hollow fiber is on the order of 0.1 μ without defects or substructure resistance.

The defect-free hollow fibers achieved the desired thin skin layer thickness through the work of the three main aspects. The hollow fiber spinning conditions were first optimized by varying the important spinning parameters, including the spinneret temperature, air gap and take-up rate. Moreover, the phase separation of the PDMC polymer was studied and the binodal was determined through the cloud point technique. With the information from binodal curve, the dope composition was reformulated to

move closer to the binodal and produce defect-free fibers with thinner skin layer. Finally, the effect of molecular weight on the separation performance was studied by using a new polymer batch with higher molecular weight. The high molecular weight polymer batch yielded the thin skin layer thickness lower to 0.1 μ without defects or substructure resistance.

7.1.2. Crosslinking of defect-free thin skin hollow fibers

The defect-free hollow fibers were crosslinked through two main approaches: thermal crosslinking and catalyst assisted crosslinking. The temperature and time of thermal crosslinking were studied on the PDMC hollow fibers. The ideal gas permeation shows that the thermal crosslinking fibers have an O_2 permeance up to 15.4 GPU with above intrinsic O_2/N_2 selectivity (dense film $\alpha_{O2/N2}$=4.8). The crosslinked fibers show delicate cross sectional morphology and robust structures.

The idea of using catalyst during crosslinking process is to reduce the aggressive crosslinking temperature and increase the productivity of hollow fibers without the loss of selectivity. P-toluenesulfonic acid (PTSA), DuPont™ Tyzor® tetra-isopropyl titanate (TPT) and methanesulfonic acid (MSA) were applied to the crosslinking and an improved O_2/N_2 selectivity was achieved. However, the O_2 permeance of catalyst crosslinked fibers dropped significantly. Further optimization work on the catalyst crosslinking must be done to produce defect-free fibers with improved permeance.

7.1.3 Natural gas purification with hollow fibers

The natural gas purification of hollow fibers were studied with the model feed gas mixture. Different CO_2 concentrations in the gas feed were applied on the hollow fibers. 50/50 CO_2/CH_4 mixed gas was used to study the fibers with aggressive feed conditions. The uncrosslinked hollow fibers yield a CO_2 permeance up to 237 GPU with a relatively

high CO_2/CH_4 selectivity. The crosslinked hollow fibers exhibit a CO_2 permeance up to 102 GPU, which is significantly improved vs. previous researchers' results. It is also found that crosslinked fibers exhibit a stable CO_2 permeance and permselectivity under a partial CO_2 pressure up to 350 psia and a period of 9 hrs exposure in 325 psia partial CO_2 pressure.

7.2 Recommendations for future work

7.2.1 Skin layer optimization of crosslinked hollow fibers

Since the crosslinked fibers are preferred in the practical application, further work to form a thinner defect-free skin of crosslinked hollow fibers must be done with the PDMC polymer. The uncrosslinked hollow fibers show a CO_2 permeance up to 237 GPU. However, after thermal crosslinking, the hollow fibers have a CO_2 permeance of ~ 102 GPU. The skin layer thickness of crosslinked fibers in this study is on the order of ~0.6 μ. This clearly suggests that there is plenty of room to improve the productivity of crosslinked hollow fibers by reducing the skin layer thickness.

As discussed in Chapter 2 and 3, catalyst can lower the crosslinking temperature by reducing the activation energy of crosslinking reaction. Chapter 4 shows that catalyst assisted crosslinking exhibits some advantages over conventional thermal crosslinking in terms of high selectivity. However, the significant loss of CO_2 permeance during catalyst crosslinking indicates that further optimization work must be pursued. This involves the study of embedding the catalyst into fibers and the optimization of crosslinking conditions (such as crosslinkng temperature and crosslinking environment). One possible way to embed the catalyst into hollow fibers is adding the catalyst during the solvent exchange step.

7.2.2 Aggressive feed conditions

The hollow fibers in this work were tested with high feed pressure up to 700 psia. 50/50 CO_2/CH_4 was applied on the hollow fibers to study the separation performance against high CO_2 content. However, high feed pressure (over 700 psia) of 50/50 mixed gas was not performed on the high permeance fibers due to the difficulties of maintaining a lower stage cut below 1%. Further optimization work must be done on mixed gas permeation of crosslinked fibers with high CO_2 content. On the other hand, impurities, such as toluene, H_2O and H_2S, may exist in the gas streams in practical feeding. The separation performance of crosslinked hollow fibers under those rigid feed condition must be further evaluated by feeding mixed gas with contaminants.

7.2.3 Dual layer hollow fiber spinning

Although the PDMC hollow fibers exhibit excellent separation performance in terms of high productivity, the PDMC polymer is expensive. The cost of polymer can be reduced significantly by dual layer hollow fiber spinning technology. In this technique, the expensive PDMC polymer is used on the sheath layer and other commercially less expensive materials are used on the core layer. The adhesion between the core layer polymer and sheath layer polymer must be considered during the dual layer spinning. Cellulose acetate is a good choice to serve as the core layer polymer and can be easily integrated with the PDMC polymer [12].

APPENDIX A: HOLLOW FIBER MODULE FABRICATION [11, 27, 71]

The hollow fiber modules are commonly used as the platform for the gas permeation of hollow fibers. Those modules connect the permeation system and the hollow fibers and have a key role in permeation test, either pure gas or mixed gas permeation. This appendix describes the parts and procedures of fabricating double-ended lab-scale hollow fibers modules.

A.1 Parts of a module

The parts used in the how fiber modules are summarized in the Table A.1.

Table A.1: Parts required for construction of hollow fiber modules

Name	Manufacturer	Notes
Ferrules	Swagelok®	Brass or Stainless Steel
Nut	Swagelok®	Brass or Stainless Steel
Female Adapter	Swagelok®	Brass or Stainless Steel
Male Adapter	Swagelok®	Brass or Stainless Steel
Tee	Swagelok®	Brass or Stainless Steel
Metal Tubing	Swagelok®	Brass or Stainless Steel
Cap	Swagelok®	Brass or Stainless Steel
Plug	Swagelok®	Brass or Stainless Steel
Tygon Tubing	Fisher Scientific	
Epoxy	GC Electronics	

A.2 Procedure of making modules

The hollow fibers modules without fibers inside, called blank modules, consist of the parts shown in Figure A.1. The procedures of making blank modules are showing in the following steps:

a) Cut a 3~10cm long ¼" S.S. tubing;

b) Cover the two ends with ¼" S.S. nut and ferrules;

c) Connect the nut with a tee on both ends;

d) Attach nuts on female adapters and connect them to the tee;

After the blank modules are constructed, the hollow fibers are added into the blank modules. The steps are as following:

a) Choose at least one hollow fiber;

b) Tie the fibers if necessary and insert into the blank modules;

c) Seal the fibers with Teflon tape or paper towel;

d) Add the epoxy to the female adapters;

e) Fill the female adapter with a male adapter and screw the male adapter until the epoxy filled the Tygon tubing part;

f) Wait till the epoxy solidified and repeat step d) and e) to fill another end of the module with male adapters;

g) After solidification of both ends, the modules are ready for permeation test.

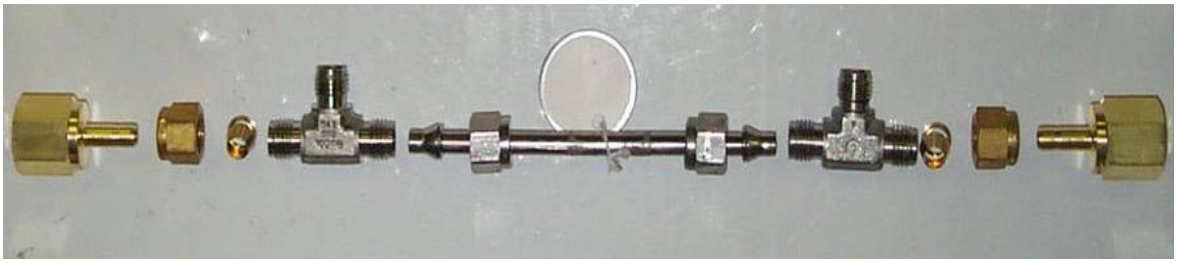

Figure A.1: Parts of a module

APPENDIX B: GAS PERMEATION OF HOLLOW FIBERS

The appendix describes the gas permeation used in this work, including the pure gas permeation and mixed gas permeation. The permeation tests are done in the permeation system.

B. 1: Pure gas permeation

B. 1.1 Permeation setup

Since the bore feed is preferred for pure gas permeation, multiple modules can be tested simultaneously. Connect the modules with tees, Union Crosses and Female-Female Unions, as shown in Figure B.1.

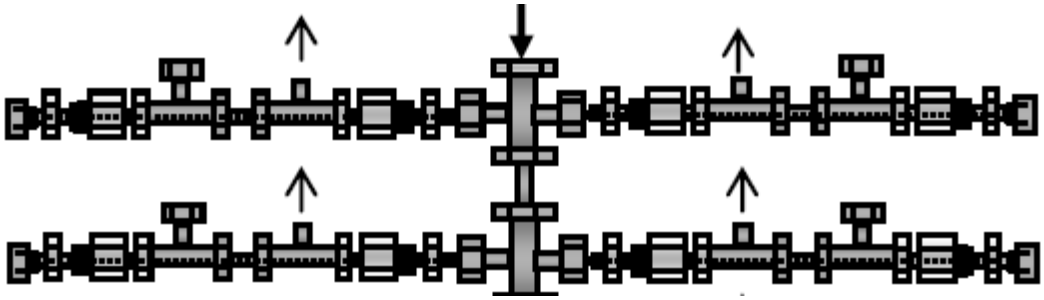

Figure B.1: Multiple modules permeation by bore feed method. Arrow shows the flow directions of feed gas [12].

B. 1.2 Permeation test

B.1.2.1 Purge all of the modules with the pure gas [11]:

a) Open the retentate outlet on all the modules and the feed gas cylinder;

b) Let the gas pressurize the all system for a few seconds and close the feed;

c) When the pressure drops to ~20psia, reopen the feed cylinder and repeat the above step for three more time;

d) Close the retentate of all modules and maintain the feed pressure at the desired level;

e) Wait ~15min for the equilibrium of permeation and temperature.

B. 1.2.2 Permeation test

a) After 15min's equilibrium, record the permeate flow rate with bubble flow meter or digital flow meter.

b) After the first record, wait 45mins and repeat the recording of the permeate flow rate;

c) Compare those two recording, if the results are within 5% difference, permeation is done; if not, repeat the aforementioned step until the difference of results below 5%;

d) Close the cylinder and remove the modules from permeation system.

B.1.2.3 Data analysis

The permeance of each pure gas is calculated according to the definition of permeance in GPU, as shown in Equation B.1:

$$\frac{P_i}{l} = 10^{-6} \frac{(\text{Permeate flow}) \cdot 273.15}{T \cdot A \cdot \Delta p \cdot 5.17} \tag{B.1}$$

a) Permeate flow is in mL/sec.

b) T is the testing temperature in Kelvin.

c) A is the area available for permeation in cm^2.

d) Δp is the pressure drop between upstream and downstream sides of the membrane in psi.

The ideal gas selectivity is ratio of the permeance of a gas pair:

$$\alpha_{ij} = \frac{P_i / l}{P_j / l} \tag{B.2}$$

B. 2: Mixed gas permeation[11, 32]

B.2.1 Gas Chromatograph (GC) Calibration

The GC must be calibrated before using. Sample gases with known gas composition are used to conduct the GC calibration.

B.2.1.1 Sample test

a) Turn on helium and set the feed pressure to 30psi (show on GC);

b) Turn on GC and set the column temperature to 90^{o}C; Turn on the integrator;

c) Set the initial oven temperature to 90^{o}C, initial time 7~10mins and final oven temperature to 90^{o}C;

d) Connect the sample gas to the GC and let the GC warm up for one hour;

e) After equilibrium of the GC, feed the GC with sample gas and control the feed pressure at certain level by vacuum valve (ideally 5 torr and above);

f) Push "start" on GC;

g) Wait until hear two sounds of pneumatic valves and open the vacuum value;

h) Once the integrator prints out the peak area for each component of the sample gas, repeat the step e)~g) at least three times;

i) Record the run number and sample gas composition.

B 2.1.2 Data analysis

In a two component mixture, the response factor, λ, is given by

$$\frac{y_i}{y_j} = \lambda \frac{A_i}{A_j} \tag{B.3}$$

Where y_i is the gas mole fraction of component i and A_i is the peak area of component i given by the gas chromatograph. In the experiments, the two components, CO_2 and CH_4, are the gas pair of interest to measure the selectivity and permeance. The response factor can be determined from gas samples of known compositions. The response factor depends on the carrier gas, feed pressure, oven temperature, and gas compositions. With the response factor, the unknown gas composition can be calculated by the GC.

B.2.2 GC setup

a) Turn on helium and set the feed pressure to 30 psia (show on GC);

b) Turn on GC and set the column temperature to 90^{o}C;

c) Set the initial oven temperature to 90^{o}C, initial time 7~10mins and final oven temperature to 90^{o}C;

d) Connect the module to the GC and let the GC warm up for one hour;

e) Turn on the integrator.

B.2.3 Modules setup

Shell feed is preferred in mixed gas permeation. That means only one module can be tested one time in the mixed gas permeation system.

a) Attach one shell side with mixed gas cylinder. The other side is connected to a flow meter;

b) Close one end of the module with a cap and connect the other end to a bubble meter. Make sure the feed flow and permeate flow are counter-current flows;

c) Attach a T-valve to the permeate side to allow the permeate to go into GC;

d) Adjust the feed pressure to the desired level, usually from 200~1000psia;

e) Set the retentate flow rate by adjusting the valve in the retentate side. The ratio of permeate flow rate to retentate flow rate (stage cut) must be below 1%;

B.2.4 Modules testing

a) After the module is setup in the permeation system, wait at least 15mins for equilibrium of both the GC and permeation cells.

b) Measure and record the following:

i. Module ID;

ii. Feed composition;

iii. Total feed pressure;

iv. Retentate flow rate;

v. Retentate pressure;

vi. Permeate flow rate;

vii. Permeate pressure rate;

viii. Operation temperature.

c) Switch the T-valve to the GC and feed the GC with the permeate gas;

d) Adjust the vacuum valve to ensure the feed pressure of GC the same as calibration work;

e) Start the GC and record the run number;

f) Repeat c~e at least three time;

g) Wait another 45mins and repeat the test. If the data gives the close results of permeation composition, the measurement is valid. If not, wait again and repeat the previous steps until close data achieved.

h) After permeation test, adjust the oven temperature to $30^{o}C$

i) Wait the oven temperature reaches $30^{o}C$ and close the GC.

j) After the GC cool down in about 1hour, close the all regulators.

B.2.5 Analysis

a) Calculate the real permeate composition by the peak area of each component in the permeance flow and GC calibration work.

b) The permeance of each component in the permeate is determined by the definition of permeance, as shown in Equation B.4.

$$\frac{P_i}{l} = 10^{-6} \frac{(\text{Permeate flow rate}) \cdot Y_i \cdot 273.15}{T \cdot A \cdot (p_X \cdot \phi_{Xi} \cdot Xi - p_Y \cdot \phi_{Yi} \cdot Y_i) \cdot 5.17} \tag{B.4}$$

1) Permeate flow is in mL/sec.

2) Y_i is the permeate mole fraction of component *i*.

3) X_i is the upstream mole fraction of component *i*. At a lower stage below 1%, X_i is approximately equal to the feed gas mole fraction.

4) T is the measurement temperature in Kelvin.

5) A is the area available for permeation in cm^2.

6) p_X and p_Y are the upstream and downstream total pressures, respectively (psi). *Py* is usually atmospheric.

7) ϕ is the fugacity coefficient. The calculation of fugacity coefficients is described in Section 2.5.4.

8) Subscripts represent upstream (*X*) or downstream (*Y*).

c) Selectivity

$$\alpha_{ij} = \frac{P_i / l}{P_j / l} \tag{B.5}$$

d) Separation Factor

$$S.F._{i/j} = \frac{Y_i}{Y_j} \cdot \frac{X_j}{X_i} \tag{B.6}$$

1) Y_i are the permeate mole fraction of component *i*.

2) X_i are the upstream mole fraction of component *i*.

APPENDIX C: MONOESTERIFICATION [11-12]

The 6FDA-DAM: DABA (3: 2) is monoesterified with 1, 3-propane diol. The reaction mechanism is shown in Figure C.1.

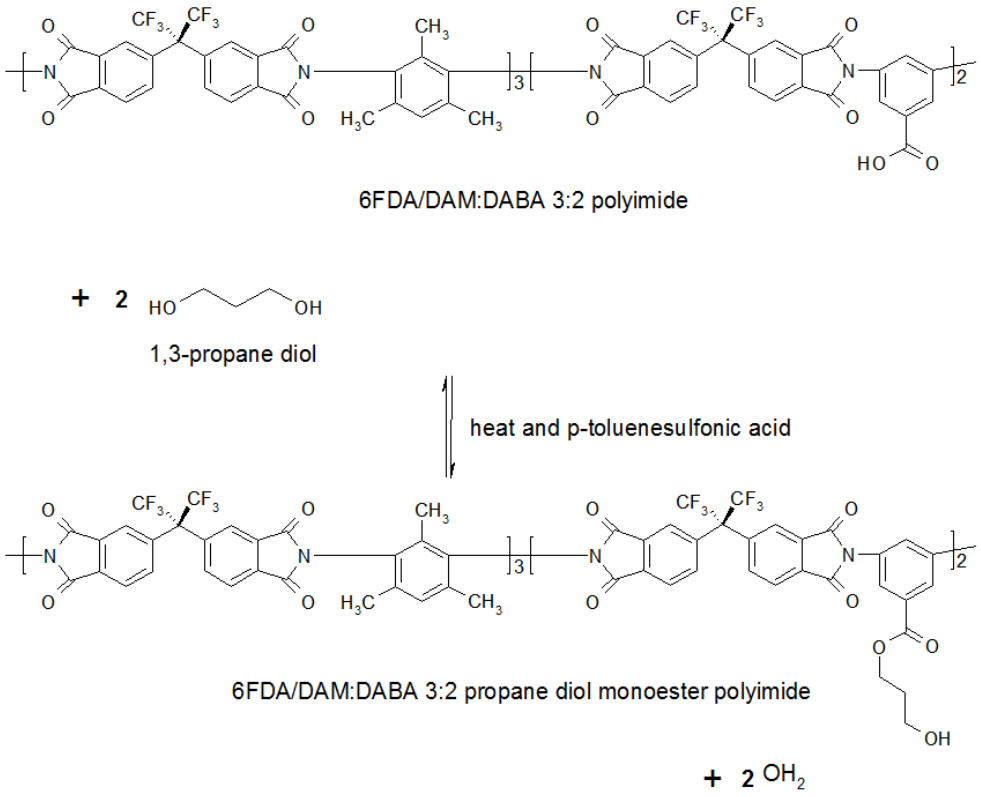

Figure C.2: Monoesterification reaction of 6FDA-DAM: DABA (3:2) polyimide with 1, 3-propane diol.

The monoesterification reaction is conducted by the following steps:

a) Dry 4A molecular sieves; clean and dry glassware.

b) Needle-transfer NMP to dry round-bottom with 4A molecular sieves.

c) Transfer ortho-dichlorobenzene (ODCB) or toluene to dry round-bottom with molecular sieves.

d) Assemble glassware in hood, as shown in Figure C.2.

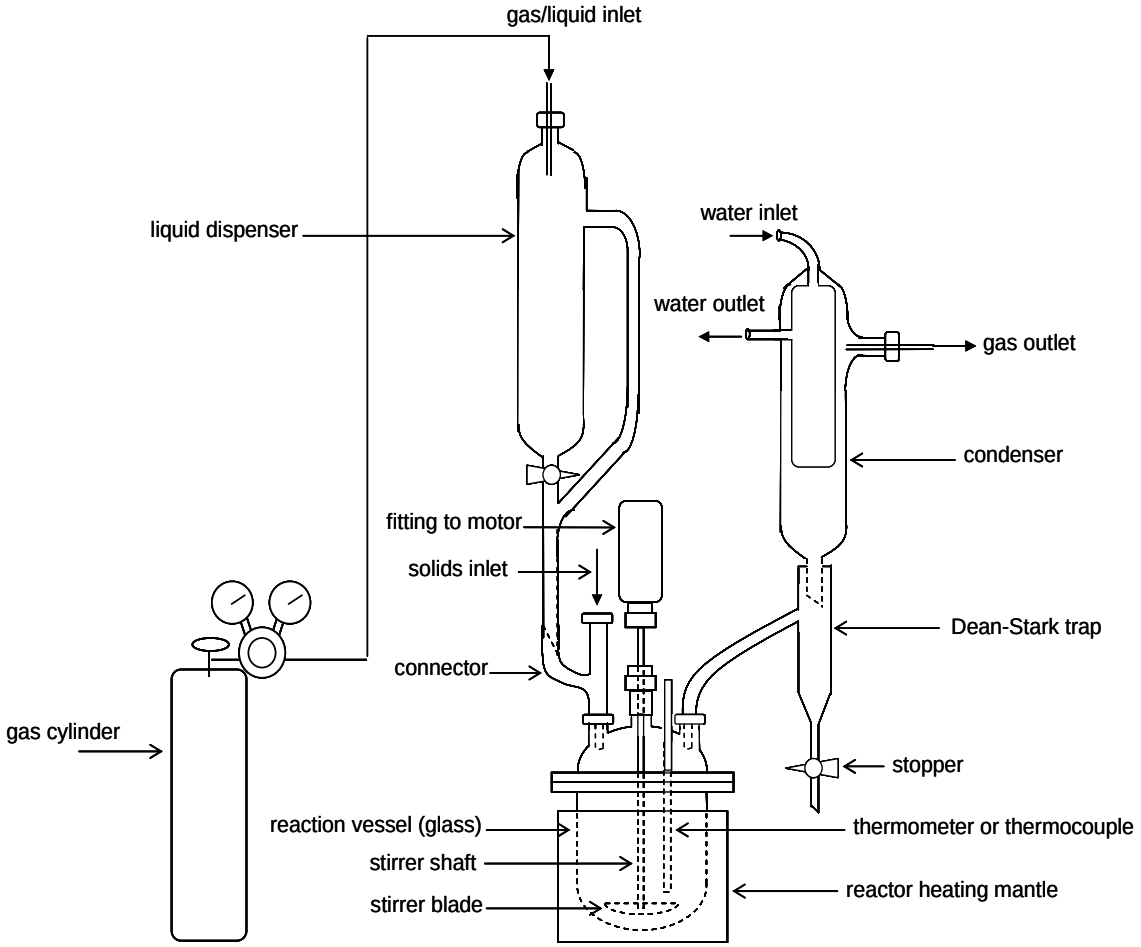

Figure C.2: Schematic showing the set-up for monoesterification reaction in this work.

e) Weight the 6FDA-DAM: DABA (3:2) polyimide precisely.

f) Dissolve the 6FDA-DAM: DABA (3:2) polyimide with enough NMP solution in the flask.

g) Heat up solution to ~140^{o}C and then add 40-70 times the stoichiometric amount of 1, 3-propanediol slowly enough to prevent large precipitates forming in reactor.

h) Add ~2.5 mg of para-toluenesulfonic acid per gram polyimide to reaction solution.

i) React for ~ 24 hrs at ~ 140^{o}C while collecting any water produced. Keep reaction always purged with nitrogen.

j) Cool reaction solution to less than ~ 50^{o}C, and then precipitate solution by pouring it slowly into methanol solvent.

k) Blend polymer, wash several times with methanol, filter, and then dry in hood overnight.

l) Dry polymer in vacuum oven at 70^{o}C for 24 hrs. The temperature was kept low to prevent cross-linking of the polymer particles.

m) The monoesterified polymer is ready for characterization and further research.

REFERENCES

1. *U.S. Energy Information Administration: Independent Statistical Analyses. International Energy Outlook 2009*. http://www.eia.doe.gov/oiaf/ieo/graphic_data_natgas.html].
2. Baker, R.W., and Lokhandwala, K., *Natural Gas Processing with Membranes: An Overview*. Ind. Eng. Chem. Res., 2008. 47: p. 2109-2121.
3. Baker, R.W., *Future Directions of Membrane Gas Separation Technology*. Eng. Chem. Res., 2002. 41: p. 1393-1411.
4. Bernardo, P., et al., *Membrane Gas Separation: A review/State of the Art*. Ind. Eng. Chem. Res., 2009, 48, 4638-4663.
5. Olajire, A., *CO_2 capture and separation technologies for end-of-pipe applications-A review*. Energy 35 (2010) 2610-2628.
6. Koros, W.J., G.K.F., *Membrane-based gas separation.* Journal of Membrane Science, 1993. 83: p. 1-80.
7. Mulder, M., *Basic Principles of Membrane Technology. Second Edition*. 1996. 564 pp.
8. Bird, A.J. and Trimm, D.L., *Carbon molecular sieves used in gas separation membranes*, in *Carbon*. 1983. p. 177-80.
9. Koros, W.J., *Evolving beyond the thermal age of separation processes: Membranes can lead the way.* AIChE Journal, 2004. 50(10): p. 2326-2334.
10. Baker, R.W., *Membrane Technology and Applications*. 2nd ed. 2004: John Wiley & Sons, Ltd. 538 pp.
11. Wallace, D.W., *Crosslinked Hollow Fiber Membranes for Natural Gas Purification and Their Manufacture from Novel Polymers*, in *Chemical Engineering*. 2004, The University of Texas at Austin: Austin, Texas. p. 202.

12. Omole, I. C., Crosslinked Polyimide Hollow Fiber Membranes for Aggressive Natural Gas Feed Streams in *Chemical Engineering. 2008*., Georgia Institute of Technology: Atlanta, Georgia. p. 199.
13. Hillock, A. M. W., *Crosslinkable polyimide mixed matrix membranes for natural gas purification*, in *Chemical Engineering. 2005*., Georgia Institute of Technology: Atlanta, Georgia. p. 199.
14. Wind, J. D., *Improving Polyimide Membrane Resistance to Carbon Dioxide Plasticization in Natural Gas Separations*, in *Chemical Engineering*. 2002, The University of Texas at Austin: Austin, Texas. p. 215.
15. Hines, A.L., et al., *Mass Transfer, Fundamentals and Applications*. 1 ed. Prentice Hall International Series in the Physical and Chemical Engineering Sciences, ed. N.R. Amundson. 1985, Upper Saddle River: Prentice-Hall PTR. 542.
16. Knudsen, M., *The Law of the Molecular Flow and Viscosity of Gases Moving through Tubes,* Annalen der Physik (Weinheim, Germany), 1909. 28: p. 75-130.
17. Cussler, E.L., *Diffusion, Mass Transfer in Fluid Systems*. 2nd ed. 1997, Cambridge, UK: Cambridge University Press. 580.
18. Graham, T., *on the law of the diffusion of gases*. Phil. Mag., 2 (1833) 175.
19. Bueche, F., *Physical Properties of Polymers*. 1962, New York: Interscience, Inc.
20. Michaels, A. S., W.R. Vieth, and J.A. Barrie, *Diffusion of Gases in Polyethylene Terephthalate.* J. Applied Physics, 1963. 14(1): p13-20.
21. Koros, W. J., et al., *A model for permeation of mixed gases and vapors in glassy polymers*. Journal of polymer Science: polymer physics edition, vol. 19, 1513-1530 (1981).
22. Robeson, M., *Correlation of separation factor versus permeability for polymer membranes polymeric membranes*. Journal of Membrane Science. *62* (1991) 165-185.
23. Kesting, R. E. and Fritzsche, A. K., *Polymeric Gas Separation Membranes*. 1993, New York: John Wiley and Sons, Inc.

24. Pinnau, I. and Koros, W. J., *Qualitative skin layer formation mechanism for membranes made by dry/wet phase inversion.* Journal of Polymer Science, Part B: Polymer Physics, 1996. 31(4): p. 419-427.

25. Clausi, D.T. and Koros, W. J., *Formation of defect-free polyimide hollow fiber membranes for gas separations.* Journal of Membrane Science, 2000. 167(1): p. 79-89.

26. Ismail, A.F. and Yean, L.P., *Review on the development of defect-free and ultrathin-skinned asymmetric membranes for gas separation through manipulation of phase inversion and rheological factor.* Journal of Applied Polymer Science, 2003. 88(2): p 442-451.

27. Carruthers, S.B., Ramos, G.L., and Koros, W. J., *Morphology of Integral-Skin Layers in Hollow-Fiber Gas-Separation Membranes.* Journal of Applied Polymer Science, 2003. 90: p. 399-411.

28. Van't Hof J. A. et al., Preparation of asymmetric gas separation membranes with high selectivity by a dual-bath coagulation method. J. Membr. Sci., 70 (1992) 17.

29. Li, D.F. et al., *Fabrication of fluoropolyimide/polyethersulfone dual-layer asymmetric hollow fiber membranes for gas separation.* J. Membr. Sci., 198 (2002) 211.

30. Peng, N. et al., *Evolution of ultra-thin dense-selective layer from single-layer to dual-layer hollow fibers using novel Extem® polyetherimide for gas separation.* Journal of Membrane Science, 360 (2010) 48–57.

31. Widijojo, N. et al., *A morphological and structural study of Ultem/P84 copolyimide dual-layer hollow fiber membranes with delamination-free morphology*, J. Membr. Sci., 294 (2007) 132.

32. Shabbir, H., *Mixed matrix dual layer hollow fiber membranes for natural gas separation*, in *Chemical Engineering*. 2006, Georgia Institute of Technology: Atlanta, Georgia. pp. 214.

33. Pinnau, I. and Koros, W. J., *Relationship between substructure resistance and gas separation properties of defect-free integrally skinned asymmetric membranes.* Industrial & Engineering Chemistry Research, 1995. 30(8): p. 1837-1840.

34. Bos, A., et al., *CO2-induced plasticization phenomena in glassy polymers.* Journal of Membrane Science, 1999. 155(1): p. 67-78.

35. Vissser. T., et al., *On the subtle balance between competitive sorption and plasticization effects in asymmetric hollow fiber gas separation membranes*. Journal of Membrane Science, 252 (2005) 265–277.

36. Paul, D. R. and Ebra-Lima, O. M., *Pressure-induced diffusion of organic liquids through highly swollen polymer membranes*. *J. Appl. Polym. Sci.*, 1970, *14*, 2201-2224.

37. Kamaruddin. H. D. et al., *Some observations about the application of Fick's first law for membrane separation of multicomponent mixtures*. Journal of Membrane Science 135 (1997) 147-159.

38. Kamaruddin, H. D., *Analysis of methanol/methyl tert-butyl ether (MTBE) separations using pervaporation*, in *Department of Chemical Engineering*. 1997, The University of Texas at Austin: Austin, TX. p. 215.

39. Peng, D. and Robinson, D. B., *New 2-constant equation of state*, *Ind. Eng.Chem. Fund.*, 1976, 15, 59-64.

40. Bertucco, A., et al., *Estimation of chemical-equilibria in high-pressure gaseous systems by a modified Redlich-Kwong-Soave equation of state*. *Ind. Eng. Chem. Res.*, 1995, *34*, 3159-3165.

41. Vu, D. Q., *Formation and characterization of asymmetric carbon molecular sieve and mixed matrix membranes for natural gas purification*. Ph.D. Dissertation, The University of Texas at Austin, 2001.17.

42. Taubert. A., et al., *Novel polyimide ionomers: CO2 plasticization, morphology, and ion distribution*. Polymer 44 (2003) 1881–1892.

43. Wind, J. D., et al., *Carbon Dioxide-Induced Plasticization of Polyimide Membranes: Pseudo-Equilibrium Relationships of Diffusion, Sorption, and Swelling*. Macromolecules, 2003, 36, 6433-6441.

44. Wind, J. D., et al, *Natural gas permeation in polyimide membranes*. Journal of Membrane Science, 228 (2004) 227–236.

45. Wind, J. D., et al., *Relaxation Dynamics of CO2 Diffusion, Sorption, and Polymer Swelling for Plasticized Polyimide Membranes*. Macromolecules, 2003, *36,* 6442-6448.

46. Wind, J. D., et al., *Solid-State Covalent Cross-Linking of Polyimide Membranes for Carbon Dioxide Plasticization Reduction*. Macromolecules, 2003, *36,* 1882-1888.

47. Wind, J. D., et al., *The Effects of Crosslinking Chemistry on CO2 Plasticization of Polyimide Gas Separation Membranes.* Ind. Eng. Chem. Res., 2002, *41,* 6139-6148.

48. Wallace, D. W., et al., *Characterization of crosslinked hollow fiber membranes*. Polymer, 47 (2006) 1207–1216.

49. Wallace, D. W., et al., *Efficient development of effective hollow fiber membranes for gas separations from novel polymers.* Journal of Membrane Science, 278 (2006) 92–104.

50. Hillock, A. M. W., et al., *Cross-Linkable Polyimide Membrane for Natural Gas Purification and Carbon Dioxide Plasticization Reduction*. Macromolecules, 2007, *40,* 583-587.

51. Hillock, A. M. W., et al., *Crosslinked mixed matrix membranes for the purification of natural gas: Effects of sieve surface modification*. Journal of Membrane Science, 314 (2008) 193–199.

52. Omole. I. C., et al., *Increased Molecular Weight of a Cross-Linkable Polyimide for Spinning Plasticization Resistant Hollow Fiber Membranes*. Macromolecules, 2008, *41*, 6367-6375.

53. Omole. I. C., et al., *Effects of CO2 on a High Performance Hollow-Fiber Membrane for Natural Gas Purification.* Ind. Eng. Chem. Res., 2010, *49,* 4887–4896.

54. Omole. I. C., et al., *Toluene impurity effects on CO2 separation using a hollow fiber membrane for natural gas*. Journal of Membrane Science, 369 (2011) 490–498.

55. Maeda, Y., and Paul, D.R., *Effect of antiplasticization on selectivity and productivity of gas separation membranes.* Journal of Membrane Science, 1987. 30(1): p. 1-9. 22.

56. Duda, J. L., Hadj Romdhane, I., and Danner, R. P., *Diffusion in glassy polymers--relaxation and antiplasticization.* Journal of Non-Crystalline Solids, 1994. 172-174 (Part 2): p. 715-720.

57. Maeda, Y. and Paul, D.R., *Effect of Antiplasticization on Gas Sorption and Transport. II. Poly (phenylene Oxide)*. Journal of Polymer Science: Part B: Polymer Physics, 1987. 25: p. 981-1003.

58. Moore, T.T., *Effects of materials, processing, and operating conditions on the morphology and gas transport properties of mixed matrix membranes*, in *Chemical Engineering*. 2004, The University of Texas at Austin: Austin, Texas. p. 283.

59. Adam, K., *Thickness dependent physical aging and supercritical carbon dioxide conditioning effects on crosslinkable polyimide membranes for natural gas purification*, in *Chemical & Biomolecular Engineering*. 2008, Georgia Institute of Technology: Atlanta. p. 200.

60. McKelvey, S.A., Clausi, D.T., and Koros, W.J., *A guide to establishing hollow fiber macroscopic properties for membrane applications.* Journal of Membrane Science, 1997. 124(2): p. 223-232.

61. Ekiner, O.M. and Vassilatos, G., *Polyaramide Hollow Fibers for H2/CH2 Separation: Spinning and Properties - II.* J. Memb. Sci., 2001(186): p. 71-84.

62. Ismail, A.F., et al., *Direct measurement of rheologically induced molecular orientation in gas separation hollow fiber membranes and effects on selectivity.* Journal of Membrane Science, 1997. 126(1): p. 133-137.

63. Sharpe, I.D., A.F. Ismail, and S.J. Shilton, *A study of extrusion shear and forced convection residence time in the spinning of polysulfone hollow fiber membranes for gas separation.* Separation and Purification Technology, 1999. 17(2): p. 101-109.

64. Bos, A., CO_2/CH_4 separation with glassy polymer membranes: Aspects of CO2-induced plasticization, University of Twente: 147(1996).

65. Bos, A., I. G. M. Punt, et al., "Suppression of gas separation membrane plasticization by homogeneous polymer blending." AIChE Journal, 47 (2001): 1088-1093.

66. Bos, A., I. G. M. Punt, et al., "Plasticization-resistant glassy polyimide membranes for CO2/CO4 separations." Separation and Purification Technology, 14 (1998): 27-39.

67. Bos, A., I. G. M. Punt, et al., "Suppression of CO2-Plasticization by Semiinterpenetrating Polymer Network Formation." J. Polym. Sci.: Part B Polym. Phys., 36(1998): 1547-1556.

68. Kuo, C.T. and Chen, S., *Kinetics of polyesterification: Adipic acid with ethylene glycol, 1,4-butanediol, and 1,6-hexanediol.* Journal of Polymer Science, Part A: Polymer Chemistry, 1989. 27(8): p. 2793-803.

69. Omole, I. C., *Personal communication*. 2009.

70. Pesek, S. C.; Koros, W. J., Aqueous quenched asymmetric polysulfone hollow fibers prepared by dry/wet phase separation. *J. Membr. Sci.*1994, *88*, 1–19.

71. Djoekita, G., D.Q. Vu, and Koros, W.J., *Pervaporative Introduction of Organic Vapors into High-Pressure Gas Feeds.* Journ. Applied Polymer Sci. 80(2): p. 311-315.